

Chemo catalytic pathways for value addition of bioglycerol

**Thesis Submitted to AcSIR for the Award of the
Degree of
DOCTOR OF PHILOSOPHY
In
Chemical Science**



By
Rajan Pandya
Registration Number: **10CC13A26024**

Under the guidance of
Dr. Chandrashekhar V. Rode

Chemical Engineering & Process Development
Division,
CSIR-National Chemical Laboratory,
Pune - 411008, INDIA

*Dedicated to my
beloved
Family and Friends...*



CERTIFICATE

This is to certify that the work incorporated in the Ph. D. thesis entitled “**Chemo catalytic pathways for value addition of bioglycerol**” submitted by **Mr. Rajan Pandya** to Academy of Scientific and Innovative Research (AcSIR) in fulfilment of the requirements for the award of the degree of **Doctor of Philosophy**, embodies original research work under my supervision/guidance. I further certify that this work has not been submitted to any other university or institution in part or full for award of any degree or diploma. Such material as has been obtained from other sources has been duly acknowledged in the thesis. Any text, illustration, table etc. used in the thesis from other sources, have been duly cited and acknowledge. It is also certified that this work done by the student, under our supervision, is plagiarism free.



Mr. Rajan Pandya

(Student)



Dr. Chandrashekhar V. Rode

(Supervisor/Research Guide)

Date- 30-07-2020

Declaration

I hereby declare that the thesis entitled “*Chemo catalytic pathways for value addition of bioglycerol*” submitted to Academy of Scientific and Innovative Research (AcSIR) for the award of degree of **Doctor of Philosophy (Ph. D.)** in chemical science is the outcome of experimental investigations carried out by me under the supervision of **Dr. Chandrashekhhar V. Rode**, Chief Scientist, Chemical Engineering and Process Development Division, CSIR–National Chemical Laboratory, Pune. I affirm that the work incorporated is original and has not been submitted to any other academy, university or institute for the award of any degree or diploma. I further declare that the material obtained from other sources has been duly acknowledged in the thesis.

July-2020

Place: Pune



Rajan Pandya

(Research Student)

CEPD Division,

CSIR-National Chemical Laboratory,
Dr.Homi Bhabha Road, Pune – 411 008,
INDIA.

Acknowledgement

In the journey of my studentship, undertaking this PhD has been a truly life-changing experience for me. It would not have been possible to do without the support and encouragement that I received from many people. Thus, without acknowledging their effort, this thesis may not be complete.

*First and foremost, I would like to express my deep and earnest gratitude to my research supervisor **Dr. Chandrashekhar V. Rode** (Emeritus Scientist and Former Chief Scientist, Chemical Engineering and Process Development Division, CSIR-National Chemical Laboratory, Pune) who made this work possible. A mere word of sincere appreciation is insufficient to express my gratitude to him. I am really grateful to him for his invaluable guidance, fruitful discussions, constructive suggestions, constant support and encouragement throughout the course, enabled me to complete this challenging task. He has been a constant source of inspiration to me during my stay at NCL and I have learnt extensively from him, including how to raise new possibilities, how to approach a problem by systematic thinking, enthusiastic attitude, innovative ideas, scientific knowledge and exploiting serendipity. I owe him lots of gratitude for his teaching and guidance in a cordial manner. It has been an intellectually stimulating and rewarding experience to work with him. I am really glad to be associated with a wonderful personality in my life.*

I would like to convey my sincere thanks to the DAC members Dr. Gopinath Chinnakonda, Dr. M. V. Badiger and Dr. S. P. Chawan for all their help, support and suggestions during the PhD coursework evaluations and presentations. I would like to thank former heads of the Chemical Engineering and Process Development Division for providing me all the divisional facilities required for my research work. I would also like to express my gratitude to Prof. Ashwini Kumar Nangia, Director of CSIR-NCL, Dr. Sourav Pal & Dr. K Vijamohanam (former Directors, CSIR-NCL), for providing the infrastructure and divisional facilities for research and giving me an opportunity to work at CSIR-NCL.

My special words of thanks should also go to Dr. Mahesh Kulkarni, Dr. B L V Prasad, Dr. C.G. Suresh, Dr. Chetan Gadgil, Dr. M. S. Shashidhar, Mr. Naveen Pavithran, Mr. P V Iyer, Mrs. Kolhe, Ms. Komal, Ms. Vaishali and SAO staff for their cooperative evaluation of AcSIR documents.. I am also grateful to CMC division for providing excellent instrumental facilities and especially Mr. Gholap, Harsha, Sheetal, Pooja, Venkatesh, Pankaj(For SEM and TEM), Dr. C.S. Gopinath, Mr. Deo (For XPS) for their help and support. I also thank the staffs from administration, accounts, Glass Blowing, medical, Engineering Section, DIRC, Stores and Purchase for providing excellent facility. The entire library staffs for providing excellent facilities are gratefully acknowledged.

I can never forget the help, love and constant encouragement from my lab seniors, Dr. Jayprakash Nadgeri, Dr. Vivek Mate, Dr. Mrs. Rasika Mane-Pol, Dr. Amol Hengne, Dr. Ajay Jha, Dr. Narayan Biradar, Dr. Sumit Kamble, Dr. Mrs. Sharda Kondawar- Parsewar, Dr. Chetana Pati, Dr. Suhas Shinde, Dr. Sanjay Jadhav, and Asst. Prof. Dr. Sachin Sakate for their help and suggestions. An individual thanks to all my labmates Mr. Bhanupratap Singh Solanki, Miss Roopa Parate, Miss Gayatri Kasar, Mr. Nandan Date, Mrs. Aarti Jadhav, Dr. Nishita Lucas, Mrs. Aparna Potdar, Mr. Sagar More, Mrs. Shobha Birajdar-Malage, Miss Priyanka Patil, Mr. Shivanand Patil, Mr. Dnyanesh Vernekar, Mr. Rameshwar Swami, Mr. Shankar Dhengale, Mr. Subhash Magar, Mr. Srinivas Charate and Mr. Anil Patil. I am also

thankful to master's trainees, Mr. Praneet Vyas, Mr. Rohit Kumbhar, Mr. Saleel Limaye, Miss Anwesha Sil, Mr. Ayush Vasishta, Ms. Kashmira Deval and Ms. Komal Tarade for maintaining the friendly and cordial atmosphere in the lab. I specially thank to Mr. David Solomon, former technician for quick solutions of technical problems and for the Kayani's cakes. I am also thankful to Mr. Chinnadurai (Annaji) for his all-time assistance in the lab. I am thankful to CEPD office staff Mr. Hasso Raheja, Mr. Patane and others for their constant cooperation. A heartfelt thanks to my dearest friends Mr. Bhanupratap Singh Solanki, Miss Roopa Parate, Miss Gayatri Kasar, Dr. Mrs. Sharda Kondawar- Parsewar (cubical bonding), Dr. Virat Pandya and Dr. Pravin Dwivedi, without your help it was impossible to complete my thesis.

A special mention of thanks to my militants friends Pratiksh, Rashid, Abhishek and to my beloved friends in Ncl Vikas, Arun, Yashpal, Shahebaz, Deepak, Rahul, Narugopal, Nirshad, Mahendra, Vir, Ravi, Dinesh, Pawan, Sayantan, Ram, Sandy, Sumanta, Golu, Kailash, Sudhakar, Ajith, Dharmendra, Rohit, Rahul, Ketan, Prabhu, Pravin, Vineeta, Yachita, Ruchi, Yogita, Geetanjali, Samrin, Rucha, Nishigandha, Divya, Parul, Swati for their priceless love, sharing, admirable support and encouragement in happy as well as unhappy situations.

I gratefully acknowledge Council of Scientific and Industrial Research-UGC, for providing me financial support to carry out this work..

*Finally, I would like to thank my family for being immensely supportive, loving and caring. I would like to pay my ultimate thanks to my father (**Mr. Vinod Pandya**) and mother (**Mrs. Harsha Pandya**) for building me to what I am. It was because of their encouragement and motivation that I could think of perusing higher education. I would like to thank my sister (Ankita) for being a strong support. I would never be able to pay back the love and affection showered upon me by my parents and family. My thanks are extended to my Brother in-laws Hardik Vyas, Mudit, Yash, Yathath, Parth and also to in-laws Mrs. Chetana and Mr. Brahmaddutt Joshi for their love and moral support.*

I owe my deepest gratitude towards my better half for her eternal support and understanding of my goals and aspirations. Her infallible love and support has always been my strength. Her patience and sacrifice will remain my inspiration throughout my life. Without her help, I would not have been able to complete much of what I have done and become who I am. It would be ungrateful on my part if I thank Chhavi in these few words.

Last but not the least, I feel very happy to express my sincere gratitude and appreciation to all those, whose direct or indirect contribution helped me during research work. Finally thanks to the almighty for giving me the strength and patience to work through all these years.

*With many thanks,
Rajan Pandya*

CONTENTS

Section	Page No.
List of Tables	ii
List of Schemes	vii
List of Figures	ix
Abbreviations	xiii
Abstract of thesis	xvi

Section No.	Title	Page No.
Chapter 1 Introduction 1-27		
1.1	Catalysis	2
1.2	Biomass	5
1.3	Biorefinery	7
1.3.1	Biodiesel production and co-generation of glycerol	8
1.3.2	Glycerol: an overview	9
1.3.3	Glycerol valorization	10
1.4	Glycerol amination to oxazoline	12
1.4.1	Background Literature	13
1.5	Aqueous phase reforming of glycerol without external hydrogen	17

1.5.1	Background Literature	21
1.6	Scope and objectives of the thesis	22
1.6.1	Glycerol amination to oxazoline	22
1.6.2	Aqueous phase reforming of glycerol without external hydrogen	23
1.7	References	24

Chapter 2	<i>Experimental methods and Characterization Techniques</i>	28- 48
------------------	--	---------------

2.1	Introduction	29
2.2	Materials	29
2.3	Catalyst preparation	29
2.3.1	Cu-Al catalyst	29
2.3.2	Supported noble metal catalysts	31
2.4	Characterization techniques	32
2.4.1	X-ray diffraction (XRD)	32
2.4.2	Surface area measurement	34
2.4.3	Scanning electron microscopy	36
2.4.4	Transmission electron microscopy	37
2.4.5	Temperature programmed desorption of NH ₃ (NH ₃ -TPD)	37
2.4.6	Pyridine FT-IR technique	38
2.4.7	Fourier transform infrared spectroscopy (FTIR)	39

2.4.8	X-ray photoelectron spectroscopy (XPS)	40
2.5	Catalyst activity testing	42
2.5.1	Glycerol conversion to oxazoline using a simple distillation method	42
2.5.2	Single-pot glycerol conversion to oxazoline in a batch reactor	43
2.5.3	APR of glycerol to 1, 2-PDO	45
2.6	Analytical methods	45
2.7	Performance criteria of a catalyst	46
2.8	References	47

<i>Chapter 3</i>	<i>Dehydrative amination of glycerol to oxazoline using a simple distillation method</i>	49-66
-------------------------	---	--------------

3.1	Introduction	50
3.2	Experimental	52
3.3	Results and Discussion	52
3.3.1	Characterization techniques	53
3.3.1.1	Surface area measurement	53
3.3.1.2	X-ray diffraction	53
3.3.1.3	XPS	54
3.3.1.4	NH ₃ -Temperature programmed desorption	57
3.3.1.5	Pyridine infrared (Py-IR) spectroscopy	58
3.3.2	Activity testing	59
3.4	Conclusion	64

3.5	References	64
-----	------------	----

Chapter 4		67-90
<i>Ru Catalyzed cascade dehydrative amination of glycerol to oxazoline</i>		
4.1	Introduction	68
4.2	Experimental	69
4.3	Results and discussion	70
4.3.1	Characterization techniques	70
4.3.1.1	X-ray diffraction	70
4.3.1.2	BET surface area	71
4.3.1.3	HRTEM	71
4.3.1.4	SEM	72
4.3.1.5	XPS	73
4.3.1.6	NH ₃ -Temperature programmed desorption	76
4.3.1.7	Pyridine infrared (Py-IR) spectroscopy	77
4.3.2	Activity testing	79
4.3.3	Process optimization studies	82
4.3.3.1	Effect of metal loading	83
4.3.3.2	Effect of glycerol concentration	83
4.3.3.3	Effect of solvent	84
4.3.3.4	Effect of temperature	85
4.3.3.5	Effect of catalyst loading	86
4.3.4	Recycling of catalysts	87

4.4	Conclusion	88
4.5	References	89

Chapter 5	Role of catalyst pre-treatment in aqueous-phase reforming of glycerol to propylene glycol	91-113
------------------	--	---------------

5.1	Introduction	92
5.2	Experimental	94
5.3	Results and discussion	94
5.3.1	Characterization techniques	94
5.3.1.1	X-ray diffraction	94
5.3.1.2	BET surface area	95
5.3.1.3	HRTEM	95
5.3.1.4	XPS	96
5.3.1.5	NH ₃ -Temperature programmed desorption	99
5.3.1.6	Pyridine infrared (Py-IR) spectroscopy	100
5.3.2	Activity testing	101
5.3.3	Process optimization studies	107
5.3.3.1	Effect of metal loading	107
5.3.3.2	Effect of glycerol concentration	108
5.3.3.3	Effect of temperature	109
5.3.4	Recycling of catalyst	109
5.4	Conclusion	110
5.5	References	111

Chapter 6 Conclusions and Future scope		114-117
6.1	Conclusions	115
6.2	Future prospects	117
	Research papers published in peer reviewed journals	118
	About the Author	120
	Erratum	125

List of tables

Table No.	Title	Page No.
Chapter 1		
1.1	Comparison of homogenous and heterogeneous catalyst	4
1.2	Physical properties of 1, 2-PDO	17
1.3	Literature study of aqueous phase reforming of glycerol without external hydrogen	22
Chapter 2		
2.1	Oven program of gas chromatography	45
Chapter 3		
3.1	Relative intensity ratio of copper species by XPS in various activated copper catalysts	57
3.2	NH ₃ -TPD results of different copper catalysts	58

3.3	Catalyst screening for dehydrative cyclised amination of glycerol	59
3.4	Effect of catalyst on acetol conversion to oxazoline	62

Chapter 4

4.1	Surface areas (BET) of supported 3% Ru catalysts	71
4.2	Percentage of Ru ⁰ in different supported catalysts from XPS curve fitting data of Ru 3p peak	76
4.3	NH ₃ -TPD results of bare supports and Ru supported catalysts	77
4.4	Py-IR results of supported Ru catalysts	78
4.5	Catalyst screening for one pot conversion of glycerol to oxazoline	80
4.6	Effect of solvent	85

Chapter 5

5.1	Effect of activation temperature on the % of Ni ⁰ from XPS curve fitting data of the Ni 2p peak	98
5.2	NH ₃ -TPD results of NiAl catalysts activated at different temperature	100
5.3	Py-IR spectroscopy results of NiAl catalysts activated at different temperature	101
5.4	Catalyst activity for APR of glycerol	102

List of schemes

Scheme No.	Title	Page No.
------------	-------	----------

Chapter 1

1.1	Roadmap of glycerol valorization	11
1.2	Process for converting glycerol to amino alcohols	14
1.3	Process for the alternating conversion of glycerol to propylene glycol or amino alcohols	14
1.4	Proposed reaction pathway for glycerol dehydration	16
1.5	Glycerol hydrogenolysis routes	19
1.6	Schematic representation of in situ generated hydrogen utilization for glycerol hydrogenolysis to 1, 2-propanediol	21
Chapter 3		
3.1	Dehydrative amination of glycerol to oxazoline	52
3.2	Reaction mechanism for the glycerol amination	62
Chapter 4		
4.1	Two pathways for glycerol amination to oxazoline [A] Dehydrative amination of glycerol to oxazoline using a simple distillation method [B] Cascade dehydrative amination of glycerol to oxazoline	68
4.2	Plausible mechanistic pathway for glycerol amination to oxazoline	82
Chapter 5		
5.1	Reaction pathway proposed for the glycerol APR on nickel catalyst	105
5.2	Proposed reaction pathway for hydrogenation /dehydration and dehydrogenation of glycerol with aqueous phase reforming over Ni-Al catalyst	106

List of figures

Figure No.	Title	Page No.
Chapter 1		
1.1	Catalyst cycle	2
1.2	Energy profile diagram for catalysed and uncatalysed reactions	3
1.3	Various sources of biomass	5
1.4	Biorefinery concept	7
1.5	Chemistry of biodiesel production	8
1.6	Global biodiesel production and crude glycerol price from 2003 to 2020	9
1.7	Distribution of the glycerol consumption by sector/application	10
1.8	Structure of 2-oxazoline, 3-oxazoline, and 4-oxazoline (from left to right)	12
1.9	Uses of Oxazoline	13
1.10	Experimental setup for semi-batch reactive distillation	15
1.11	Industrial application of 1, 2-PDO	18
Chapter 2		
2.1	General setup for catalyst preparation of Cu-Al	30
2.2	Method for preparation of copper catalyst by co-precipitation	31

	method	
2.3	Setup for supported catalysts preparation by impregnation method	32
2.4	Schematic representations of X-ray diffractometer and Bragg's equation	33
2.5	IUPAC classifications of isotherms	35
2.6	Chemisoft TPx (Micromeritics-2720) instrument	35
2.7	Features of an optical microscope TEM and SEM	36
2.8	FTIR instrumentation	40
2.9	Basic principle of XPS	41
2.10	Schematic presentations of XPS	42
2.11	Reactive distillation set up	43
2.12	Schematic of a batch reactor set-up	44

Chapter 3

3.1	Examples of 3-oxazoline-containing natural products (a, b) – Two dimeric diterpenoids, taxodikaloids and (c) - Intermediate for synthesis of <i>ent</i> -alantrypinone	51
3.2	XRD patterns of different activated copper catalysts. (*)Cu ⁰ , (#) Cu ₂ O, (+) CuO, (ϕ) t-ZrO ₂	54
3.3	XPS spectra for the Cu 2p _{3/2} region A) Cu-Al, B) Cu-Zr and C) Cu-Mg	56
3.4	NH ₃ -TPD profiles of different activated copper catalysts	57
3.5	Py-IR of different activated copper catalysts	59
3.6	¹ H-NMR spectra of Oxazoline	60

3.7	^{13}C -NMR spectra of Oxazoline	60
3.8	IR spectra of oxazoline	61

Chapter 4

4.1	XRD spectra of supported Ru catalysts: (a) 3% Ru/C, (b) 3% Ru/SiO ₂ , and (c) 3% Ru/Al ₂ O ₃	70
4.2	TEM images of (a) 3% Ru/C, (b) 3% Ru/C(enlarged), (c) Ru/SiO ₂ (d) Ru/SiO ₂ (enlarged), (e) 3% Ru/Al ₂ O ₃ , (f) 3% Ru/Al ₂ O ₃ (enlarged), (g) fifth recycled 3% Ru/C (h) fifth recycled 3% Ru/C (enlarged) catalyst	72
4.3	SEM images of a) 3% Ru/C, b) 3% Ru/SiO ₂ and c) 3% Ru/Al ₂ O ₃ catalysts	73
4.4	XPS spectra for the Ru 3d region (a) 3% Ru/C, (b) 3% Ru/SiO ₂ and (c) 3% Ru/Al ₂ O ₃ catalyst	74
4.5	XPS spectra for the Ru 3d region (a) Ru/C, (b) Ru/SiO ₂ and (c) Ru/Al ₂ O ₃ catalyst	75
4.6	NH ₃ -TPD profiles of supported Ru catalysts	77
4.7	Py-IR profiles of supported Ru catalysts	78
4.8	Leaching of catalyst a) non-noble catalyst b) noble metal catalyst	79
4.9	Effect of Ru metal loading on cascade dehydrative amination of glycerol	83
4.10	Effect of glycerol loading on cascade dehydrative amination of glycerol	84
4.11	Effect of temperature on cascade dehydrative amination of glycerol	86
4.12	Effect of catalyst loading on cascade dehydrative amination	87

of glycerol

4.13	Recycling studies on the 3% Ru/C catalyst on cascade dehydrative amination of glycerol	88
-------------	---	----

Chapter 5

5.1	XRD spectra of activated NiAl catalysts at different temperature: (a) NiAl-calcined (b) NiAl-400 (c) NiAl-600 and (d) NiAl-800	95
5.2	TEM images of activated NiAl catalysts at different temperature: (a) NiAl-calcined (b) NiAl-400 (c) NiAl-600 and (d) NiAl-800	96
5.3	XPS spectra for the Ni 3p region (a) NiAl-400 (b) NiAl-600 (c) NiAl-800	98
5.4	NH ₃ -TPD profiles of NiAl catalysts activated at different temperature	99
5.5	Py-IR profiles of NiAl catalysts activated at different temperature	101
5.6	Catalyst activity of NiAl catalysts activated at different temperature	103
5.7	Effect of metal loading on glycerol APR reaction	108
5.8	Effect of glycerol loading on glycerol APR reaction	108
5.9	Effect of temperature on APR of Glycerol	109
5.10	Recycling studies on the NiAl-600 catalyst for the APR reaction	110

Abbreviations

AC	Activated carbon
NH ₃	Ammonia
AlCl ₃	Aluminium trichloride
APR	Aqueous phase reforming
BET	Brunauer, Emmett and Teller
BD	Biodiesel
Conc.	Concentrated
Cu-Al	50% Cu and 50% Al
°C	Degree Celsius
CDCl ₃	Deuterated chloroform
eV	Electron volt
EDS	Energy-dispersive X-ray spectroscopy
EtOH	Ethanol
EG	Ethylene glycol
FAME	Fatty acid methyl esters
FID	Flame ionization detector
FT-IR	Fourier transform infrared spectroscopy
FFAP	Free fatty acid phase
GC	Gas chromatography
G	Gram
HR-TEM	High-resolution transmission electron microscopy

HPLC	High performance liquid chromatography
HP-5	Hewlett Packard-5
ICP-AES	Inductively coupled plasma atomic emission spectroscopy
M	Moles
MeOH	Methanol
Mmol	Millimoles
mg	Milligram
OXZ	Oxazoline
1, 2 PDO	1, 2-propanediol
2-PrOH	2-Propanol
Py-IR	Pyridine infrared
SAED	Selected area electron diffraction
SEM	Scanning electron microscope
S-ZrO ₂	Sulfated zirconia
TG and DTA	Thermogravimetric and differential thermal analysis
NH ₃ -TPD	Temperature programmed desorption of ammonia
TPR	Temperature programmed reduction
TEM	Transmission electron microscopy
θ	Theta
TCD	Thermal conductivity detector
TOF	Turnover frequency

TOS	Time on stream
H ₂ O	Water
WGSR	Water gas shift reaction
XRD	X-ray diffraction
XPS	X-ray photoelectron spectroscopy
ZrOCl ₂ · 8 H ₂ O	Zirconium (IV) oxychloride octahydrate

ABSTRACT

Chemo catalytic pathways for value addition of bioglycerol

Introduction

In recent years, downstream processing of biomass resources has attracted much attention for the development of sustainable industrial processes and efficient management of greenhouse gas emission. Biomass represents a prominent and easily accessible renewable source of organic carbon and its processing needs viable catalytic routes. Glycerol is a byproduct of biodiesel production involving transesterification of vegetable oils and animal fats. As a consequence of government mandates in various countries to blend biodiesel with diesel, the production of biodiesel is forecasted to reach 37 million metric tons in 2020, ultimately leading to the surplus availability of glycerol [1]. Therefore, although glycerol has a traditional market, it is incapable of absorbing the huge surplus quantity of glycerol in the near future which already resulted in a crash in the price of glycerol. Hence, value addition of glycerol is through catalytic conversion to commodity and fine chemicals is highly desirable for improving the process economics of biodiesel production and also to develop sustainable processes. Thus, the valorization of glycerol will not only improve the biodiesel economy but also provide an excellent opportunity for the usage of renewable resources in synthetic chemistry [2].

For last couple of decades, several efforts have been made towards the carbon-neutral production of H₂ from biomass resources. This approach is a credible alternative to the polluting and non renewable fossil energy sources [3]. Several biomass-derived oxygenated compounds, such as alcohols (methanol, ethanol) and polyols (ethylene glycol, glycerol, and sorbitol) have been considered as some of the active compound capable of undergoing aqueous phase reforming to generate hydrogen [4].

Among possible downstream products from glycerol, hydrogen production from glycerol has been considered as an attractive process [5]. Some of the reforming techniques studied for the

production of hydrogen from glycerol include steam reforming (SR), pyrolysis, gasification, aqueous phase reforming (APR), and the supercritical water reforming process [6]. Depending on the nature of catalyst and process conditions, glycerol APR leads to in-situ hydrogenation to produce various industrially important products such as 1, 2-propanediol (1, 2-PDO), acetol, ethylene glycol (EG) and 2-propanols (2-Prop). These are commonly used as solvents, in antifreeze formulations and additives in many fields such as polymer (polyesters, polyurethanes), cosmetics and pharmaceuticals [7]. All the strategies mentioned above only offer oxygen containing chemicals from glycerol. However, the scope of reactions for converting glycerol into nitrogen containing molecules and aqueous phase reforming, often have higher commercial value, which have received much less attention and further research in this area is essential.

In this work, we aimed at we focused on the transformation of glycerol into value added chemicals by 2 distinct strategies; (i) glycerol amination to oxazoline and (ii) Aqueous phase reforming of glycerol to 1, 2-PDO without external hydrogen.

Methodology:

A brief introductions of methodologies used in the work are discussed below in respective research chapters.

Thesis chapters and content:

Chapter I: This chapter includes an introduction to catalysis, biomass and the biorefinery concept of using renewable bio-feedstock. The basic information of different types of catalysis and mechanism is summarized. In particular, this chapter also highlights the valorisation of glycerol as it is a co-product of biodiesel production. This is followed by detailed literature survey on glycerol amination and aqueous phase reforming of glycerol highlighting the challenges and selection of best catalysts for both the reactions. Last section of the chapter describes the objectives and scope of present work.

Chapter 2: In this chapter, the first section deals with general experimental procedures followed for the preparation of various catalysts are discussed. The second section of the chapter describes details various characterization techniques such as X-Ray Diffraction, Thermo gravimetric analysis, X-ray Photoelectron Spectroscopy, BET, surface area measurements, and electron microscopy (SEM and TEM), which are indispensable for

catalyst characterization and activity testing. Analytical methods used for identification of gaseous and liquid products are also described in this chapter.

Chapter 3: Synthesis of valuable nitrogen-containing compounds directly from biomass feedstock is highly desirable but at the same time quite challenging. Here, we report a non-noble metal Cu–Zr catalyst developed method for the direct conversion of bio glycerol to oxazoline involving glycerol dehydration to acetol followed by its amination using an aqueous solution of ammonia. In this two-step strategy 78% of glycerol conversion was achieved with complete selectivity to acetol while, the amination of acetol carried out separately gave 95% selectivity to oxazoline. The excellent activity performance of the catalyst was explained based on its detailed characterization by XRD, NH₃-TPD and Py-IR. The novelty of this catalyst was its multifunctional active sites responsible for glycerol dehydration to acetol, followed by its amination to oxazoline.

Chapter 4: N-heterocyclic compounds are ubiquitous building blocks in chemical industry. Our previous work suggests that heterogeneous catalysts are promising to promote the formation of nitrogen-containing compounds from cheap and abundant raw materials. Here, we report a simple and efficient method for the single pot cascade conversion of bioglycerol to oxazoline involving glycerol dehydration to acetol followed by its amination using an aqueous solution of ammonia. We have demonstrated a single-pot oxazoline synthesis using 3% Ru/C as the most stable catalyst to achieve 95% selectivity to oxazoline without any leaching. XPS studies revealed the co-existence of multivalent Ru species in different percentages depending on the nature and structure of the support. These multivalent species (RuO₂ and RuO₃) have a synergistic effect on the activation of the carbonyl group, whereas Ru⁰ is an active site for ammonia dissociation. NH₃-TPD and Py-IR spectroscopy results also suggest that the presence of relatively moderate acid sites and a higher Brønsted /Lewis acid ratio in the catalyst promote the selective production of oxazoline. The reaction pathway involves first glycerol dehydration to acetol while in the subsequent step, NH₃ is dissociatively adsorbed on the catalyst surface and the imine thus formed is condensed with a second molecule of acetol gives oxazoline. The catalyst developed in this work could be recycled successfully without any significant loss of catalytic activity.

Chapter 5: The aqueous phase reforming (APR) of glycerol over supported nickel-based catalysts was investigated. A series of Ni catalysts on different supports (C, Al₂O₃, ZnO₂, Mont, ZrO₂ or SiO₂) were prepared by wet impregnation method and tested in glycerol APR which gave in situ glycerol hydrogenolysis product, 1,2-propanediol (propylene glycol) at

220 °C and 5 h in a batch reactor. The effect of catalyst reduction temperature, between 400-800 °C, on physicochemical properties and catalytic performance in the APR of glycerol were investigated for NiAl catalyst. The excellent activity performance of the catalyst was explained based on its detailed characterization by XRD, XPS, NH₃-TPD and Py-IR. Without external hydrogen, the reaction pathway involves glycerol dehydration to acetol with simultaneous reforming to H₂ and CO₂; this hydrogen generated *in situ* is used for the hydrogenation of acetol to propylene glycol. Under these conditions, the Ni/Al₂O₃ activated at 600 °C catalysts exhibited the highest glycerol conversion, 35 %, with propylene glycol yield around 40 %. The good stability of the spinel phase of the studied catalyst resulted in successful recycling without any significant loss of the catalytic activity.

Chapter 6: The salient features and specific conclusions of my research work, illustrated from all the above findings are summarised in this chapter.

References:

1. R. Pandya, R. Mane, C. V. Rode, *Catalysis Science & Technology* 8(11) (2018) 2954-65.
2. C. V. Rode, R. Pandya, R. B. Mane, US 10385029 B2 (2019).
3. R. B. Mane, C. V. Rode, *Green Chem.* 14 (2012) 2780-2789.
4. N. H. Tran, G. S. K. Kannangara, *Chem. Soc. Rev.* 42 (2013) 9454-9479.
5. Y. Nakagawa, K. Tomishige, *Catal. Sci. Technol.* 1 (2011) 179-190.
6. R. B. Mane, A. Yamaguchi, A. Malawadkar, M. Shirai, C. V. Rode, *RSC Adv.* 37 (2013) 16499-16508.
7. A. Seretis, P. Tsiakaras, *Fuel Process. Technol.* 142 (2016) 135–146.

Chapter 1

Introduction

This chapter includes an introduction to catalysis, biomass and biorefinery concept. The basic information on different types of catalysis and mechanism is summarized. In particular, this chapter also highlights the valorisation of glycerol (a co-product during biodiesel production). This is followed by a detailed literature survey on glycerol amination and also its aqueous phase reforming highlighting the challenges and selection of best catalysts for both the reactions. The last section of the chapter describes the objectives and scope of the present work.

1.1 CATALYSIS

Catalysis is commonly encountered while studying chemistry particularly, and chemical reactions. While some of the chemical reactions occur quickly, some take a protracted time and need additional materials or effort. This is where a catalyst comes in. Catalysts are those substances that alter the rate of reaction by changing the path of the reaction. When a catalyst is employed to increase the rate of a chemical reaction this phenomenon is known as catalysis. The term “catalysis” was first defined by Berzelius in 1835 [1], “Catalysis is a phenomenon in which chemical reactions are accelerated by small quantities of foreign substances”. The catalytic reaction is a cyclic process. Figure 1.1 shows that the reagent A and B forms a complex with catalyst on its surface and get converted to the product. After completion of the reaction, product and catalyst leave each other, and the catalyst can take part in the new cycle [2]. As catalyst is not consumed in the reaction, it can be recycled many times without a drop of its original activity.

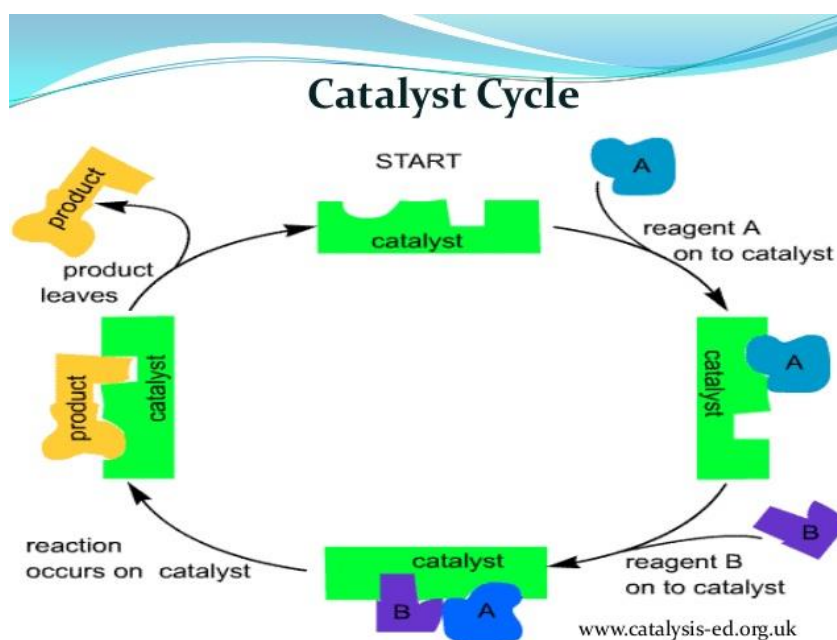


Figure 1.1 Catalyst cycle

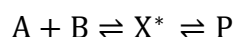
The rate of any chemical reaction at a given temperature is usually decided by the ‘activation energy’. Activation energy or threshold energy was introduced by Arrhenius in 1889. It is defined as “the energy that must be overcome in order for a chemical reaction to occur”. The term activation energy is commonly represented by E_a and measured in kilojoules per mole. The relation between the E_a and temperature is given by the Arrhenius equation,

$$k = A e^{-E_a/RT} \dots\dots\dots 1.1$$

Thus, $E_a = -RT \ln (k/A) \dots\dots\dots 1.2$

Where A represents the pre-exponential factor for the reaction, R is the gas constant, T is the temperature (K), and k is the reaction rate constant.

For Example: For a reaction $A + B \rightarrow P$, it is necessary that the molecules of A and B must form an activated complex or a transition state X^* before they get converted into product P. A state of equilibrium exists between $A + B$, P, and X^* which is represented as,



The energy profile diagram for the above reaction with and without catalyst is presented in Figure 1.2.

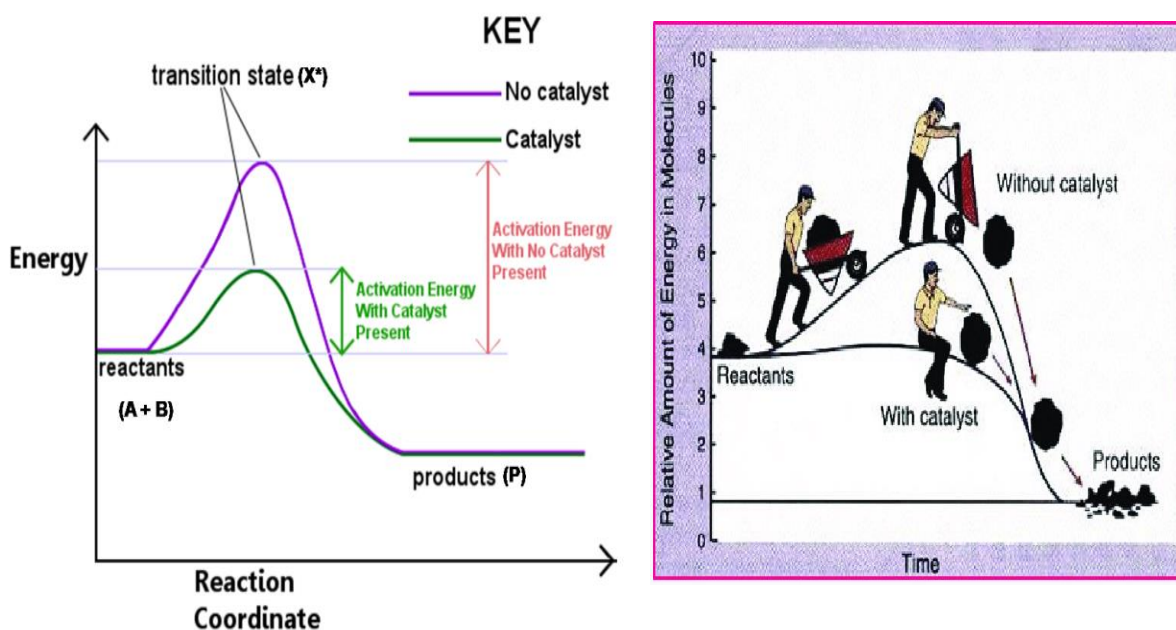


Figure 1.2 Energy profile diagram for catalysed and uncatalysed reactions

The absorption of energy E_a (energy of activation) by molecules of A and B forms an activated complex X^* . When X^* gets converted into product P, more heat will be evolved, since the energy of P is lower than that of A + B. The energy of activation is lower for a

reaction carried out in the presence of a catalyst as compared to an uncatalysed reaction. Therefore, the rate of a catalytic reaction is very high as compared to that in the absence of a catalyst [3].

Catalysis is divided into two parts, depending upon the physical state of catalyst:-

1. **Homogeneous catalysis:** - if the reactants and catalyst are present in the same phase. For example, hydrolysis of sugar is catalysed by sulphuric acid.
2. **Heterogeneous catalysis:** - if the reactants and catalyst are present in a different phase. For example, manufacture of sulphuric acid by contact process.

Heterogeneous catalysis has several intrinsic advantages and disadvantage over its homogeneous counterparts, which are shown in Table 1.1

Table 1.1 Comparison of homogenous and heterogeneous catalyst

Features	Homogeneous Catalyst	Heterogeneous catalyst
Phase	liquid	different
Reaction conditions	mild	harsh
Selectivity	high	irregular
Temperature	mild	drastic
Recycling	difficult	simple
Ease of separation	challenging	easy
Diffusivity problem	none	high
Mechanism	familiar	poorly known
Catalyst deactivation	low	high

Surface adsorption theory [4] proposed five stages for the heterogeneous catalysis:

1. Diffusion of reactant to the catalytic surface.
2. Adsorption of reactants.
3. A chemical reaction between reactant molecules on the surface.
4. Product desorption.
5. Diffusion of product.

Due to increasing awareness of the environmental issues, the importance of heterogeneous catalysis is exponentially enhanced during the last couple of decades. A particular area where the catalysis is contributing significantly by substitution of the traditional procedure by a new catalytic procedure, which permits efficient use of resources, energy and gives rise to minimize waste. More than 81% of the current industrial processes within the field of pharmaceutical, chemical, petrochemical, biochemical as well as polymer industries are catalytic. For my Ph.D. work, I studied heterogeneously catalyzed chemo catalytic transformation of biomass derived glycerol.

1.2 Biomass

Biomass refers to the organic matters that arise from plants and animals and are used for energy production. The most common biomass materials used for energy are plants, wood, and waste as shown in Figure 1.3. These are called biomass feedstock. Biomass gets its energy from the sunlight. Plants transform sunlight energy to chemical energy by a process called photosynthesis. On biomass burning, the stored energy is released in the form of heat. For energy production, it can be burnt directly or transformed into bio fuels or bio gas.

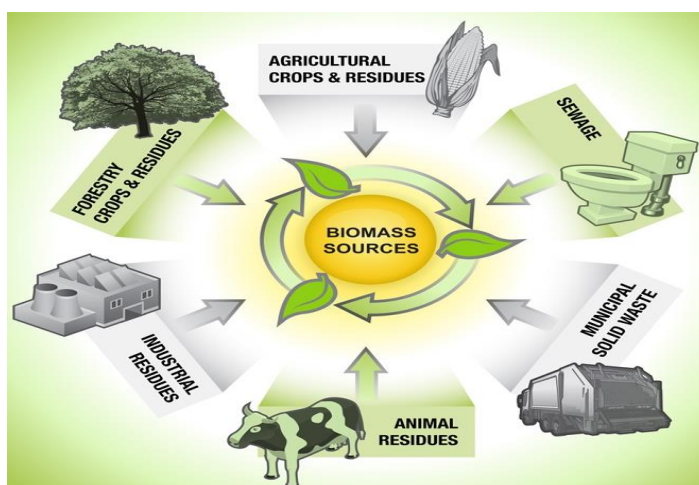


Figure 1.3 Various sources of biomass

We use four types of biomass today: -

1. Wood waste - to generate electricity in industry.
2. Agricultural products - burnt directly or transformed to bio fuels.

3. Municipal Solid Wastes and Sewage - burnt to get electricity or transformed to energy in landfills.
4. Animal waste - transformed to bio gas that can be used as an indirect fuel.

With an increase in population, low power utilization, fast urban expansion and economic development in last few decades; India is having a dominant position in the power industry of the world. Fossil fuels are finite non-renewable resources and it prolongs consumption will increase global warming. This realisation has led to aggressive development in the quest for alternative energy resources. The on-going price increase of fossil fuels, their uncertainty and impact on environmental, it is predicted that the feasibility of fuel exploitation would reduce very soon. The only way out is fossil-free resources, such as bio-based, which are also renewable in nature. Therefore new suitable sources of energy have been substituted, which can environment friendly and lower the dependence on fossil fuels. Most of the research is focussed on bio-based processes with the precondition that the products must be cheaper than traditional ones.

Biomass energy has quickly set off an essential part of the global renewable energy resources. Recently few reports counsel that biomass energy is probably going to create 33% of global energy mix by 2050. In fact, bio fuels supply approximately 3% of the global fuel for transport [5]. The shift towards biomass energy has played a vital role in lowering our need for fossil fuels. Biomass fuels outstandingly diminish global warming. Biomass is sustainable, renewable and is a low-carbon choice.

Bioenergy systems supply vital potentialities for minimizing global warming due to their huge potential to replace traditional fossil fuel use. In addition, bio energy decreases emissions and enhances bio sequestration. Bioenergy can also play a vital role in reducing carbon emissions [6].

Furthermore, bio fuels will be significant for employment creation in addition to environmental benefits. The development of small and large-scale biomass-based power plants can offer attractive opportunities for rural development.

With affordability and sustainability in mind, researchers turned their attention to the production of bio fuel, a greener alternative to conventional fuel that can be used to power trucks, planes and heavy equipment. This has led to the concept of biorefinery.

1.3 Biorefinery

A biorefinery is a facility that transforms biomass to energy and other value added products. A biorefinery is similar to today's crude oil refinery, which refines biomass to produce biofuel, power and chemical products. Bio-refinery has a key role in the bio-based economy. Its goal is to use all the synergies for sustainable and efficient production to efficiently utilize biomass for economical, eco friendly and social benefits.

A biorefinery could, for example, produce a broader spectrum of value added products, in addition to bio fuel. At the same time, it can also generate power. The value added products enhance profitability, the bio fuel helps meet energy needs, and the power generation contributes to reducing energy costs.

Figure 1.4 shows two essential platforms of bio refining processes: "sugar" and "thermo chemical" [7]. Sugar platform biorefineries are based on the breakdown of biomass into an aqueous sugar solution. Fermenting sugars can be further processed into various fuels and chemicals. On the other hand, thermo chemical biorefineries convert biomass into synthesis gas via the gasification process to pyrolysis oil. The thermo chemical refining is a complex process where bio-oils can be further converted into liquid fuels and several other chemical products.

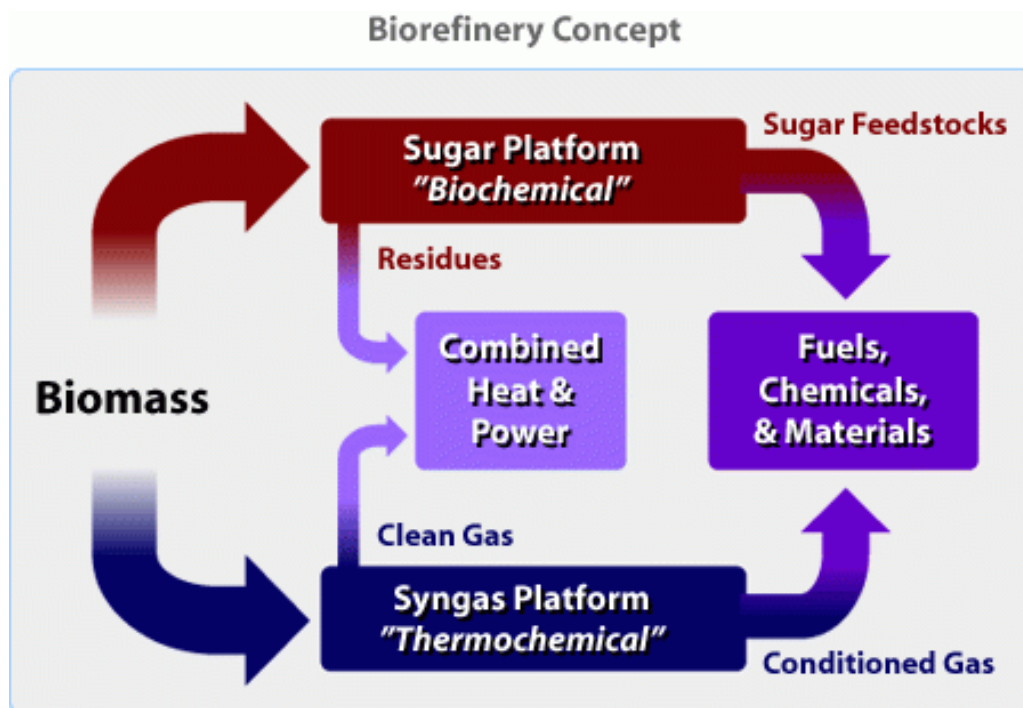


Figure 1.4 Biorefinery concept

Although the concept is still in embryonic stages, it will play a vital role in the future for the perfect usage of wastes and natural resources that humans have always struggle to achieve.

1.3.1 Biodiesel production and co-generation of glycerol

Biodiesel (BD) production under the biorefinery concept is proved to be one of the initial and best alternatives to replace traditional fossil fuel. It has lubricity benefits, is a clean-burning fuel and can be used in existing, unmodified diesel engines. It is the best alternative fuel that offers such flexibility. Biodiesel is simple to use, emit fewer air pollutants, comes from renewable sources, biodegradable, improves air quality and provides safety benefits. BD can be used alone and can be blended in many different concentrations, from additive levels to 100% BD. India has set an indicative target of 22% blending of ethanol with gasoline and 6% blending of biodiesel with diesel by 2025.

BD is a form of diesel fuel derived from transesterification of vegetable oils, animal fats or waste cooking oils. Transesterification is a process in which triglyceride is allowed to chemically react with alcohol to produce fatty acid methyl esters (FAME), which is also known as biodiesel and glycerol is a co product (Figure 1.5) [8, 9].

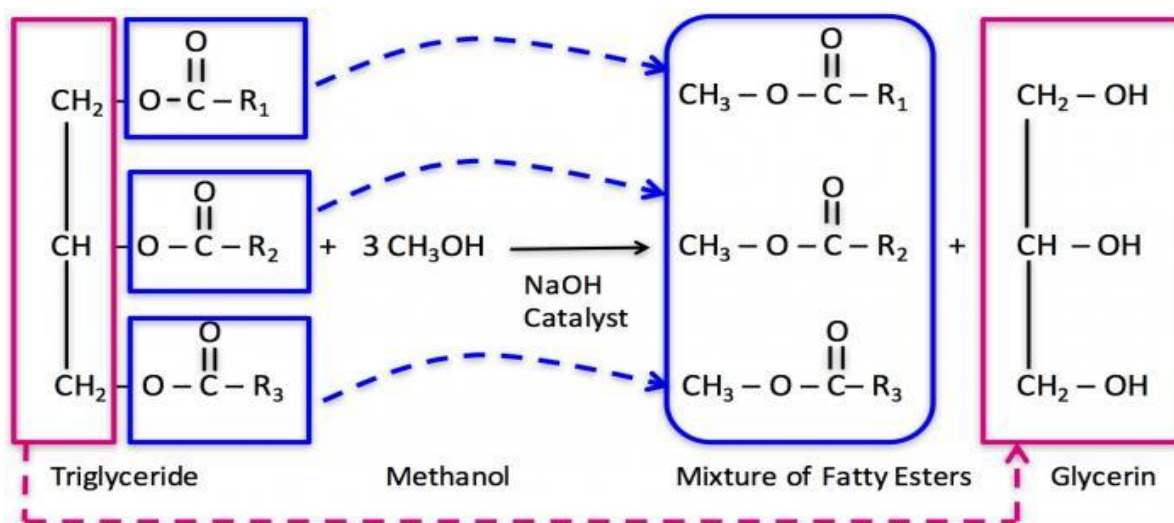


Figure 1.5 Chemistry of biodiesel production

It was estimated that the world biodiesel consumption steadily increases to 36 billion gallons by 2020 (Figure 1.5), which will provide approximately 4 billion gallons of crude glycerol [10]. As per the stoichiometry, 10% of crude glycerol is generated in the process of biodiesel production (Figure 1.6).

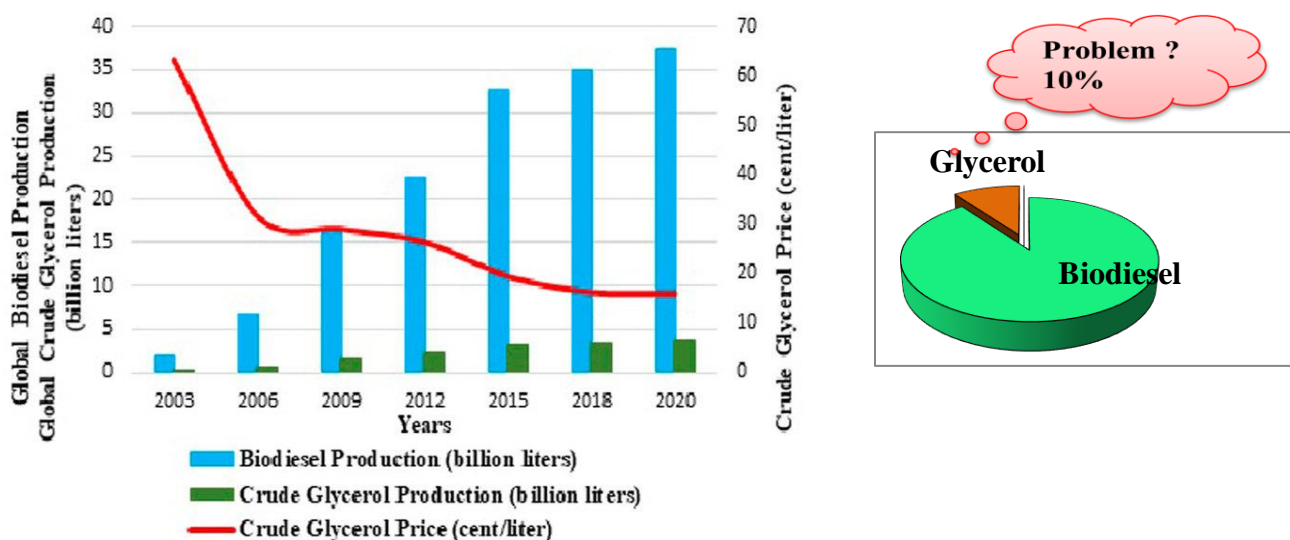


Figure 1.6 Global biodiesel production and crude glycerol price from 2003 to 2020

The current market price of pure glycerol is US\$ 0.27–0.41 per pound; however, the cost of 80% pure crude glycerol obtained in biodiesel production is as low as US\$ 0.04–0.09 per pound [11]. This shows that rapid growth of biodiesel production; affects the price of glycerol in the market. Therefore, the management of crude glycerol has become a serious problem in the biodiesel industry. BD production is usually costly due to dumping of crude glycerol. Hence, downstream processing of glycerol is necessary to enhance its economics. Considering the market scenario, the transformation of glycerol to value-added products makes the biodiesel industry more profitable.

1.3.2 Glycerol: an overview

Glycerol (1, 2, 3-propanetriol) is a simple polyol compound with chemical formula $C_3H_8O_3$. It is a colourless viscous liquid with a sweet taste and non toxic at low concentration. Glycerol was first isolated in 1783; when the Swedish chemist Carl Wilhelm Scheele (1742-1786) described it as the “sweet principle of fat” [12]. Today, it is obtained as a by-product in making soaps.

Pure glycerol melts at 17.8 °C and has a boiling point of 290 °C. Glycerol is hygroscopic in nature and easily miscible with water, due to the hydrogen bonding between hydroxyl groups and a water molecule. It is used as a constituent in numerous products in the pharmaceutical, medical, food, and personal care industries. Figure 1.7 shows that the global market of glycerol can be categorised into pharmaceuticals & healthcare, food & beverages, personal care, and automotive, etc.

Despite the several uses of glycerol, the current market is not capable of absorbing the massive supply of glycerol produced as a co product during biodiesel manufacture. There is a big space between the amount of glycerol produced and the market absorption capacity. This gap will expand shortly if no new applications are found [13]. Its distinctive structure and properties offer us numerous opportunities for chemo catalytic or biological conversions for producing value-added chemicals.

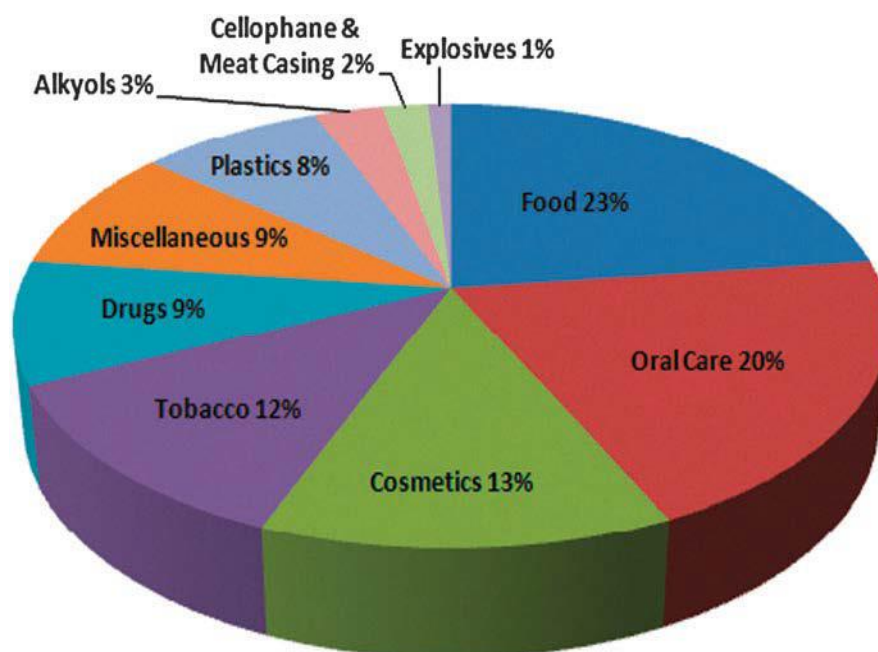
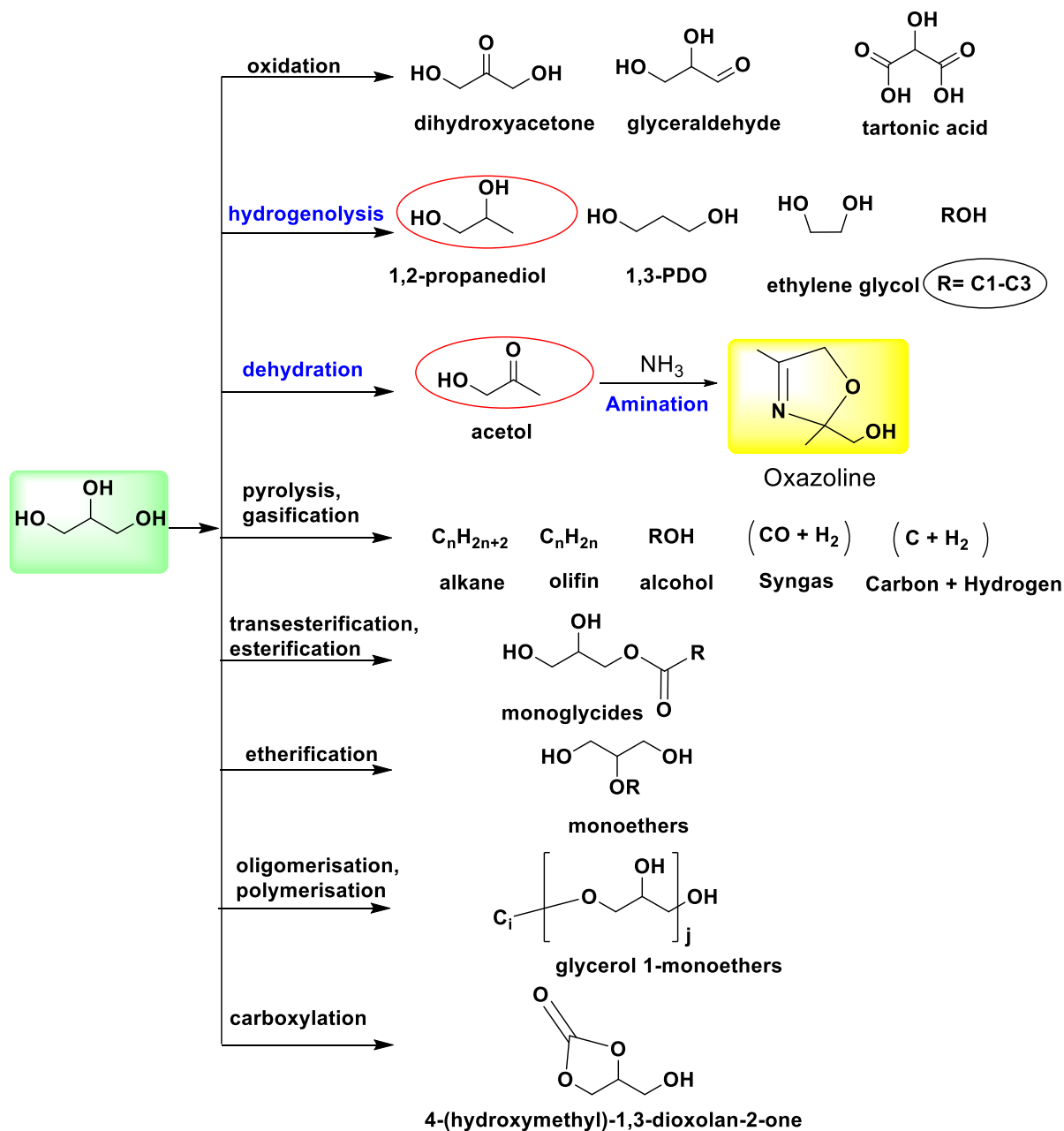


Figure 1.7 Distribution of the glycerol consumption by sector/application

1.3.3 Glycerol valorization

Glycerol has emerged as powerful and versatile building blocks within the biorefinery due to numerous opportunities for chemical production, and with the expected drop in cost. The glycerol valorization could facilitate the price reduction of biofuel and, consequently, make the production process of biofuel more economically favourable [14]. Glycerol has important potential in terms of conversion to valuable products, as shown in Scheme 1.1. At lower projected prices, there's an incredible opportunity to develop a range of latest processes and products from glycerol. The most commonly studied reactions of glycerol are oxidation [15, 16], hydrogenolysis [17, 18], reforming [19, 20] and dehydration [21, 22]. The selective oxidation of glycerol gives rise to a new derivative that would serve as a chemical intermediate, or as monomers of latest branched polymer. A technical hurdle for the production of those materials embodies the requirement to develop selective oxidation technology using simple oxidants, such as oxygen or air.

Hydrogenolysis of glycerol can result in the formation of a variety of valuable intermediates. The development of selective catalytic systems produces potential derivatives like propylene glycol (1, 2-PDO) and 1, 3-propanediol from glycerol. 1, 2-PDO offers an enormous potential market for glycerol with the capacity to produce 1.5 billion lb/yr of 1, 2-PDO in the US. The major hurdle for this transformation is to make it economical compared to the present petroleum route. Again, a crucial technical challenge is to design a selective catalyst that may differentiate between C-C and C-O bonds.



Scheme 1.1 Roadmap of glycerol valorization

Most of the strategies mentioned in the literature only offer oxygen containing chemicals from glycerol. However, the scope of reactions for converting glycerol into nitrogen containing molecules and aqueous phase reforming, often have higher commercial value, which has received much less attention and further research in this area is essential. In this thesis, we concentrated on the transformation of glycerol into value added products by 2 distinct strategies; (i) glycerol amination to oxazoline and (ii) Aqueous phase reforming of glycerol to 1, 2-PDO.

1.4 Glycerol amination to oxazoline

Oxazolines are 5-membered heterocyclic chemical compounds containing O and N as a heteroatom. Depending on the position of the double bond, oxazolines are classified into three isomers, as shown in Figure 1.8. Oxazoline chemistry, including their preparation, reactions, and use, was extensively discussed in previous literature. Historically, oxazolines have been popular since the 19th century. Earlier, it was prepared in 1884 [20] by dehydrohalogenation of allyl urea, But the correct chemical structure is not known. In 1890, oxazolines were synthesis successfully [21] and after that, oxazoline chemistry started to be increasingly investigated.

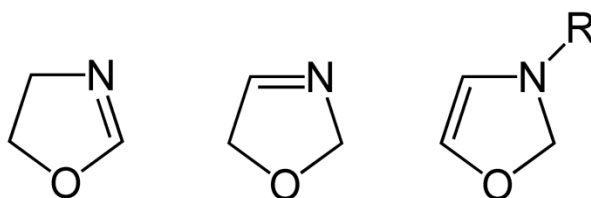


Figure 1.8 Structure of 2-oxazoline, 3-oxazoline, and 4-oxazoline (from left to right)

The preparation of 2-oxazoline is well known via the cyclisation of 2-amino alcohol with a suitable functional group [22]. 4-Oxazolines are less common and found as intermediates during the preparation of azomethine ylides [23]. 3-Oxazolines are even rare but have been prepared photo chemically [24] and by the opening of azirine ring [25].

The distinctive structure of oxazoline ring offers us numerous opportunities for producing a wide variety of compounds with numerous applications.

Oxazolines have a wide variety of uses as pharmaceuticals, flavouring agents, gasoline and lube oil additives, adhesives, monomers for the production of polymers, as a protecting group for carboxylic acids in asymmetric catalysis and in photography as shown in Figure 1.9 [26].

2-Oxazolines derivatives can undergo cationic ring-opening polymerisation to form poly (2-oxazoline) [27]. These polyamides have numerous potential applications [28] and received much attention for their biomedical uses [29, 30].

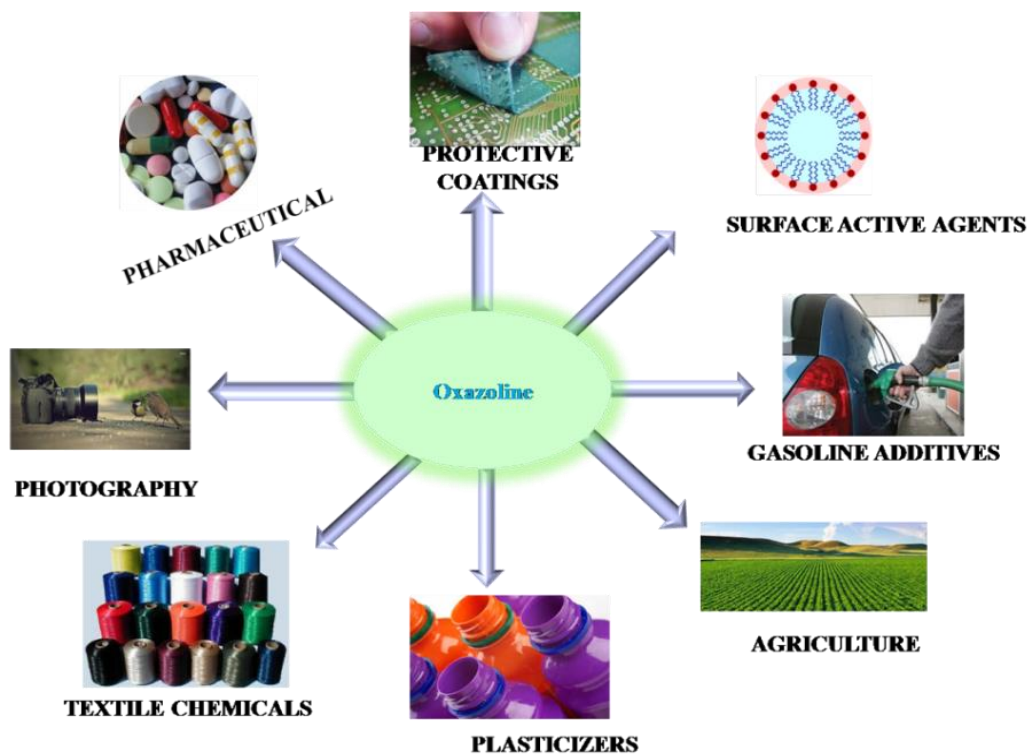


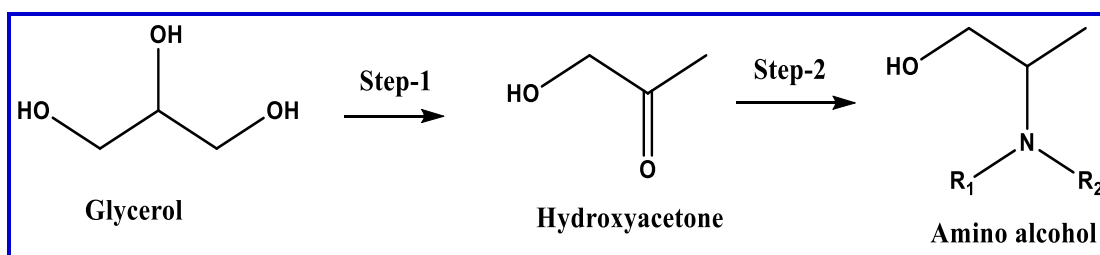
Figure 1.9 Uses of Oxazoline

1.4.1 Background Literature

Despite the compelling synthetic utility and various applications of 3-oxazolines, their synthesis is less common. There is no direct claim for the formation of 3-oxazoline from glycerol, but only a few literatures available for the transformation of glycerol to amino alcohol where oxazoline is intermediate.

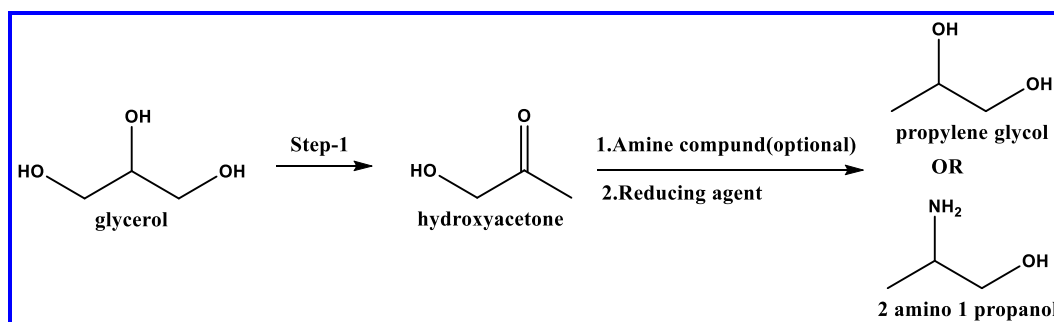
U.S. patent no. 4105669 discloses manufacture of 2-amino-1-alcohols carried out by reacting the acetol with ammonia, without using extraneous solvents at a temperature range from 0° to 120° C, preferably 20° C to 80° C, at a pressure range from 1 to about 300 bars, preferably 100 bars. But reaction takes place in two steps with less conversion and selectivity about less than 85 percent and also reaction took place in harsh conditions [31].

U.S. patent no. 7619119 shows that glycerol conversion to amino alcohol requires two steps. Initially, glycerol in the presence of metal catalysts gives acetol and this acetol is further reacted with an amine compound to obtain unknown adduct. In second step, obtained adduct further reduced to amino alcohol by using a reducing agent (Scheme 1.2). To carry out this reaction, a series of metal catalysts are selected from the group consisting of Cu, Cr, Ni, Zn, Co, Mn, Si, Al, Cu-Cr, Cu-Zn and combinations of any thereof [32].



Scheme 1.2 Process for converting glycerol to amino alcohols

U.S. patent application no. 20080045749 discloses two steps industrial process for the alternating production of amino alcohol or 1, 2-PDO from glycerol comprising: 1) glycerol in presence of metal catalyst gives acetol; 2) optionally acetol is reacted with an amine compound to obtain unknown adduct, and 3) acetol or the adduct is further reduced by a reducing agent to obtain a product. Reduction of acetol with the reducing agent gives the product as 1, 2-PDO while reduction of unknown adduct gives another product as amino alcohol. To carry out this reaction, a series of metal catalysts are selected from the group consisting of Cu, Cr, Ni, Zn, Co, Mn, Si, Al, Cu-Cr, Cu-Zn and combinations of any thereof [33].



Scheme 1.3 Process for the alternating conversion of glycerol to propylene glycol or amino alcohols

U.S. patent no. 8809593 discloses a process for the preparation of the hydroxyacetone or 1, 2 propylene glycol. This process is catalyzed by metal catalysts that result in 80 to 100% selectivity towards the conversion of glycerol to hydroxyacetone (acetol) or 1,2 propylene glycol. The metal catalysts are selected from the group Cu, Cr, Al, Ba, Zn, Si, Zr, Mg, or in combinations thereof [34].

Shu et al. reported the reaction between an ammonia precursor and acetoin under mild conditions gives two major products, tetramethylpyrazine (TMP) and unknown compound. The major compounds formed from the reactions between alpha-hydroxy carbonyls and ammonium hydroxide has been identified by MS, IR and NMR [35].

There are very few reports on selective dehydration of glycerol to acetol. An article titled “Dehydration of glycerol to acetol via catalytic reactive distillation” by Chiu et al. reports glycerol dehydration to obtain acetol in the presence of various metallic catalysts including Al, Mg, Ru, Ni, Pt, Pd, Cu, raney nickel, and Cu-Cr catalysts under mild conditions in a semi-batch reactive distillation mode as shown in Figure 1.10 [36]. The highest selectivity of acetol (> 90%) was achieved using Cu-Cr catalyst.

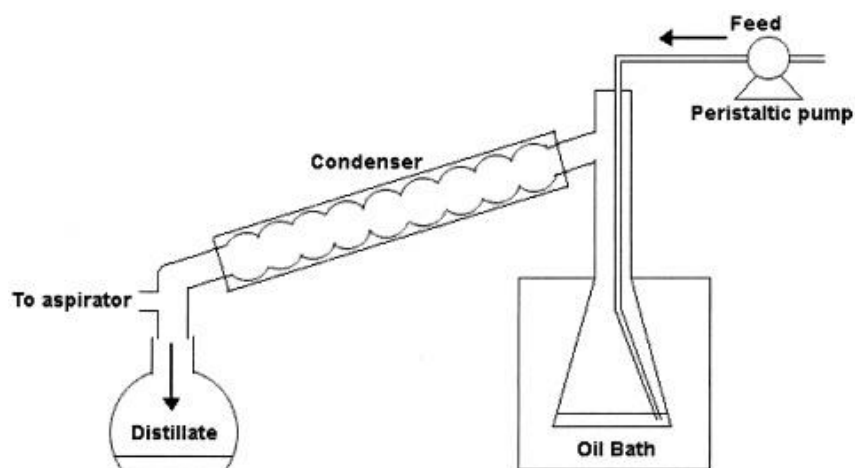


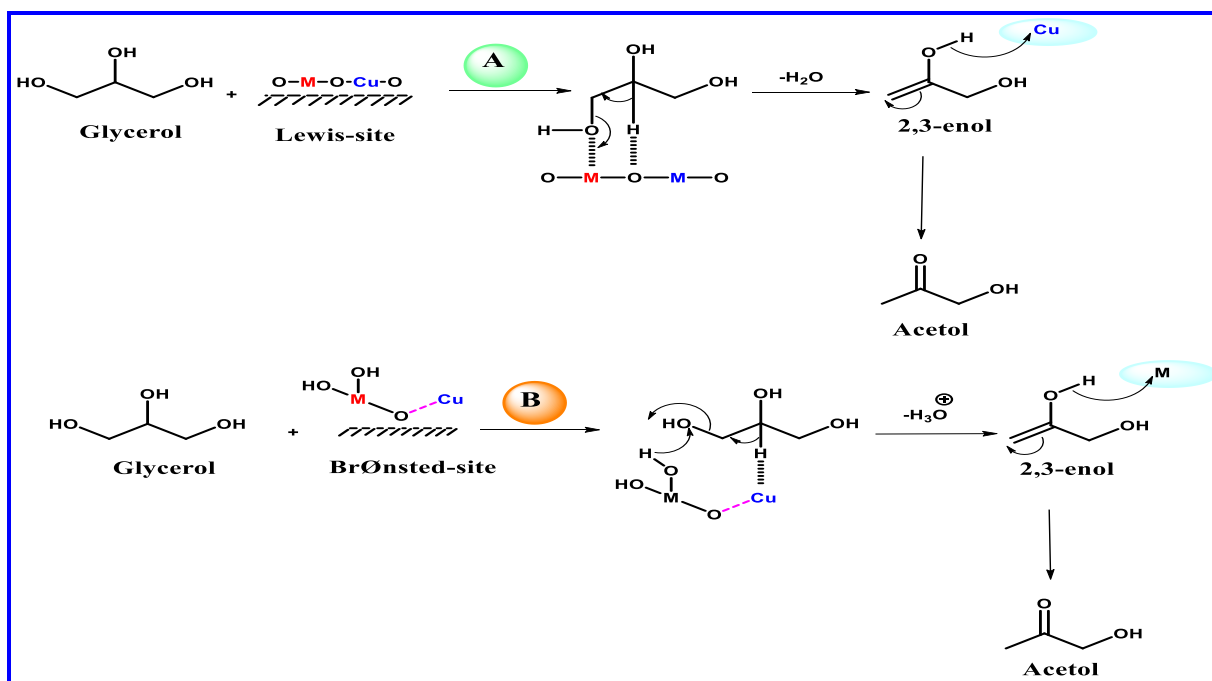
Figure 1.10 Experimental setup for semi-batch reactive distillation

Bayramoglu et al. describe single-pot conversion of renewable chemical, glycerol into the important heterocyclic compounds pyridine and its derivative 3-methylpyridine, in an acidic medium by thermal conversion reactions. In situ study of condensation or cyclization

reactions of glycerol degradation products were investigated using different inorganic ammonium salts produced under thermal conditions. But the major disadvantage is harsh conditions are required. [37].

Mohamad et al. describe that catalyst presence greatly influence the glycerol to acetol reaction. The most popular catalyst used for this reaction is the metal supported acidic catalyst. In nitrogen flow, unreduced Cu-Al₂O₃ reduces glycerol conversion and acetol selectivity was increased with time on stream (TOS). Meanwhile, when Cu-Al₂O₃ was activated with hydrogen, glycerol is fully converted and selectivity of acetol increases with TOS for the first 5 hours.

Mainly, dehydration of glycerol to acetol has been studied under gas phase conditions at very high temperature in the literature [39-44]. The selectivity of acetol was affected because of many by product formations. Other challenges are catalyst deactivation due to coke deposition. Hence, dehydration of glycerol in liquid phase would be achieved by Mane et al. as shown in Scheme 1.4. The metal sites along with the Lewis and Bronsted acidity of catalyst greatly influence each step of glycerol dehydration reaction [45].



Scheme 1.4 Proposed reaction pathway for glycerol dehydration

1.5 Aqueous phase reforming of glycerol without external hydrogen

US National Renewable Energy Laboratory (NREL) listed 12 top value added chemicals from biomass in 2004 [46]. In 2019 the European Union, too, identified the chemicals that can be made from biomass [47]. On comparing the top 12 NREL list and European Union project on the 49 road to bio chemicals, 4 chemicals appeared in both lists are 1, 2-propanediol (1, 2-PDO), succinic acid, para-xylene, and glycerol [48]. From an economic point of view, 1, 2-PDO is the 2nd best product from glycerol. The worldwide production of the 1, 2-PDO is >1.5 billion lb/yr with a yearly growth rate of 5% [49].

1, 2-PDO ($\text{CH}_3\text{CHOHCH}_2\text{OH}$) is a three-carbon diol aliphatic organic compound. It is clear, viscous, colorless, practically having no odor and the presence of two hydroxyl groups makes it water soluble. Table 1.2 presents the physical properties of 1, 2-PDO [50].

Table 1.2 Physical properties of 1, 2-PDO

Physical properties	Value
Boiling point, °C	187.3
Flash Point, °C (Open Cup)	107
Melting point (°C)	-60
Heat of Vaporization at 1 atm, (cal/g)	165
Specific Heat at 25 °C, (cal/g)	0.59
Specific Gravity at 20/ 4 (°C)	1.0363
Refractive Index,(nD)	201.43
Surface tension at 25 °C (dynes/cm)	0.37
Viscosity at 20 °C (cps)	60.5
Density (g cm ⁻³)	1.04

Several physical properties of 1, 2-PDO are useful in many industrial applications such as industrial solvent, thermo set plastics, antifreeze, flavours and fragrances, and approved additive in food, cosmetic and pharmaceutical industries, which are presented in Figure 1.11.

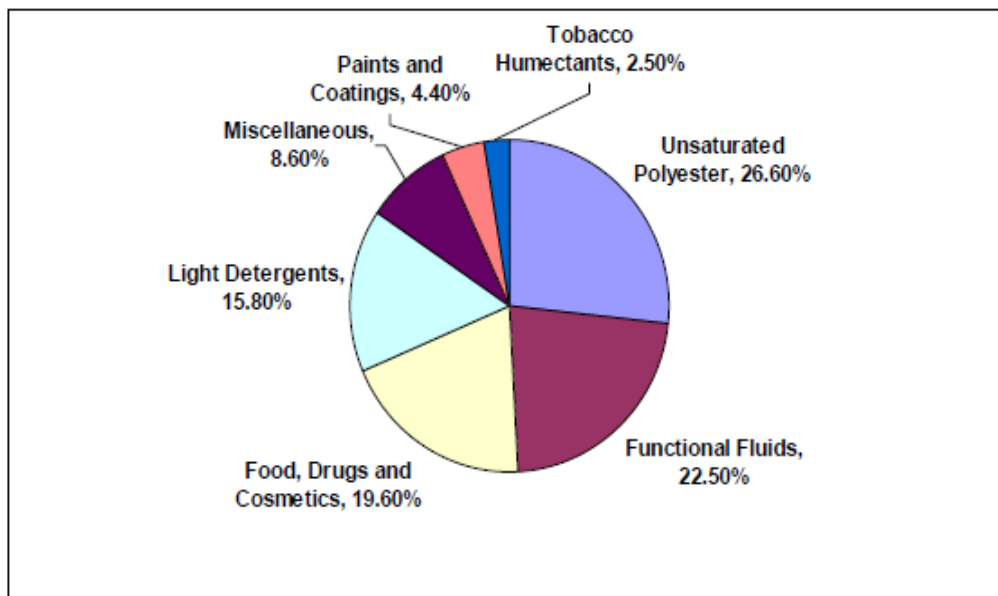


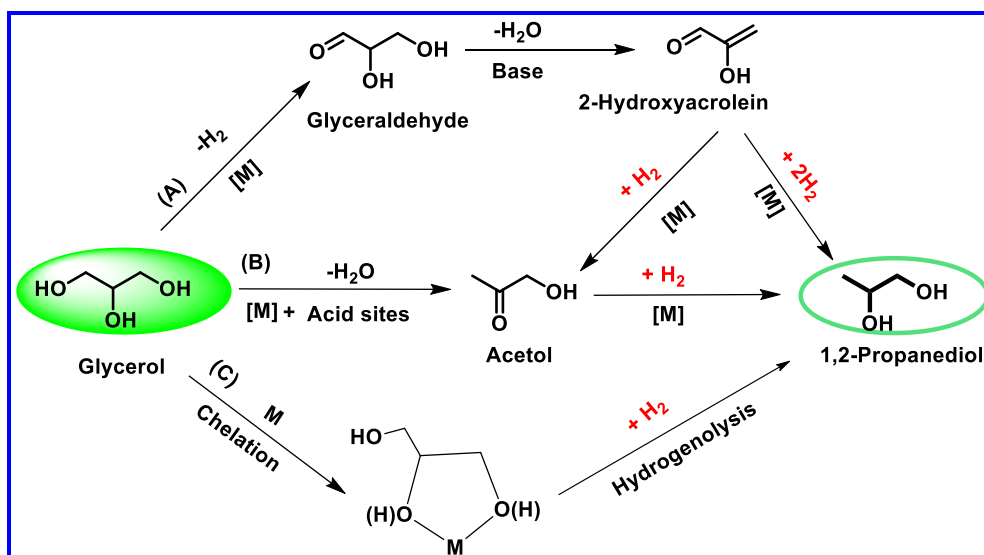
Figure 1.11 Industrial application of 1, 2-PDO

In 1859, Wurtz reported first synthesis of 1, 2-PDO by hydrolysis of propylene glycol diacetate [51]. Currently, selective hydrolysis of propylene oxide gives 1, 2-PDO using chlorohydrin route [52]. In this route, starting material propylene gives propylene chlorohydrin intermediate, which is further converted to 1, 2-PDO. Major drawbacks of this route are dependency on the non-renewable petroleum derived source propylene, multistep and generation of HCl as a byproduct.

Moreover, due to the limited fossil crude oil resources, this process cannot be sustained for the long term. To overcome these drawbacks, the focus is changed from non renewable to renewable resources. In this path, glycerol to 1, 2-PDO by catalytic hydrogenolysis provides an alternative option in a simpler and more sustainable way, which involves C-O and C-C bond cleavage and subsequent addition of hydrogen [53].

It is elemental to understand the reaction mechanism, in order to design efficient catalysts. Scheme 1.5 given below shows three reaction pathways through which reaction can occur:-

- (A) Glyceraldehyde route,
- (B) Dehydration to acetol and hydrogenation,
- (C) Chelation of glycerol with metal and hydrogenolysis.



Scheme 1.5 Glycerol hydrogenolysis routes

In this path, major priority is designing a catalyst of high performance. In the past literature, the hydrogenolysis of glycerol has been extensively investigated in both liquid and gas phases [54-58]. Major focuses thus far have been carrying out towards optimising the process and developing the effective catalysts and these studies were well reviewed in past literature [59-61].

For the hydrogenolysis of glycerol, mostly noble metal based catalysts were widely tested due to their higher potential to activate hydrogen molecules. In past literature, Ru [62, 63], Rh [64], Pt [65, 66] and Pd-based [67] catalysts were reported by several groups.

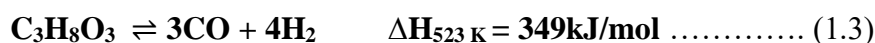
Despite the fact that noble metal based catalysts were widely used for the glycerol hydrogenolysis, non noble transition-metal catalysts were still competitive due to its high recyclability and low price. Among these, copper [68, 69], nickel [70–71], and cobalt [72, 73] were leading for their high performance toward the formation of 1, 2-PDO.

However, the hydrogenolysis of glycerol in the presence of these catalysts has a requirement of high temperatures, in the addition of external hydrogen under very high pressure. Many studies show that external hydrogen under very high pressure is essential for a good yield of 1, 2-PDO, due to less solubility of H₂ in an aqueous solution of glycerol [74] therefore; considerable risks are associated with this hazard of working at high pressures. Hydrogenolysis of glycerol at low pressure is desirable to ensure operational safety and minimise energy consumption.

The need for external hydrogen could be avoided if the required hydrogen for hydrogenolysis was to be generated in-situ, allowing a process with cost-effective, environmental-friendly, energy-saving, lower working pressure, sustainable process and inert atmosphere.

In particular, catalytic transfer hydrogenation (CTH) and aqueous phase reforming (APR) of glycerol appear as two promising methods in this direction. APR is also minimising energy consumption, since glycerol and water are not vaporized. Hydrogen production from the APR process is a well-reported [75].

In general, glycerol reforming with water for production of H₂ (and CO) is possible over a wide range of temperatures, either in gas phase, supercritical phase or in an aqueous liquid phase. This reaction is strongly endothermic; the stoichiometry is given below:



The rate of reaction is proportional to temperature. The conversion of CO into CO₂ in a water-gas-shift (WGS) reaction mainly depends on temperature and forms additional H₂:

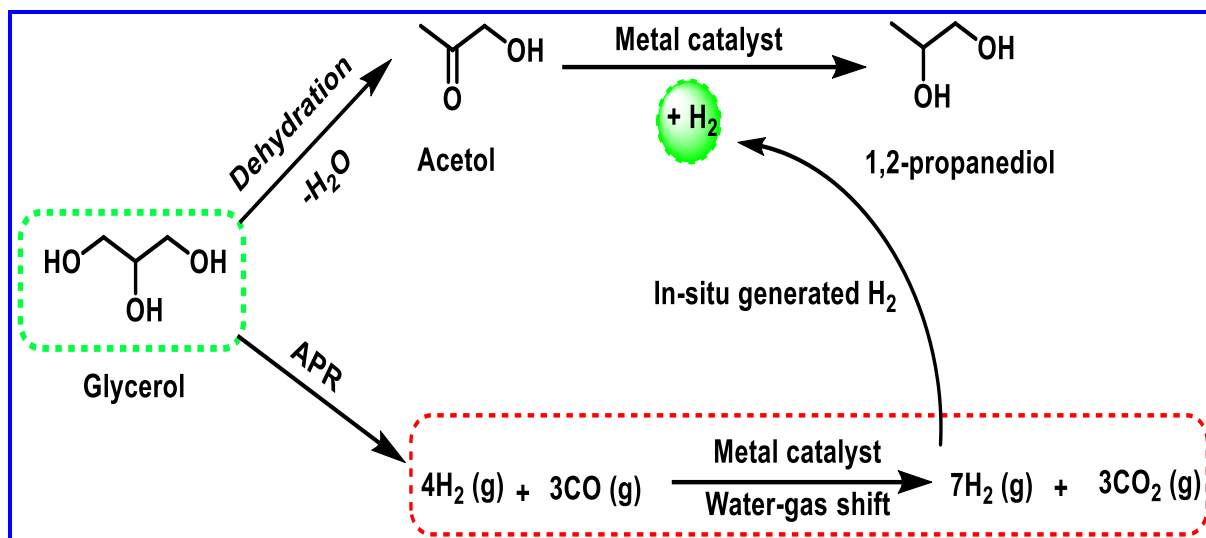


Conversely, glycerol APR required mild reaction conditions. At low temperature and moderate pressure, where water can be kept in liquid state, the equilibrium shifts toward right side and favours CO₂ and H₂ formation at slow rate. In contrast to steam reforming, the presence of excess water in APR favours a mixture of H₂ with CO₂, instead of CO. The sum of these two equations corresponds to the overall equation for APR as follows [76]:



This equation summarises that the equilibrium shift of the reaction is towards CO₂ side. If not, methane formation is facilitated as side reactions at high pressure and may form hydrocarbons as by-products [77].

Glycerol hydrogenolysis using in situ hydrogen generated by reforming step, leading to an overall glycerol conversion to 1, 2-PDO. The concept is presented in Scheme 1.6.



Scheme 1.6 Schematic representation of in situ generated hydrogen utilization for glycerol hydrogenolysis to 1, 2-propanediol [68]

The other advantages of using low temperature for an APR process are comparatively low energy input required for heating water, moderate water pressure and process efficiency is promoted by hydrolysis or dehydration reactions, whereas carbon deposition is negligible. The production of 1, 2-PDO by APR of glycerol has already been studied in previous literature as shown below.

1.5.1 Background Literature

The use of in situ generated hydrogen for the glycerol hydrogenolysis would provide alternative to high pressure fossil derived external hydrogen and would make the process safer and more sustainable, the detailed literature of which is summarized in Table 1.3.

D'Hondt *et al.* reported hydrogenolysis of glycerol using in situ hydrogen generated by APR on Pt catalyst, which gave 84% glycerol conversion with 65% 1, 2-PDO selectivity [78]. For the efficient utilisation of biomass-derived products, APR studies play a significant role and were widely studied during the past decade. In this path, the effects of metal, support, additive and synthesis procedure on catalyst performance were investigated. These studies shared several key insights and interesting observations about improved catalysts and reaction conditions. Many reports suggest that use of a combination of bimetallic catalyst compared to respective individual catalysts for in situ hydrogenolysis of glycerol was more favourable [79-81]. The recent report appeared on the use of a combination of different

support like Ni catalyst supported on $\text{SiO}_2\text{-Al}_2\text{O}_3$ was recognized to play an important role for both the APR and the glycerol hydrogenolysis [82].

Some other approaches to replacing expensive Pt and Ru catalysts by using cheap Ni and Cu catalysts have also been attempted for in situ glycerol hydrogenolysis, which is an alternative cost-effective option. Some research suggests the dehydration of glycerol and in situ hydrogenolysis in presence of Cu-Al oxide catalyst with considerable enhancement in the selectivity of 1, 2-PDO (36%) for an aqueous bio-glycerol feed during 400 h of testing [68]. A recent report shows continuous hydrogenolysis of glycerol to 1, 2-PDO with in situ hydrogen over Cu-Ni catalysts exhibited 82% glycerol conversion with propylene glycol yield around 24% [83]. Another route for hydrogenolysis of glycerol reported in the literature by using hydrogen donor molecules (catalytic transfer hydrogenation) like 2-propanol, methanol, and formic acid [84].

Table 1.3 Literature study of aqueous phase reforming of glycerol without external hydrogen

Catalyst	P (bar)	Temp.	Time (h)	Glycerol conv. (%)	PG Selectivity / yield (%)	Ref
Pt/NaY	-	230	15	85	64 (S)	78
Pt-Fe/ Al_2O_3	-	240	12	60	26.9 (s)	79
Ru/ Al_2O_3	14	220	6	50.1	47.2 (s)	80
Cu-Ni/ Al_2O_3	1	220	10	60	20 (y)	81
Ni/ $\text{SiO}_2\text{-Al}_2\text{O}_3$	33.5	240	4	80	22 (y)	82
Cu-Al	20	220	50	90	75 (s)	68
CuNi/ Al_2O_3	40	250	6	82	24 (y)	83
Ni-Cu/ Al_2O_3 (sol-gel)	-	220	24	60	65 (s)	84

In this thesis, Ni catalysts supported on Al_2O_3 and effect on reduction temperature on their activity is studied for glycerol hydrogenolysis using hydrogen generated in situ.

1.6. Scope and objectives of the thesis

1.6.1 Glycerol amination to oxazoline

Selective conversion of glycerol to oxazoline mainly involves multi steps with low yields in the above reported literature. However, the scope of reactions for converting glycerol into

oxazoline derivatives has been a subject of enduring interest. This can be accomplished by fundamental understanding of roles of each component involved in the catalyst systems along with reaction mechanism. Hence, in this thesis, our aim was on the development of different methods for selective amination of glycerol to oxazoline and to study new catalysts and their structure activity correlation. The major objectives and scope of this work are:-

- To develop different methods for the synthesis of oxazoline viz. (i) a two-step route involving glycerol dehydration to acetol followed by its subsequent amination that gave maximum glycerol conversion and oxazoline selectivity using a simple distillation method and (ii) a single-pot reaction without active metal leaching.
- To study the effect of various preparation methods on the acid sites dispersion, surface acidity, particle size, morphology and stability of the prepared catalysts.
- Optimization of the reaction parameters and catalyst stability testing.
- Identification of active sites to understand structure-activity relationship.
- To propose plausible reaction pathways.

1.6.2 Aqueous phase reforming of glycerol without external hydrogen

The generation of renewable hydrogen from glycerol relies on the cleavage of C-C and C-H, but preserving C-O bonds. Pt, Ru and in general, metals from Group VIII exhibit high APR activity. In recent years, nickel based catalysts have attracted considerable attention for the APR process due to economic criteria. Ni has an unquestionable advantage over Pt primarily due to its lower cost; additionally, this non-noble metal holds a remarkable ability to break C-C bonds, as well as its good intrinsic activity in C-C scission. The reduction step, indeed, can alter the structural properties. Thus, if metal support interaction is improved, better catalytic behaviour could be obtained. Therefore in this thesis, we mainly focused on the synthesis of Ni/alumina catalyst. The specific objectives of this work are given below:-

- Ni-Alumina catalyst synthesis by wet impregnation method and role of catalyst pre-treatment was studied for glycerol APR.
- To study the effect of activation temperature on the acid sites dispersion, surface acidity, particle size, morphology and stability of the prepared catalysts.
- Identification of active sites to understand the structure-activity relationship.
- To propose plausible reaction pathways.
- Detailed physicochemical characterization of various catalyst systems and recycle study.

1.7 References

1. J. J. Berzelius, *Ann. Chim. Phys.* 61 (1836) 146.
2. K. J. Laidler, J. H. Meiser, *Physical Chemistry*, Benjamin/Cummings (1982).
3. S. A. Topham in: J. R. Anderson, M. Boudart, *Cat. Sci. Tech.* 7 (1987) 1-5.
4. J. Burwell, L. Robert, *Chemical Reviews* 57 (1957) 895-934.
5. W. V Reid, M. K. Ali, C. B. Field, *Glob. Chang. Biol.* 26 (2020) 274–286.
6. D. L. Klass, *Biomass for renewable energy, Fuels and Chemicals*, Academic Press, London (1998)
7. U.S. Department of Energy, *Report Top Value Added Chemicals from Biomass* (2004).
8. J. D. Hooker, US Patent 027137 (2005).
9. F. J. Luxem, US Patent 254387 (2004).
10. N. M. Saifuddin, R. Hussein, *Green Chem. Lett. Rev.* 11 (2018) 135–157.
11. A. A. A. Raman, H. W. Tan, A. Buthiyappan, *Front. Chem.* 7 (2019).
12. <http://en.wikipedia.org/wiki/Glycerol>
13. B. Katryniok, S. Paul, V. Bellière-Baca, P. Rey, F. Dumeignil, *Green Chem.* 12 (2010) 2079–2098.
14. M. R. A. Arcanjo, I. J. da Silva Jr, C. L. Cavalcante Jr, J. Iglesias, G. Morales, M. Paniagua, J. A. Melero, R. S. Vieira, *Biofuels, Bioprod. Biorefining* 14 (2020) 357–370.
15. M. S. Gross, B. S. Sánchez, C. A. Querini, *Appl. Catal. A* 501 (2015) 1–9.
16. M. Zhang, J. Shi, Y. Sun, W. Ning and Z. Hou, *Catal. Commun.* 70 (2015) 72–76.
17. M. Besson, P. Gallezot and C. Pinel, *Chem. Rev.* 114 (2014) 1827–1870.
18. A. M. Ruppert, K. Weinberg, R. Palkovits, *Angew. Chem. Int. Ed.* 51 (2012) 2564-2601.
19. Y. Li, M. Nielsen, B. Li, P. H. Dixneuf, H. Junge, M. Beller, *Green Chem.* 17 (2015) 193–198.
20. R. Andreasch, *Monatshefte für Chemie und verwandte Teile anderer Wissenschaften* 5 (1884) 33–46.
21. S. Gabriel, *Berichte der Dtsch. Chem. Gesellschaft* 22 (1889) 1139–1154.
22. J. A. Frump, *Chem. Rev.* 71 (1971) 483–505.
23. E. Vedejs, J. W. Grissom, *J. Am. Chem. Soc.* 110 (1988) 3238–3246.
24. D. Armesto, M. J. Ortiz, R. Pérez-Ossorio, W. M. Horspool, *Tetrahedron Lett.* 24 (1983) 1197–1200.
25. M. C. M. Sá, A. Kascheres, *J. Org. Chem.* 61 (1996) 3749–3752.
26. G. C. Hargaden, P. J. Guiry, *Chem. Rev.* 109 (2009) 2505–2550.

27. S. Kobayashi, H. Uyama, *J. Polym. Sci. Part A Polym. Chem.* 40 (2002) 192–209.
28. R. Hoogenboom, *Angew. Chemie Int. Ed.* 48 (2009) 7978–7994.
29. N. Adams, U. S. Schubert, *Adv. Drug Deliv. Rev.* 59 (2007) 1504–1520.
30. A. M. Kelly, F. Wiesbrock, *Macromol. Rapid Commun.* 33 (2012) 1632–1647.
31. W. Himmele, L. Hupfer, H. Toussaint, G. Paul, US Patent 4105669 (1978).
32. V. M. Arredondo, P. J. Corrigan, A. C. Cearley, D. J. Back, M. S. Gibson, N. T. Fairweather, US Patent 7619119 (2009).
33. V. Arredondo, P. Corrigan, A. Cearley, N. Fairweather, M. Gibson, US Patent 20080045749 (2008).
34. C. V. Rode, A. M. Hengne, A. A. Ghalwadkar, R. B. Mane, P. H. Mohite, H. S. Potdar, US Patent 8809593 (2014).
35. C.K. Shu, B. M. Lawrence, *J. Agric. Food Chem.* 43 (1995) 2922–2924.
36. C. Chiu, M. A. Dasari, G. J. Suppes, W. R. Sutterlin, *AIChE J.* 52 (2006) 3543–3548.
37. D. Bayramoğlu, G. Gürel, A. L. I. Sinag, M. Gullu, *Turkish J. Chem.*, 38 (2014) 661–670.
38. M. H. Mohamad, R. Awang, W. M. Z. W. Yunus, *Am. J. Appl. Sci.* 8 (2011) 1135.
39. S. Sato, D. Sakai, F. Sato, Y. Yamada, *Chem. Lett.* 41 (2012) 965–966.
40. C. W. Chiu, A. Tekeei, W. R. Sutterlin, J. M. Ronco, G. J. Suppes, *AIChE J.* 54 (2008) 2456–2463.
41. S. Sato, M. Akiyama, R. Takahashi, T. Hara, K. Inui, M. Yokota, *Appl. Catal. A* 347 (2008) 186–191.
42. W. Suprun, M. Lutecki, T. Haber, H. Papp, *J. Mole. Catal. A* 309 (2009) 71–78.
43. A. Yamaguchi, N. Hiyoshi, O. Sato, C. V. Rode, M. Shirai, *Chem. Lett.* 37 (2008) 560–561.
44. A. Yamaguchi, N. Hiyoshi, O. Sato and M. Shirai, *Top. Catal.* 53 (2010) 487–491.
45. R. B. Mane, A. Yamaguchi, A. Malawadkar, M. Shirai, C. V Rode, *RSC Adv.* 3 (2013) 16499–16508.
46. U.S. Department of Energy, Report Top Value Added Chemicals from Biomass (2004).
47. J. Michels, *Bioeconomy for Beginners*, Springer (2020) 77–103.
48. J. A. Posada, L. E. Rincón, C. A. Cardona, *Bioresour. Technol.* 111 (2012) 282–293.
49. <http://www.cargill.com/news-center/news-releases/2007/NA3007798.jsp>
50. J. A. Monick, *Alcohols, Their Chemistry, Properties and Manufacture*, Reinhold Book Corporation (1968) 315.
51. A. Wurtz, *Ann. Chim. Phys.* 55 (1859) 438.
52. I. MeHan, *Polyhydric Alcohols*, Spartan Books, Washington, D.C. (1962) 46.

53. C. Ellis, *Hydrogenation of Organic Substances*, 3rd ed., Van Nostrand Company, New York (1930) 564.
54. S. Wang, K. Yin, Y. Zhang, H. Liu, *ACS Catal.* 3 (2013) 2112–2121.
55. E. S. Vasiliadou, T. M. Eggenhuisen, P. Munnik, P. E. de Jongh, K. P. de Jong, A. A. Lemonidou, *Appl. Catal. B* 145 (2014) 108–119.
56. E. Vasiliadou, A. Lemonidou, *Chem. Eng. J.* 231 (2013) 103–112.
57. J. T. Dam, U. Hanefeld, *Chemsuschem* 4 (2011) 1017–1034.
58. A. M. Ruppert, K. Weinberg, R. Palovits, *Angew Chem. Int. Ed.* 51 (2012) 2564–2601.
59. D. M. Alonso, S.G. Wettstein, J.A. Dumesic, *Chem. Soc. Rev.* 41 (2012) 8075–8098.
60. Y. Wang, J. Zhou, X. Guo, *RSC Adv.* 5 (2015) 74611–74628.
61. M. J. Gilkey, B. Xu, *ACS Catal.* 6 (2016) 1420–1436.
62. T. Miyazawa, Y. Kusunoki, K. Kunimori, K. Tomishige, *J. Catal.* 240 (2006) 213–221.
63. R. Mane, S. Patil, M. Shirai, S. Rayalu, C. Rode, *Appl. Catal. B Environ.* 204 (2017) 134–146.
64. Y. Shinmi, S. Koso, T. Kubota, Y. Nakagawa, K. Tomishige, *Appl. Catal. B Environ.* 94 (2010) 318–326.
65. W. Oberhauser, C. Evangelisti, R. P. Jumde, R. Psaro, F. Vizza, M. Bevilacqua, J. Filippi, B.F. Machado, P. Serp, *J. Catal.* 325 (2015) 111–117.
66. A.V. H. Soares, G. Perez, F.B. Passos, *Appl. Catal. B Environ.* 185 (2016) 77–87.
67. T. Jiang, Q. Huai, T. Geng, W. Ying, T. Xiao, F. Cao, *Biomass Bioenergy* 78 (2015) 71–79.
68. R. B. Mane, C. V. Rode, *Green Chem.* 14 (2012) 2780–2789.
69. R. B. Mane, C.V. Rode, *Org. Process Res. Dev.* 16 (2012) 1043–1052.
70. I. C. Freitas, R.L. Manfro, M.M.V.M. Souza, *Appl. Catal. B Environ.* 220 (2018) 31–41.
71. M. N. Gatti, M.D. Mizrahi, J.M. Ramallo-Lopez, F. Pompeo, G.F. Santori, N.N. Nichio, *Appl. Catal. A Gen.* 548 (2017) 24–32.
72. V. Rekha, C. Sumana, S.P. Douglas, N. Lingaiah, *Appl. Catal. A Gen.* 491 (2015) 155–162.
73. Q. Liu, X. Cao, T. Wang, C. Wang, Q. Zhang, L. Ma, *RSC Adv.* 5 (2015) 4861–4871.
74. I. Gandarias, J. Requies, P. L. Arias, U. Armbruster, A. Martin, *J. Catal.* 290 (2012) 79–89.
75. G.W. Huber, R.D. Cortright, J.A. Dumesic, *Angew. Chem. Int. Ed.* 43 (2004) 1549.
76. A. Seretis, P. Tsiakaras, *Fuel Process. Technol.* 142 (2016) 135–146.

77. M. El Doukkali, A. Iriondo, P. L. Arias, J. Requies, I. Gandarías, L. Jalowiecki-Duhamel, F. Dumeignil, *Appl. Catal. B Environ.* 125 (2012) 516-529.
78. E. D'Hondt, S. Van de Vyver, B. F. Sels, P. A. Jacobs, *Chem. Commun.* (2008) 6011-6012.
79. A. V. H. Soares, G. Perez, F. B. Passos, *Appl. Catal. B Environ.* 185 (2016) 77-87.
80. D. Roy, B. Subramaniam, R. V. Chaudhari, *Catal. Today* 156 (2010) 31-37.
81. Y. S. Yun, D. S. Park, J. Yi, *Catal. Sci. Technol.* 4 (2014) 3191-3202.
82. A. Seretis, P. Tsiakaras, *Fuel Process. Technol.* 142 (2016) 135–146.
83. I. C. Freitas, R. L. Manfro, Mariana, M. V. M. Souza, *Appl. Catal. B Environ.* 220 (2018) 31-41.
84. I. Gandarias, P. L. Arias, J. Requies, M. El Doukkali, M. B. Güemez, *J. Catal.* 282 (2011) 237-247.

Chapter 2

Experimental Methods and Characterization Techniques

In this chapter, the first section deals with general experimental procedures followed for the preparation of various catalysts are discussed. The second section of the chapter describes details various characterization techniques such as X-Ray Diffraction, X-ray Photoelectron Spectroscopy, Thermo gravimetric analysis, BET, surface area measurements, and electron microscopy (SEM and TEM), which are indispensable for catalyst characterization and activity testing. This chapter also includes the description of different analytical methods used for identification of gaseous and liquid products.

2.1 Introduction

The key aspect for ensuring the efficient utilization of the catalyst lies in the method of its preparation and the pre-treatment conditions such as calcination, reduction, etc. These Synthetic protocols have a major role in controlling the morphology as well as various textural properties such as particle and crystallite size, surface area, extent of reduction, planes and/or phases of the active species, acidity, and morphology. The most widely used catalyst preparation methods include co precipitation method and wet impregnation. The detailed characterization of the active catalysts is also very crucial in order to understand the structure-activity correlation. The present chapter highlights various methods for the catalyst preparation, their activity testing, characterization and the different analytical methods used for the identification of gaseous and liquid products of glycerol amination and aqueous phase reforming reactions.

2.2. Materials

Refined glycerol (99%), was purchased from Merck Specialities, Mumbai (India). The assay of the bio-glycerol calculated by GC was 50%, which was obtained by transesterification of vegetable oil and methanol (1:6) in the presence of KOH. This bioglycerol was directly used for making a desired concentration. 1, 2-Propanediol (1,2-PDO), acetol, ethylene glycol (EG), 2- propanol, methanol, ethanol and isopropanol were purchased from Aldrich Chemicals, Bangalore (India). 30% Aqueous ammonia, γ -Alumina, fumed silica, Nitrate precursors of Cu, Al, Mg, Zr, and potassium carbonate (K_2CO_3) were purchased from Loba Chemie, Mumbai (India). Anhydrous sodium carbonate (Na_2CO_3), zirconium oxychloride, sodium hydroxide (NaOH), hexane and sulphuric acid, were purchased from Thomas Baker, India. Hydrochloric acid (HCl, 35.4%) and potassium hydroxide (KOH, 98%) were purchased from Loba Chemie, Mumbai, India. Chloride precursor of $[(RuCl_3).3H_2O]$, 3% Pd/C and 3% Pt/C were purchased from Sigma-Aldrich, Bangalore, India.

2.3 Catalyst preparation

Various catalysts were used for amination and APR of glycerol and the preparation methods used are given below.

2.3.1 Cu-Al catalyst

Figure 2.1 shows a schematic of the experimental setup for catalyst preparation. A co-precipitation technique was used for the preparation of copper–alumina (Cu–Al) catalyst. In a typical procedure, 0.05 M aqueous solutions of $\text{Al}(\text{NO}_3)_3 \cdot 9\text{H}_2\text{O}$ [4.6 g] and $\text{Cu}(\text{NO}_3)_2 \cdot 3\text{H}_2\text{O}$ [3 g] were mixed in a round bottom flask with 5 mL water at room temperature and was further precipitated by using 0.2 M [7.0 g] aqueous potassium carbonate. The obtained precipitate was digested for 5 h and then filtered. The ppt was rinsed and washed further with double-distilled water to free potassium. The ppt was dried at 100 °C in an oven for 5–8 h and calcined for 3 h at 400 °C which is activated further at 200 °C for 12 h under a H_2 flow.

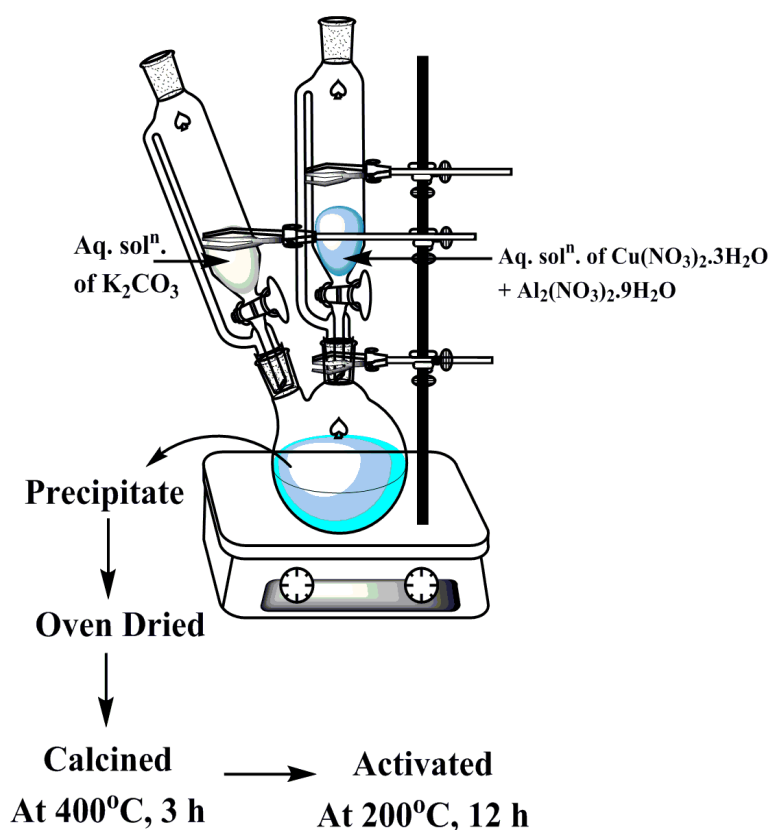


Figure 2.1 General setup for catalyst preparation of Cu-Al

Copper catalysts with various metals such as Zr and Mg were prepared by using the same co-precipitation method. The prepared catalysts were nominated as Cu-Zr and Cu-Mg. The Cu content in all these catalysts was kept constant (50 wt. %). In a typical preparation, 0.05 M of $\text{Cu}(\text{NO}_3)_2 \cdot 3\text{H}_2\text{O}$ and the other metal nitrate, each was dissolved in water and precipitated by K_2CO_3 (0.2M). Other procedure is same as the flow chart shown in Figure 2.2.

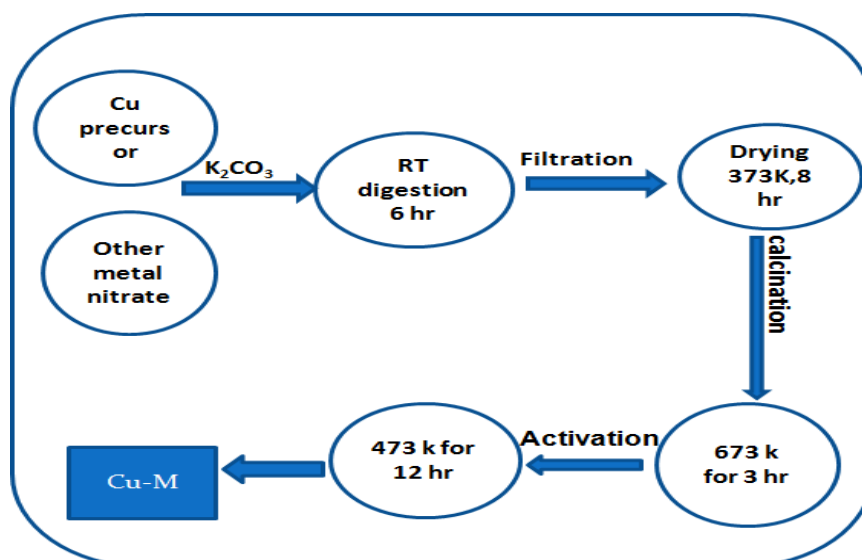


Figure 2.2 Method for preparation of copper catalyst by co-precipitation method

2.3.2 Supported noble metal catalysts

Figure 2.3 shows a schematic representation of supported Ru, Pt, Pd catalysts preparation by a wet impregnation method. In a typical procedure, calculated amounts of the respective metal precursors were added drop wise to the 2 g of support suspended in water. The suspension was stirred for 2h. It was further reduced using 5 mL of NaBH₄ (1 mol). The solid was rinsed with water and dried at 110 °C for 12 h.

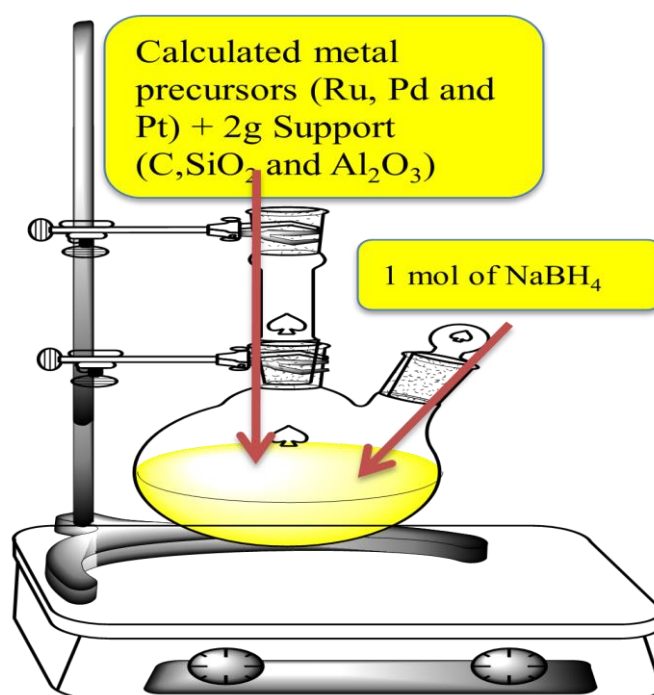


Figure 2.3 Setup for supported catalysts preparation by impregnation method

2.4 Characterization techniques

The performance of heterogeneous catalyst in a reaction was measured by its physical and chemical characteristics. Several techniques have been used to characterize the properties of catalyst. Thus, characterization of catalyst plays a pivotal role in field of catalysis for design and process optimization. The main purpose of characterization of catalyst is to understand the relationship between catalytic, physical, and chemical properties. In several cases, there are needs of more than one technique to evaluate various parameters. For this purpose, a combinatorial characterization approach is needed to relate various properties with its activity and selectivity.

The characterization of catalyst is also important to observe the changes in various properties during its synthesis and reaction stage. Characterization of used catalysts can help to determine the stability and deactivation causes during catalytic reactions. It also helps to minimise cause of catalyst deactivation. The principal objective of this chapter is to summarize the use of various experimental techniques that are available for the characterization of catalyst.

2.4.1 X-ray diffraction (XRD)

XRD is a non destructive technique and plays a critical role in identify crystalline phases and orientation [1, 2]. It gives information about structural properties like lattice parameters (10-4Å), grain size, thermal expansion, atomic arrangement, phase composition, interlayer spacing, and strain present in the lattice of nano materials [3].

Crystalline materials having comparable distances between the atoms in the crystal structure interact with X-ray waves in such a way as to produce interference. The scattering of X-rays from atoms produces a diffraction pattern and this phenomenon of diffraction is known as X-ray diffraction. Thus, the diffractogram is like a unique “finger print” of materials because it contains information about the arrangement of atoms within the crystal.

The atomic distance of crystalline materials directly influences the intensity in X-ray diffraction pattern. Figure 2.4 shows the interaction of incident x-ray with the atoms in the crystal structure (green spheres).

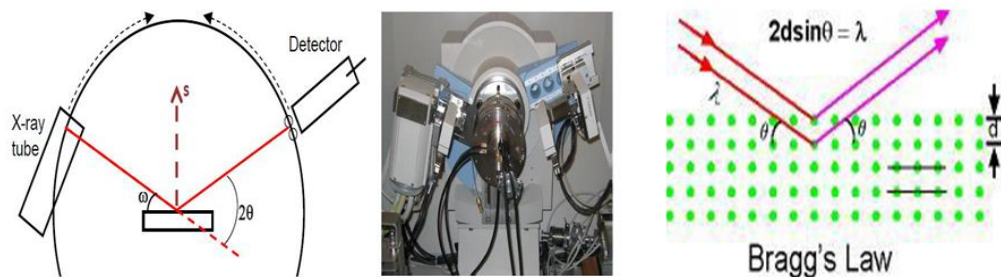


Figure 2.4 Schematic representations of X-ray diffractometer and Bragg's equation

The relationship describing the angle at which diffraction of incident x-ray with a particular wavelength with the atoms in the crystal structure is known as Bragg's Law. It was discovered by by Sir William H. Bragg and Sir W. Lawrence Bragg.

$$n\lambda = 2d\sin\theta \dots \dots \dots (2.1)$$

Where, n is an integer, representing order of the diffraction peak

λ is the wavelength of the X-rays,

d is the inter planar spacing generating the diffraction,

θ is the scattering angle

The Scherrer's equation is used to calculate average crystallite size (D), which is as follows

$$D = k\lambda/\beta\cos\theta \dots \dots \dots (2.2)$$

Where,

k = Scherrer's constant (0.9)

λ = wavelength of X-rays used, Å

β = full width at half maximum (FWHM), radian.

θ = diffraction angle, deg.

In this work, all the data was obtained using Ni-filtered Cu K α radiation ($k = 0.154$ nm) as a source (current intensity, 30 mA; voltage, 40 kV) and an Xcelerator detector on a PAnalytical PXRD Model X-Pert PRO-1712. All the samples have been scanned in the 2θ range of 10–80°. The surface species is marked by the characteristic 2θ values of the corresponding crystalline phases and obtained pattern was compared with the standard international centre

for diffraction (ICDD) or Joint Committee on Powder Diffraction Standards (JCPDS) data [5]. Before data analysis, the software program X-Pert High Score Plus was used to deduct the contribution of the line Cu K α 2. Before data analysis.

2.4.2 Surface area measurement

In order to understand the extent of possible dispersion for active metals, the determination of the surface area of catalysts is important. Mostly, supports of higher surface area are desirable because the surface area of support is proportionate to the dispersion of the active metal. Hence, Brunauer, Emmett and Teller (BET) analysis can be used to determine surface area of a monolayer adsorption model [6]. It describes the link between the volume adsorbed at monolayer coverage and volume adsorbed at a given partial pressure. The BET equation can be written in the following form:

$$\frac{P/P_0}{V(1-P/P_0)} = \frac{1}{cV_m} + \frac{c-1}{cV_m}(P/P_0) \dots\dots\dots (2.3)$$

P = partial pressure; P₀ = saturation pressure at the experimental temperature; V = volume adsorbed at p; V_m = volume adsorbed at monolayer coverage; C = constant which is a function of the adsorbate heats of condensation and adsorption.

The above equation 2.3 can be plotted as P/P₀ on the x-axis and 1/V [(P₀ / P) – 1] on the y-axis. It gives a straight line at very low pressure range of 0.05 < P / P₀ < 0.35. Monolayer capacity is determined by the slope and intercept of this linear plot {V_m = 1/(Slope + Intercept)} [7-9]. The catalyst surface area (S_{BET}) is connected with V_m by equation:

$$S_{BET} = (V_m/22414) N_a \sigma \dots\dots\dots (2.4)$$

Where N_a is the Avogadro number and σ is mean cross sectional area covered by one adsorbate molecule. The σ value generally used for N₂ is 0.162 nm².

The isotherm obtained from a physisorption experiment gave us surface and porosity information. It helps us to determine the type of porosity in unknown samples. Figure 2.5 shows the six types of adsorption isotherms as recommended by the IUPAC.

Type I shows monolayer adsorption on microporous solids (Langmuir isotherm).

Type II represents monolayer-multilayer adsorption on nonporous/macroporous solids.

Type III also indicates unrestricted multilayer formation on non-porous/macroporous solids with weak adsorption.

Type IV represents stepwise multilayer adsorption on a uniform non-porous surface.

Type V is similar to Type IV with weak adsorbate-adsorbent interaction.

Type VI represents stepwise multilayer adsorption on a uniform non-porous surface.

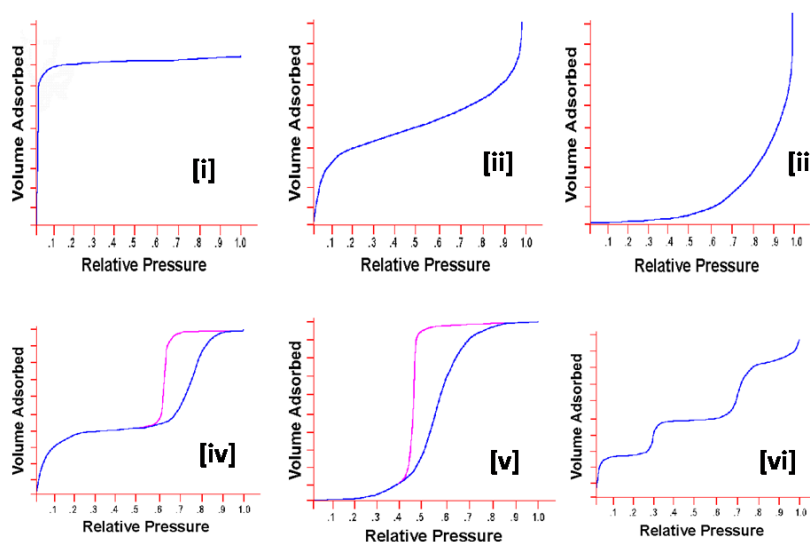


Figure 2.5 IUPAC classifications of isotherms [10]

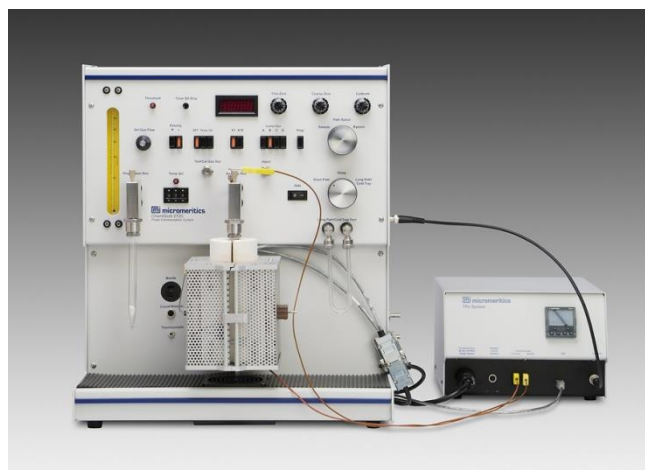


Figure 2.6 Chemisoft TPx (Micromeritics-2720) instrument

In this work, all the data was obtained using N_2 adsorption at 77 K on a Chemisoft TPx (Micromeritics-2720) instrument (Figure 2.6). The t-plot method of De Boer was used to calculate pore volumes. The pore size distribution was calculated by the BJH method from the isotherms [11].

2.4.3 Scanning electron microscopy

This microscopy relies upon a finely focused beam of high-energy electrons that is blasted on sample surface, which produces a variety of signals. It is non destructive technique and used to obtain information about the crystal morphology, particle size, surface defects and magnetic domains [12]. The surface reflected electrons (and secondary electrons emitted) are detected to give topography of surface. Gold or graphite coating is required on the electrically insulating sample to stop charge build-up on the surface.

The schematic diagram of the SEM is shown in Figure 2.7. SEM uses a focused electron beam over a surface to create an image. First, electrons are generated at the top of the column by the electron source. Accelerated electron collimated by electromagnetic condenser lenses and electron-sample interactions produces a variety of signals. The secondary electrons released by the samples are commonly used in primary imaging. The secondary electrons are then magnified and eventually dropped on a fluorescent screen to get the final image.

SEMs also generate and can collect X-rays that are characteristic of the elements in the sample. This is usually done with an energy dispersive X-ray spectrometer or EDS system. EDS X-ray data can be used to determine the sample elements [13, 14]. The detection limit for EDS is generally on the order of 0.5% by weight within the X-ray generation volume. A magnifying range with the best ~ 2 nm is possible.

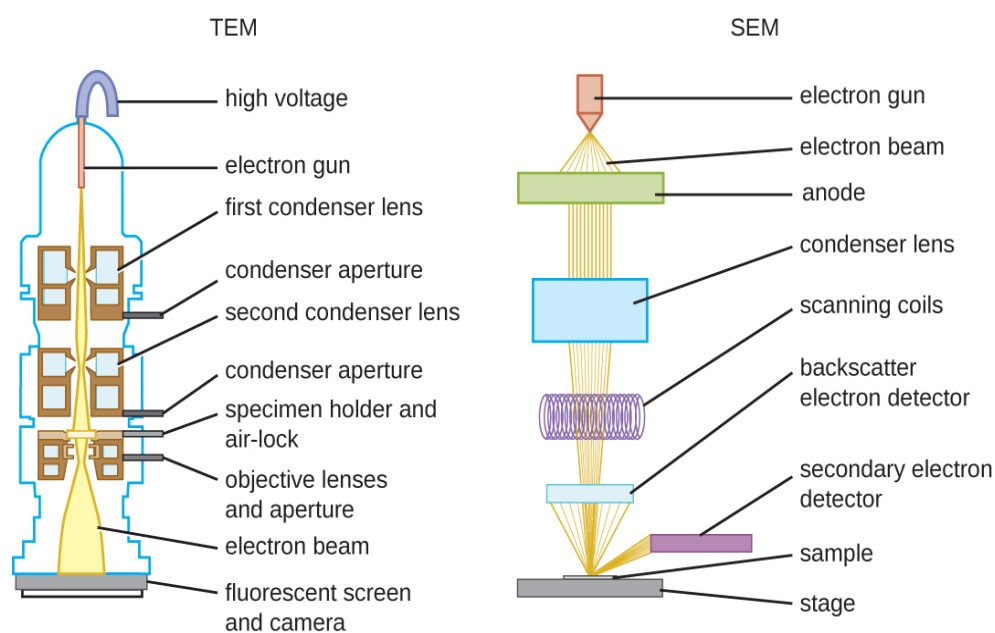


Figure 2.7 Features of an optical microscope TEM and SEM

In the present work, chemical composition and morphology of the samples were examined by using Quanta 200 3D, FEI scanning electron microscope (SEM).

2.4.4 Transmission electron microscopy

The TEM is operating on the same basic concepts as the light microscope. TEM can magnify objects up to 2 million times [15, 16]. It was developed in the 1930s. The schematic diagram of the TEM is shown in Figure 2.7. TEMs consist of the following components: Electron source, vacuum chamber, sample stage, 2 condenser lens, objective lens and projector lens and Phosphor or fluorescent screen. Information that can be accessed from the TEM includes:

1. Morphological: The size and shape of the particles
2. Topographical: The texture and surface features of the object.
3. Compositional: The elements and compounds that the object is composed of and their relative amounts
4. Crystallographic: atoms arrangement in the object.

TEMs have a wide-range of applications in different fields such as nanotechnology, forensic analysis, life sciences, medical, biological and material research, educational and industrial fields. TEMs produce high-resolution, 2D images. The imaging mechanism of HRTEM is phase contrast, in which the instrument may be operated in the bright field or dark field and electrons may be elastically or inelastically scattered. TEM works like a slide projector. The electrons transmitted through the thin sample are detected to form an image that is why the electron microscopy is called “transmission”. However, the transmission of electron beam is highly dependent on the properties of material being examined (typically, depends on the density, sample composition and sample thickness).

In the case of SAED, a chosen area aperture is placed into the image plane virtually so that a selected area from sample can form the diffraction pattern. SAED can be used to identify nano wire growth direction, crystal structures and defects and for dark field imaging [17].

Sample preparation includes suspension of solid sample in 2-propanol for 1 min. A drop of prepared suspension was supported on a 3 mm grid (typically made from Cu) coated with a carbon layer. All the samples were examined by using a HR-TEM, JEOL 1200 EX model.

2.4.5 Temperature programmed desorption of NH₃ (NH₃-TPD)

The temperature programmed desorption technique measures the desorption rate of molecules from surfaces as a function of temperature. The catalyst samples are pre-treated at 200 °C in an oxidative atmosphere to eliminate any adsorbed species on the surface. The adsorbing gas (NH₃) then adsorbed to the sample until the equilibrium was reached. After the complete adsorption of gas molecules, excess gas is flushed out of the reactor by inert gas stream. Now, through the programmed heating of the sample holder, we desorb adsorbents in effluent gas. A thermal conductivity detector is set up for collecting these desorbed gas molecules, and then correlation between desorption temperature and concentration of the desorbing gas in the effluent gas will show us certain important information. The total amount of ammonia molecules desorbed is calculated from the total area under the curve.

NH₃-TPD is one of the most widely used and flexible techniques for characterizing acid sites on surfaces. The number of acid sites is the amount of ammonia desorbed in μmol/gm of catalysts. However, ammonia desorption only determines the overall acidic sites and cannot differentiate between Lewis or Bronsted acid sites. TPD spectra are influenced by particle size, catalysts bed depth, inert gas flow rate, and catalysts pore size [18].

NH₃-TPD experiments were performed with a Chemisoft TPx (Micromeritics-2720) instrument (Figure 2.6). The acidity of the catalyst was investigated by NH₃-TPD studies, and the measurements were carried out by (i) Before TPD characterization, He at 25 ml/min was supplied to the reactor at 200 °C to desorb any contaminants from the surface of the catalyst (ii) The catalyst was then cooled to 50 °C for adsorption of NH₃ gas and (iii) heated up to 700 °C for NH₃ desorption at a heating rate of 10 °C min⁻¹. The evolved ammonia was detected by a thermal-conductivity detector.

2.4.6 Pyridine FT-IR technique

Pyridine FT-IR is helpful in determining the nature of acidic sites. Acid sites may be Brønsted acids sites that donate proton or Lewis acid sites that accept electrons [19]. Pyridine (C₅H₅N) is a frequently used probe molecule for this method because of its basic nature, which can adsorb on both Brønsted and Lewis acid sites. The band at 1540 cm⁻¹ is assigned to pyridine adsorption at Bronsted acid sites, whereas IR bands for pyridine coordinated to Lewis sites give peaks at 1450 cm⁻¹.

According to Knouzinger, the nitrogen lone pair electrons affect vibration modes of the ring by the nature of intermolecular interactions [20]. The band observed at 1490 cm⁻¹ is

corresponds to both pyridinium ion and coordinate bonded pyridine and band at 1449 and 1599 cm^{-1} is for hydrogen bonded pyridine [21].

In this thesis, Py-IR analyses were performed using the Perkin-Elmer Spectrum 2000 FTIR instrument. FTIR spectrum is recorded between range of 400 to 4000 cm^{-1} using the praying mantis assembly and KBr as background. The quantitative measurement of Brønsted and Lewis acid sites was done by using Eq. (2.5) and (2.6) developed by Emeis [22]. The samples were pressed onto self-supporting disks (30 mg, 0.25 cm radius) and placed in an IR cell. In order to remove physisorbed water, the disk was heated under vacuum at 400 °C for 1 h. After cooling, IR spectra were recorded at room temperature using KBr background. The sample cell was then exposed to pyridine vapors at room temperature until equilibrium was reached, and then a second spectrum was recorded. Difference spectra were obtained by subtracting the spectra recorded before and after pyridine adsorption.

$$C_L = K_L \times A_{1450} = (\pi/\text{IMEC}_L) \times (r^2/w) \times A_{1450} \dots\dots\dots (2.5)$$

$$C_B = K_B \times A_{1540} = (\pi/\text{IMEC}_B) \times (r^2/w) \times A_{1540} \dots\dots\dots (2.6)$$

Where,

C_L and C_B = concentration of pyridine on Lewis and Brønsted acid sites,

A_{1450} and A_{1540} = integrated area of band at 1450 cm^{-1} and 1540 cm^{-1} ,

K_L and K_B = molar extinction constant for Lewis and Brønsted acid sites,

IMEC_L = integration molar extinction coefficient for Lewis acid sites which is 2.22 $\text{cm} \mu\text{mol}^{-1}$,

IMEC_B = integration molar extinction coefficient for Brønsted acid sites which is 1.67 $\text{cm} \mu\text{mol}^{-1}$,

r = radius of the self-supporting disk of the praying mantis assembly, and

w = weight of sample pressed into the self supporting disk of the praying mantis assembly.

2.4.7 Fourier transform infrared spectroscopy (FTIR)

Infrared spectroscopy involves the analysis of infrared radiation with a molecule. The rays of the infrared region have a longer wavelength and lower frequency than visible light. IR

spectroscopy is vibrational spectroscopy and molecular vibration is responsible for the absorption of infrared radiation. IR spectroscopy used by chemists to determine functional groups in both organic and inorganic molecules. For a molecule to be infrared active, vibrational mode must lead to a change in dipole moment [23].

All FTIR spectra were measured at room temperature in the range $400\text{--}4000\text{ cm}^{-1}$, with 20 scans and 4 cm^{-1} resolution by a Perkin-Elmer FT-IR instrument. FTIR analysis was performed on KBr pellets (1 mg of the catalyst per 100 mg of KBr) and the instrumentation of FTIR spectroscopy is shown below (Figure 2.8): -

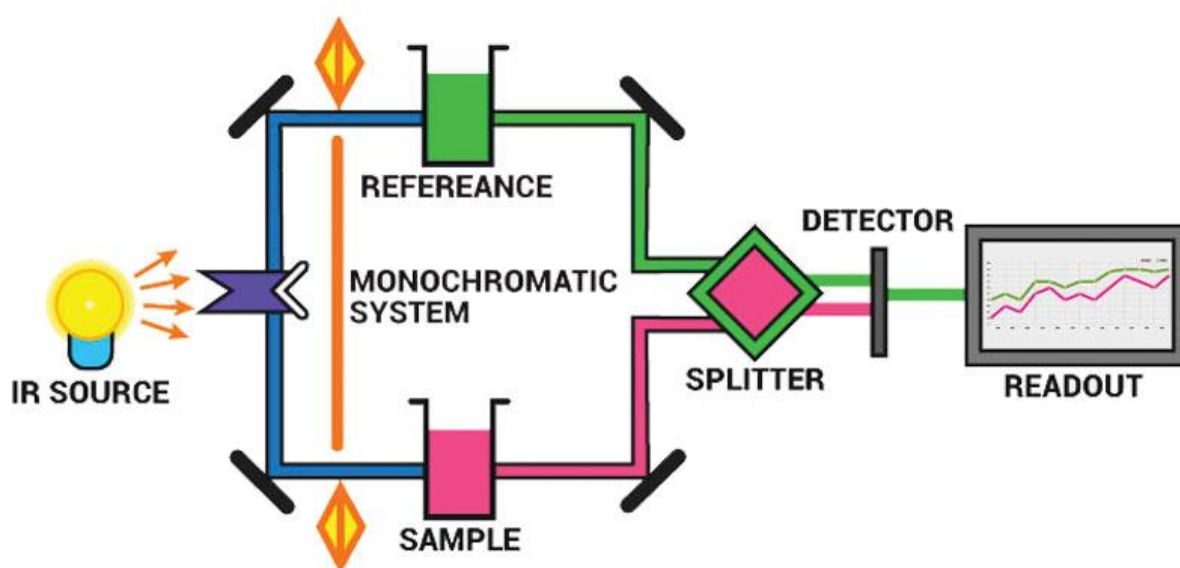


Figure 2.8 FTIR instrumentation

2.4.8 X-ray photoelectron spectroscopy (XPS)

XPS is widely used to determine the oxidation state of metals, elemental composition, and chemical information in addition to elemental information of the samples [24, 25]. XPS is a surface chemical analysis technique. XPS (also referred to as Electron Spectroscopy for Chemical Analysis or ESCA) is an analytical technique where x-rays are used to bombard a specimen and the energies of emitted electrons are analyzed. Typical x-ray sources are AlK_α at 1486.6 eV and MgK_α at 1253.6 eV.

X-rays penetrate the specimen surface to a depth of a few micrometers but only the electrons near the surface can be emitted without losing energy due to collisions with other atoms. The basic principle of XPS is based on the photoelectron effect (Figure 2.9), which was first

observed by Heinrich Hertz in 1887. In 1981, Prof. Kai Siegbahn was honoured by the Nobel Prize for the contribution to the XPS. The kinetic energy (KE) and the binding energy (BE) of the electrons can be determined with a simple relationship:

$$h\nu = \text{KE} + \text{BE} + \phi \dots\dots\dots (2.7)$$

Where $h\nu$ is the x-ray energy and ϕ is the spectrometer work function (few eV).

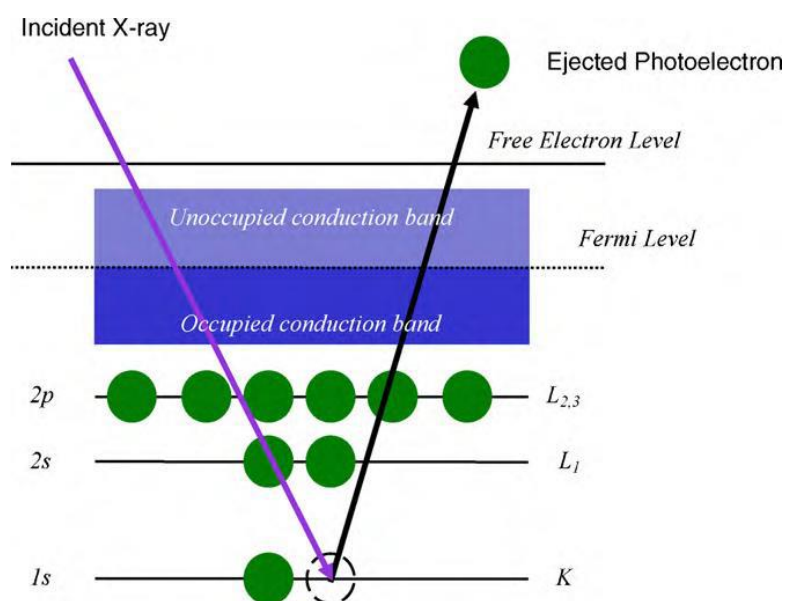


Figure 2.9 Basic principle of XPS

The spectrum is given as the photoelectron count as a function of binding energy. The binding energy of the electron shells is a characteristic feature of each element. XPS instrument consists of the X-ray source, a sample introduction chamber, sample stage, an ultrahigh vacuum (UHV) chamber with UHV pumps, an electron energy analyzer, an electron collection lens, Mu-metal magnetic field shielding and detector system as shown in Figure 2.10.

An energy spectrum is obtained with a scan over the kinetic energy range from 0 eV to the incident x-ray energy. The energy spectrum is different for each element and permits elemental identification of the species present in the top 1-2 nm. The detection limit is approximately 0.1% atomic. XPS is more sensitive to higher atomic number elements [26].



Figure 2.10 Schematic presentations of XPS

The energy resolution of the spectrometer is sufficient to resolve differences in binding energy for different chemical bonds. For example, it is possible to separate C-C from C-O and O-C=O. The area under the peak for each bond represents the percentage of that bond that is present.

In the present work, XPS analyses were performed with a VG Scientific ESCA-3000, equipped with a non-monochromatised Mg K α radiation (1253.6 eV). Survey spectra were made at 50 eV pass energy at a pressure of about 1×10^{-9} Torr (electron take-off angle 55). Usually, C 1s signal with binding energy 284.6 eV is used as an internal standard. The XPS samples were prepared by suspending catalytic quantity in 2-propanol and then mounting a drop of the suspension on the sample holder.

2.5 Catalyst activity testing

2.5.1 Glycerol conversion to oxazoline using a simple distillation method

A two-step route involving glycerol dehydration to acetol followed by its subsequent amination were carried out in the reactive distillation setup (Figure 2.11).

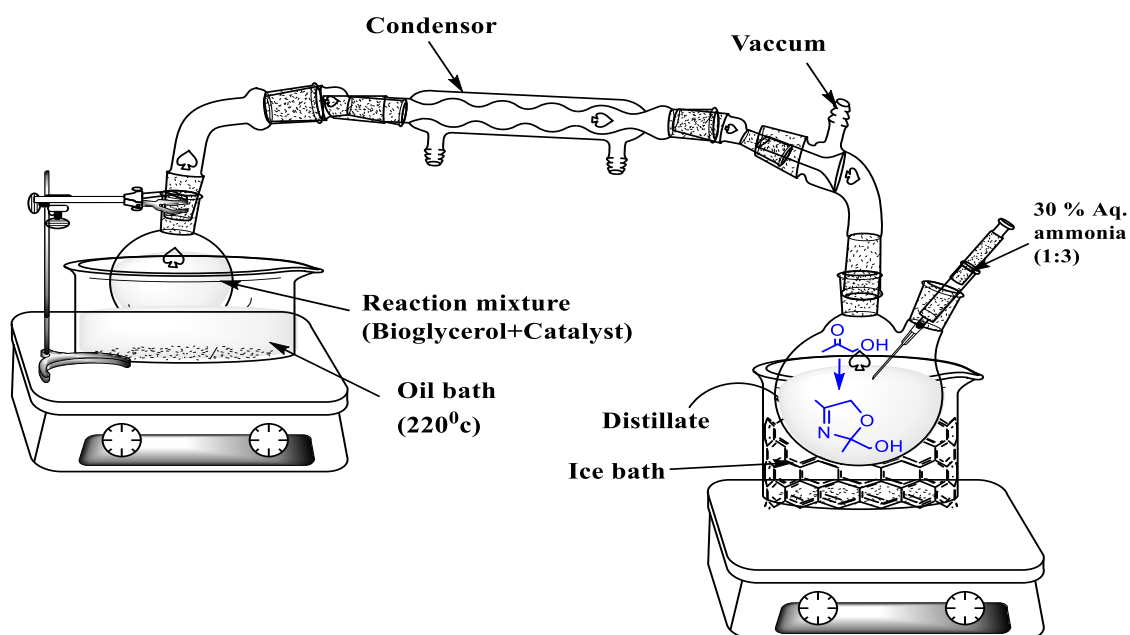


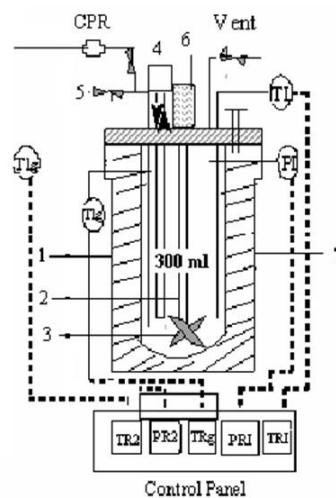
Figure 2.11 Reactive distillation set up

To carry out this experiment, 20 g of pure bio glycerol and 0.8 g of catalyst was charged into the 100 mL capacity round bottom flask. This reaction mixture was stirred with a magnetic stirrer at speed of 600 rpm and the temperature was maintained at 220 °C by using a silicon oil bath. The top of the round bottom flask was connected with a condenser, from which cooling water circulated. The reaction was continued for about 3 h and the acetol formed was continuously distilled out during the reaction. The obtained distillate was analyzed by GC. The distillate was cooled to 0 °C and then 30% aqueous ammonia solution (15 mL) was added to 5 g distillate with stirring in the presence of 0.05 g catalyst. After the complete addition of ammonia, the reaction temperature was increased up to 50 °C with continuous stirring for 2 h and the reaction progress was monitored by GC.

2.5.2 Single-pot glycerol conversion to oxazoline in a batch reactor

All amination batch tests were performed in 300 mL capacity autoclave (Make: Parr Instrument Co., USA). Figure 2.12 shows the schematic set-up batch reactor, which was equipped with overhead stirrer, reactor heating chamber, heating coil, gas inlet and outlet, internal cooling coil, safety rupture disc, solenoid valve, liquid sampling valve, pressure regulator and transducer for digital display, temperature controlling device, and manometer. The solenoid valve system with an automatic cut-off arrangement is installed for controlling

the flow of water in any reactor. This system is particularly advantageous for holding the temperature inside the reactor with an accuracy of ± 1 °C.



(1) Reactor (2) Stirrer shaft (3) Impeller (4) Cooling water (5) Sampling valve (6) Stirrer (7) Electric furnace

Figure 2.12 Schematic of a batch reactor set-up

TI: Thermocouple **PI:** Pressure transducer **TIg:** Thermocouple for gas **N:** Nitrogen cylinder
H₂: Hydrogen gas cylinder **PR:** Pressure regulator **CPR:** Content pressure regulator **TR1:**
 Reactor temperature indicator **PR1:** Reactor pressure indicator **TR2:** Reservoir temperature
 Indicator **TRg:** Gas temperature indicator **PR2:** Reservoir pressure indicator

In a typical amination experiment, 20% w/w bioglycerol (20g) and 80 g of water were charged into the reactor along with 0.8 g of the catalyst at an ambient pressure of nitrogen. An appropriate amount of water has been added to the reactor such that the total volume of the solution is 100 mL. For the removal of trapped air the contents were first flushed 2-3 times with N₂ gas and then the temperature was ramped to the required temperature. Before turning on the stirrer, the initial liquid sample was taken out and the reaction progress was monitored by GC. The reaction was carried out for 3 h at 220 °C. The reactor was cooled to 20 °C after completion of the reaction with ice-cold water and then 30% aq. Ammonia solution (15 mL) was fed into the reactor by applying a vacuum. After complete addition of ammonia, the reaction was carried out at 50 °C for 2 h under stirring at 1000 rpm. The intermittent liquid samples were withdrawn regularly and analyzed by a gas chromatograph.

2.5.3 APR of glycerol to 1, 2-PDO

The APR of glycerol was studied in a bench-scale Parr-reactor as shown in Figure 2.12. These reactions were performed in a 300 mL autoclave stirred Parr reactor, in which 10% w/w bioglycerol (10g) and 90 g of water were added along with 0.8 g of the catalyst at an ambient pressure of nitrogen. The reaction was carried out for 5 h at 220 °C. The reactor was cooled to 20 °C after completion of the reaction with ice-cold water and the intermittent liquid samples were analyzed by GC.

2.6. Analytical methods

The liquid products mentioned in this thesis such as oxazoline, 1, 2-propanediol, imidazole, acetol, 1-propanol, 2-propanol, ethylene glycol, and methanol were analysed by GC (model Shimadzu (GC-2025)). The analytical method details are provided below: -

Gas chromatography conditions:

- Instrument: Shimadzu GC-2025
- Column: HP- Free fatty acid phase column (FFAP) capillary column
- Stationary phase: Polyethylene glycol (highly polar)
- Column details: 30 m x 0.53 mm I.D., 1 µm film thickness.
- Detector: FID
- Injector temperature: 250 °C
- Detector temperature: 300 °C
- Injection volume: 1µL.
- Total run time: 25.30 min.
- Carrier: He

Table 2.1 Oven program of gas chromatography

Sr. No.	Temperature (°C)	Ramp (°C/min)	Hold time (min)	Total time (min)
1	60	-	1	
2	140	20	1	25.30
3	180	5	3	
4	200	15	10	

The identification of by products was done by GC-MS. The products were analysed by ^1H NMR and ^{13}C NMR using D₆-DMSO (0.01 % TMS) and CDCl_3 (0.01 % TMS) as solvents on a Bruker 200 MHz NMR-instrument. The gas phase reaction products were analyzed by a Shimadzu GC-2014 having a Shin Carbon ST column (2 m, 100/120 mesh micro packing) with a TCD detector.

2.7 Performance criteria of a catalyst

The catalyst performance is studied by its reaction activity and product selectivity. The catalyst showing a higher reaction rate is said to have improved activity at the specified conditions. The catalyst activity expressed as the ratio of reaction rate in the presence of catalyst at specified reaction conditions.

The overall activity of the catalyst is evaluated via the conversion. The activity of the catalyst for given reaction is proportionate to the conversion at given conditions. The conversion is defined as follows

$$\%, \text{ Conversion} = \frac{\text{Initial moles of substrate} - \text{Final moles of substrate}}{\text{Initial moles of substrate}} \times 100 \dots\dots\dots (2.8)$$

Selectivity for a specific product is the next significant parameter that defines catalyst efficiency. The selectivity can be defined as ability of catalyst to yield a particular product in the reaction. The selectivity is defined as follows

$$\text{Selectivity} = \frac{\text{moles of desired product}}{\text{converted moles of the reactant}} \dots\dots\dots (2.9)$$

Moreover, metal sites are also more crucial for defining their activity in the aspect of supported metal catalyst, because the metal sites actually act as the active sites for chemical reactions. The catalytic activity can be described by the turnover frequency or TOF. TOF is defined as the molecules reacting per active site per time (s^{-1}). Although the TOF value for a particular metal catalyst should be constant under specified conditions for a given reaction, however, a significant deviation can be observed in reality due to differences in metal support interaction, catalyst preparation, surface structure, crystallite size and morphology, etc.

$$\text{TOF} = \frac{\text{Converted moles of substrate}}{\text{moles of catalyst used} \times \text{time}} \dots\dots\dots (2.10)$$

Another major parameter for evaluating the catalyst stability is the Turnover Number (TON) value. TON defined as the amount of reactant (moles) reacted divided by amount of catalyst (moles).

$$\text{TON} = \frac{\text{Converted moles of substrate}}{\text{moles of catalysts used}} \dots\dots\dots (2.11)$$

TON is a unitless quantity. The TON term specifies the amount of substrate (moles) that a catalyst (mole) will transform up to decay of its activity. The amount of product obtained in a chemical reaction is given by % yield

$$\% \text{ Yield of product} = \frac{\text{Moles of product formed}}{\text{Initial moles of substrate}} \times 100 \dots\dots\dots(2.12)$$

2.8 References

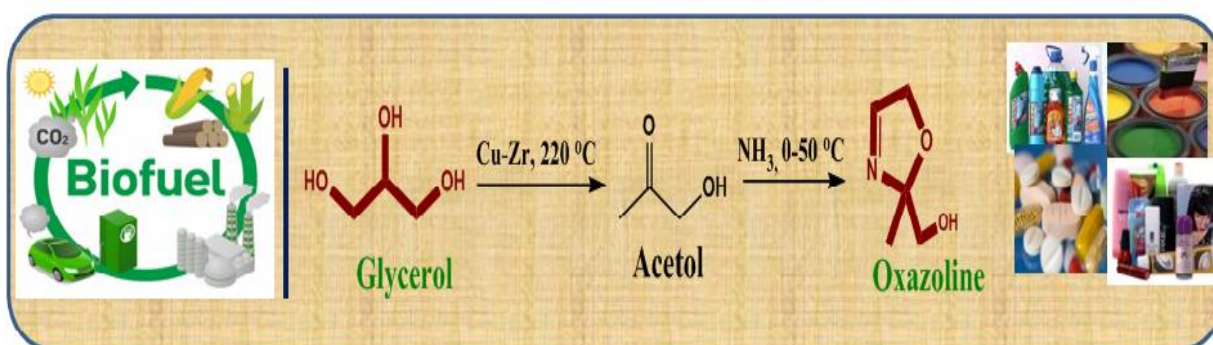
1. B. D. Cullity, Am. J. Phys. 25 (1957) 394-395.
2. V. Pecharsky, P. Zavalij, Fundamentals of powder diffraction and structural characterization of materials, Springer Science & Business Media, (2008).
3. A. R. West, Solid state chemistry and its applications, John Wiley & Sons, (2014).
4. A. L. Patterson, Phys. Rev. 56 (1939) 978.
5. X. Zhou, D. Liu, H. Bu, L. Deng, H. Liu, P. Yuan, P. Du, H. Song, Solid Earth Sci. 3 (2018) 16-29.
6. S. Brunauer, P. H. Emmett, E. Teller, J. Am. Chem. Soc. 60 (1938) 309-319.
7. E. Lopez-Capel, S. P. Sohi, J. L. Gaunt, D. A. C. Manning, Soil Sci. Soc. Am. J. 69 (2005) 136-140.
8. D. Dollimore, P. Spooner, A. Turner, Surf. Technol. 4 (1976) 121-160.
9. K. S. Walton, R. Q. Snurr, J. Am. Chem. Soc. 129 (2007) 8552–8556.
10. K. Sing, D. H. Everett, R. A. W. Haul, L. Moscou, R. A. Pierotti, J. Siemieniewska, Handbook of heterogeneous catalysis, Wiley, New York, (2008).
11. E. P. Barrett, L. G. Joyner, P. P. Halenda, J. Am. Chem. Soc. 73 (1951) 373-380.
12. J. I. Goldstein, D. E. Newbury, J. R. Michael, N. W. M. Ritchie, J. H. J. Scott and D. C. Joy, Scanning electron microscopy and X-ray microanalysis, Springer (2017).
13. L. Reimer, Scanning electron microscopy: physics of image formation and microanalysis, Springer, 45 (2013)
14. W. Zhou, Z. L. Wang, Scanning microscopy for nanotechnology: techniques and applications, Springer science & business media, (2007).
15. D. B. Williams, C. B. Carter, Transmission electron microscopy, Springer, (1996) 3-17.

16. B. Fultz, J. M. Howe, Transmission electron microscopy and diffractometry of materials, Springer Science & Business Media, (2012).
17. J. Duan, S. Yang, H. Liu, J. Gong, H. Huang, X. Zhao, R. Zhang, Y. J. Du, *Am.Chem. Soc.* 127 (2005) 6180-6181.
18. Y. Kamiya, Y. Ooka, C. Obara, R. Ohnishi, T. Fujita, Y. Kurata, K. Tsuji, T. Nakajyo, T. Okuhara, *J. Mol. Catal. A* 262 (2007) 77-85.
19. E. Modrogan, M. H. Valkenberg, W. F. Hoelderich, *J. Catal.* 261 (2009) 177-187.
20. H. Knouzinger, *Adv. Catal.* 25 (1976)184-271.
21. M. C. Kung, H. H. Kung, *Catal. Rev. Sci. Eng.* 27 (1985) 425-460.
22. C. A. Emeis, *J. Catal.* 141 (1993) 347-354.
23. J. Hagen, in *Industrial catalysis*, 2nd edition, Wiley-VCH, Germany, (2006) 215.
24. A. Cros, *J. Electron Spectros. Relat. Phenomena* 59 (1992) 1-14.
25. I. Lindgren, *J. Electron Spectros. Relat. Phenomena* 137 (2004) 59-71.
26. C. J. Corcoran, H. Tavassol, M. A. Rigsby, P. S. Bagus, A. Wieckowski, *Journal of Power Sources* 195 (2010) 7856-7879.

Chapter 3

Catalytic dehydrative amination of glycerol to oxazoline

Synthesis of valuable nitrogen-containing compounds directly from biomass feedstock is highly desirable but at the same time quite challenging. Here, we report a direct method developed for the conversion of bio glycerol to oxazoline by non-noble metal Cu–Zr catalyst, which involves the dehydration of glycerol into acetol followed by its amination using an aqueous NH₃ solution. In this two-step approach, 78% of glycerol conversion was achieved with complete selectivity to acetol while, the amination of acetol carried out separately gave 95% selectivity to oxazoline. The excellent activity performance of the catalyst was explained based on its detailed characterization by XRD, NH₃-TPD and Py-IR. The novelty of this catalyst was its multifunctional active sites responsible for glycerol dehydration to acetol, followed by its amination to oxazoline.



❖ C. V. Rode, R. Pandya, R. B. Mane, US Patent 10385029 (2019)

3.1 Introduction

In recent years, downstream processing of biomass resources has attracted much attention in order to control greenhouse gas emissions effectively and to develop sustainable industrial processes as already discussed in chapter 1 (section 1.3.1). Biomass represents a prominent and easily accessible renewable source of organic carbon and its processing needs viable catalytic routes. Glycerol derived as a by-product of biodiesel synthesis involving transesterification of animal fats and vegetable oils and is expected to reach an annual level of 3.7 million tons in upcoming days [1] as a consequence of government mandates in various countries to blend biodiesel with diesel will lead to the surplus availability of glycerol. Therefore, although glycerol has a traditional market - it is incapable of absorbing the huge surplus quantity of glycerol in the near future which already resulted in a crash in the price of glycerol. Thus, the valorisation of glycerol will not only improve the biodiesel economy but also provide an excellent opportunity for the usage of renewable resources in synthetic chemistry [2].

Glycerol is a tri hydroxy reactive molecule and extensive research has been carried out to transform glycerol into value-added chemicals, with diverse applications [3]. The most commonly studied reactions of glycerol are oxidation [4, 5], hydrogenolysis [6, 7], reforming [8], and dehydration [9]. The selective oxidation converts glycerol into dihydroxyacetone, glyceric acid, tartronic acid, or others depending on the degree of oxidation and/or regioselectivity [10, 11]. Hydroxy ketones, like acetol, are produced through the dehydration pathway [12]. Hydrogenolysis of glycerol involves either partial or full removal of oxygen from glycerol, offering 1, 2-PDO, propanols and/or ethylene glycol as products [13] as mentioned earlier in chapter 1 (Scheme 1.1).

All of the above mentioned strategies are limited to oxygen-containing chemicals from glycerol. Much less attention has been paid to converting glycerol into nitrogen containing chemicals, which often have a higher commercial value [14]. There are limited reports where glycerol is transformed into oxazoline, amino alcohols, amines, diamines and serinol by amination [15, 16]. Therefore, the conversion of glycerol to oxazoline is a challenging route.

Oxazolines have a wide variety of uses as pharmaceuticals, flavouring agents, adhesives, gasoline additives, monomers for the production of polymers, as a protecting group for carboxylic acids in asymmetric catalysis and photography [17]. Some of the 3-oxazoline derivatives (or 2, 5-dihydro oxazoles) are recognized as useful intermediates [18] and have been used in various total syntheses (Figure 3.1). Two dimeric diterpenoids were recognised

from the *Taxodium ascendens* seeds (taxodikaloids a and b), which possess an unprecedented oxazoline ring linkage between two monomers, and ent-alantrypinone (c) is the enantiomer of a natural product produced by the fungus *Penicillium thymicola* [19].

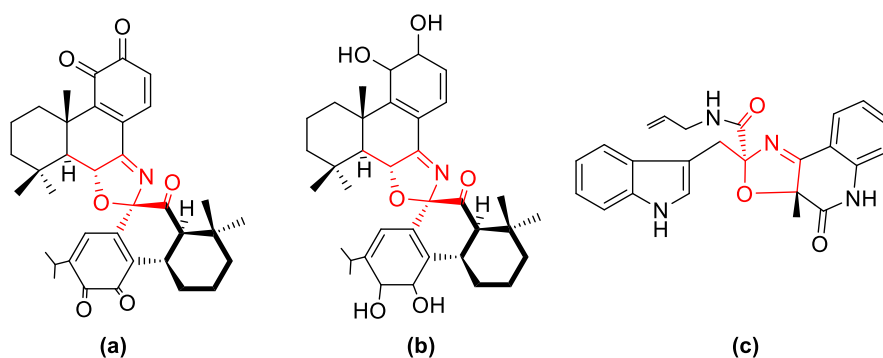
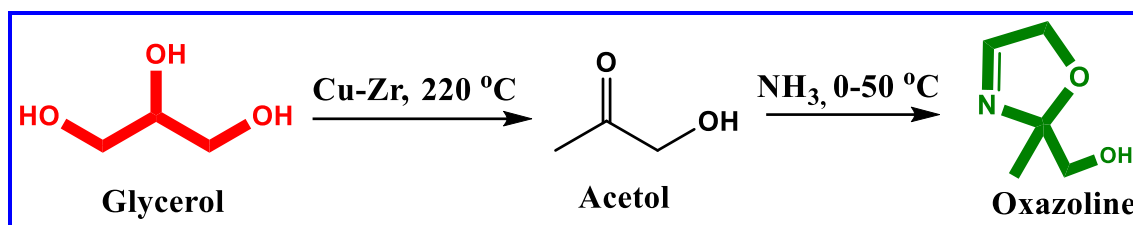


Figure 3.1 Examples of 3-oxazoline-containing natural products (a, b) – Two dimeric diterpenoids, taxodikaloids and (c) - Intermediate for synthesis of *ent*-alantrypinone

Despite the immense synthetic use and significant material as well as biological applications of 3-oxazolines, their synthesis is less common, which includes photo catalytically induced ring opening of 2H-azirines [20], reaction of α -amino perfluoronitrile [21] or diazo derivatives [22], condensation of dihydroxyketones with carbonyl compounds in liquid ammonia [23] and oxidation of the corresponding 1,3-oxazolidines [17]. The photochemical route has its disadvantage like the requirement of special conditions to deal with free radicals and other organic transformation routes were based on complex multistep reactions and are of limited industrial use due to their low stability. Therefore, it has been subject of enduring interest to develop efficient processes for the synthesis of oxazoline derivatives.

In this regard, the use of renewable bioglycerol for the synthesis of oxazoline offers a better alternative; however, it has not been much studied so far. There are few reports available on the amination of glycerol under reduction conditions to give amino alcohol [24, 25] and oxidation products of glycerol (2, 3-dihydroxypropanoic acid or dihydroxyacetone) give (\pm)-2-amino-3-dihydropropanoic acid [16]. Nevertheless, oxazoline was only reported as an adduct and/or intermediate formed during the reductive amination of acetol (1-hydroxy-2-ketones) with ammonia [26]. Oxazoline (2, 4- dimethyl-2-oxazoline-4-methanol) has also been identified as one of the products formed during the conversion of glycerol to allyl alcohol using ammonia or organic acids as sacrificial reductants [27]. From this, it was clear that catalytic glycerol amination to oxazoline has not been studied so far.

Selective conversion of glycerol to oxazoline mainly includes dehydration of glycerol to acetol (that requires an acidic catalyst) followed by subsequent cyclization and amination in the presence of ammonia [28]. In this work, we have screened several non-noble metal catalysts for two-step (Scheme 3.1) glycerol conversion to oxazoline.



Scheme 3.1 Dehydrative amination of glycerol to oxazoline

In this chapter, bimetallic Cu catalysts were prepared and evaluated for improved yield of oxazoline. It was found that for the two-step reaction, increased yield of oxazoline (95% selectivity) was achieved by Cu–Zr catalysts, because acetol was continuously removed through the distillation process which helped in shifting the equilibrium towards the right. Other salient features of this process are i) use of inexpensive commodity chemicals like ammonia for the amination reaction, ii) elimination of the step of separation of intermediates and iii) solvent less process. The aim of this study was to demonstrate the feasibility of producing acetol in a reactive distillation unit by dehydrating glycerol using heterogeneous metallic catalysts and further convert acetol to the oxazoline.

3.2 Experimental

The co-precipitating approach was employed for the production of heterogeneous Cu catalysts with specific metals such as Al, Zr and Mg and a detailed experimental process was discussed in chapter 2 (section 2.3.1). The catalytic sites were characterized by BET-surface area, XRD, XPS, NH₃-TPD and Pyridine-IR techniques according to the process discussed in chapter 2 (sections 2.4.1- 2.4.8). The activity testing for the prepared catalysts was done for the reactive distillation setup as mentioned earlier in chapter 2 (section 2.5.1). Liquid samples were analysed by gas chromatography in order to monitor the reaction progress (chapter 2, section 2.6).

3.3 Results and discussion

Our primary aim was to explore the potential commercial application of the glycerol amination process to oxazoline; hence a two-step route was developed involving glycerol dehydration to acetol followed by its subsequent amination that gave maximum glycerol conversion and oxazoline selectivity which involved a simple distillation of acetol prepared

in the first step of glycerol dehydration to acetol. In continuation of our previous work on glycerol dehydration to acetol [29] over Cu-based catalysts, we used the same catalysts for the conversion of glycerol to acetol which was recovered by distillation and then reacted with ammonia to give oxazoline. In this work, the reduced Cu-Al and Cu-Zr showed excellent conversion and selectivity for dehydration of glycerol and its further amination to oxazoline among several copper-based catalysts examined. Therefore, their characterization attempted to identify active sites within these catalysts and the data were compared with the catalytic activity of other catalysts.

3.3.1 Characterization techniques

3.3.1.1 Surface area measurement

The surface area is one of the primary causes of activity variation in different catalysts, was determined by a single point BET method. The highest surface area value of the activated Cu-Al catalyst was $57 \text{ m}^2 \text{ g}^{-1}$. The second largest surface area value was shown by Cu-Mg sample ($46.2 \text{ m}^2 \text{ g}^{-1}$), while Cu-Zr exhibited the lowest surface area value of $22 \text{ m}^2 \text{ g}^{-1}$. The influence of different metals oxides *viz.* Al, Zr and Mg in modified copper catalysts dramatically influenced their surface areas, showing a descending trend as follows: Cu-Al ($57 \text{ m}^2 \text{ g}^{-1}$) > Cu-Mg ($46.2 \text{ m}^2 \text{ g}^{-1}$) > Cu-Zr ($22 \text{ m}^2 \text{ g}^{-1}$).

3.3.1.2 X-ray diffraction

Figure 3.2 shows the X-ray diffraction pattern of different copper based catalysts. XRD patterns of activated Cu-Al, Cu-Zr and Cu-Mg catalysts indicate the presence of referenced diffraction lines at $2\theta = 43.5^\circ$ (111), 50.7° (200) and 74.2° (220). This confirmed the formation of metallic copper phase [29] in all the samples (JCPDS file no. 85-1326). The appearance of peaks at $2\theta=36.5^\circ$ (101); 29.5° (110); 61.4° (220)] and another peak with $2\theta= 34.7^\circ$ and 38.8° are corresponding to Cu_2O (JCPDS file nos. 78-2076) and CuO phases [JCPDS file no. 80-1268], respectively. In the Cu-Al sample, peaks for Cu^0 were predominant while, peaks for CuO phases were less intense compared to that observed in Cu-Zr and Cu-Mg samples, indicating that during the activation, zirconium and magnesium phases suppressed the CuO reduction. XRD results of Cu-Zr also showed the presence of distinct tetragonal phase of zirconia at $2\theta = 30.5^\circ$ [30]. The particle sizes of various Cu catalysts prepared, were evaluated from Scherrer equation using the peak at $2\theta = 43.5^\circ$ having maximum intensity, was found to be in the following order, Cu-Mg (5.5 nm) < Cu-Al (14.4 nm) < Cu-Zr (38.8 nm).

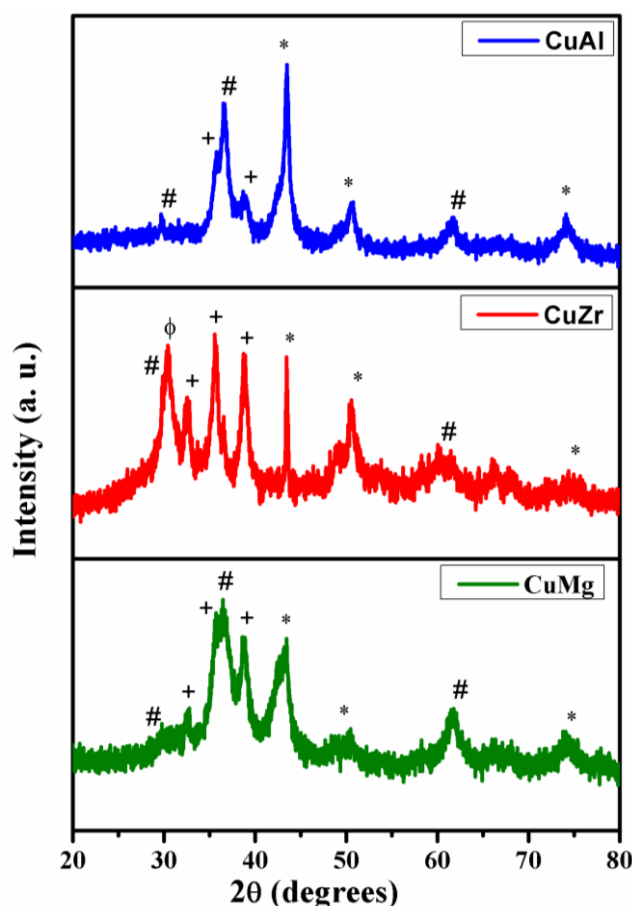
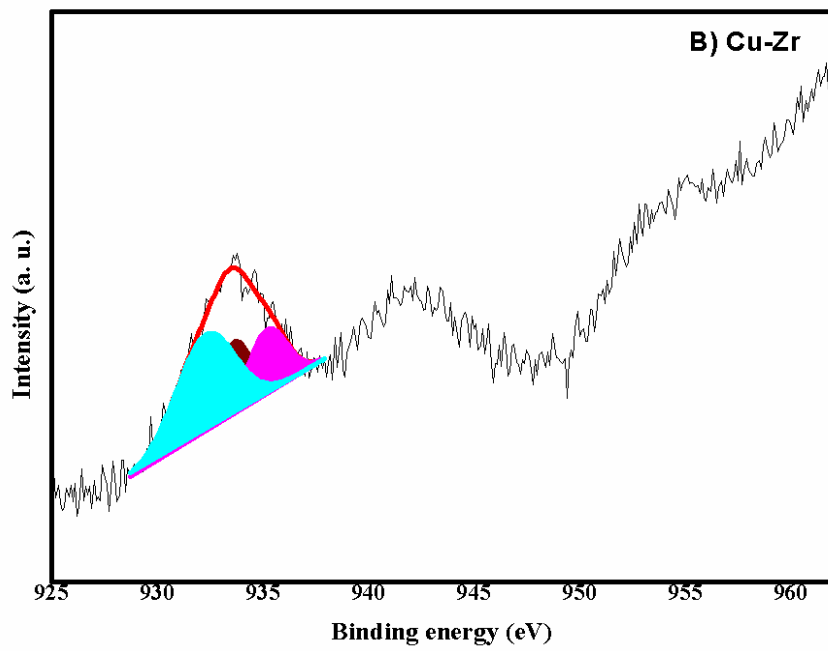
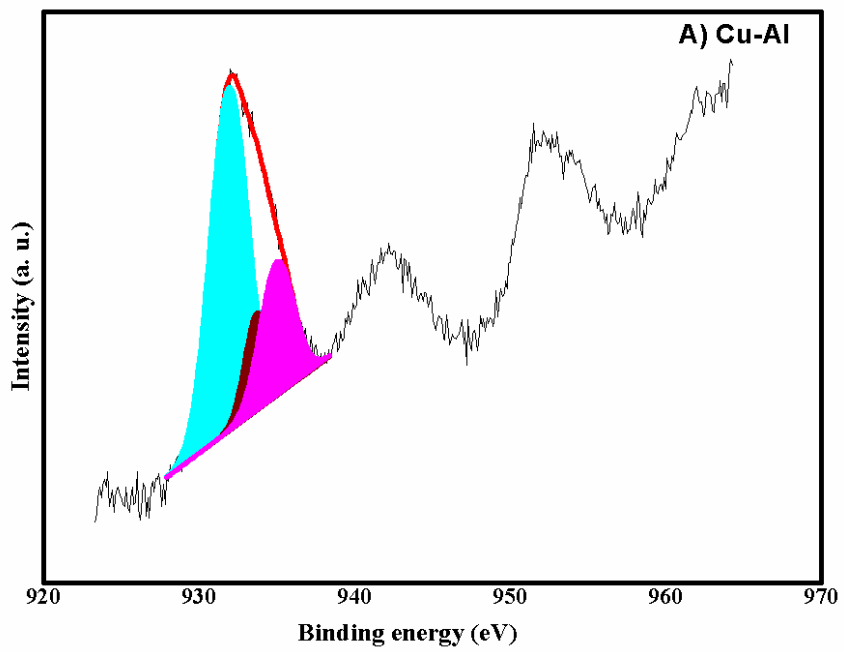


Figure 3.2 XRD patterns of different activated copper catalysts. (*)Cu⁰, (#) Cu₂O, (+) CuO, (φ) t-ZrO₂

3.3.1.3 XPS

Figure 3.3 shows the deconvoluted XPS spectra of activated copper catalysts in order to find the different Cu species formed. The XPS spectrum of Cu 2p_{3/2} shows a broad peak at B.E. of 932-935 eV. These spectra revealed the presence of three different oxidation states of Cu, viz. Cu⁰, Cu₂O and CuO, in all the three catalysts. All the samples showed a peak at 932.4 eV corresponding to either Cu⁰ or Cu⁺ in Cu₂O [31]. Other peaks at higher binding energies of 933.5 and 935 eV (Figure 3.3) were assigned to Cu²⁺ of CuO [32].



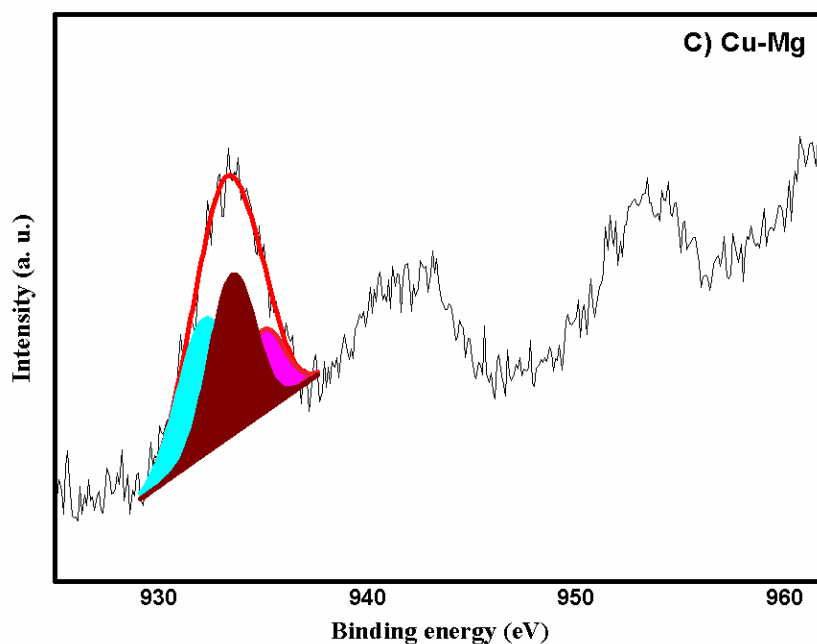


Figure 3.3 XPS spectra for the Cu $2p_{3/2}$ region A) Cu-Al, B) Cu-Zr and C) Cu-Mg

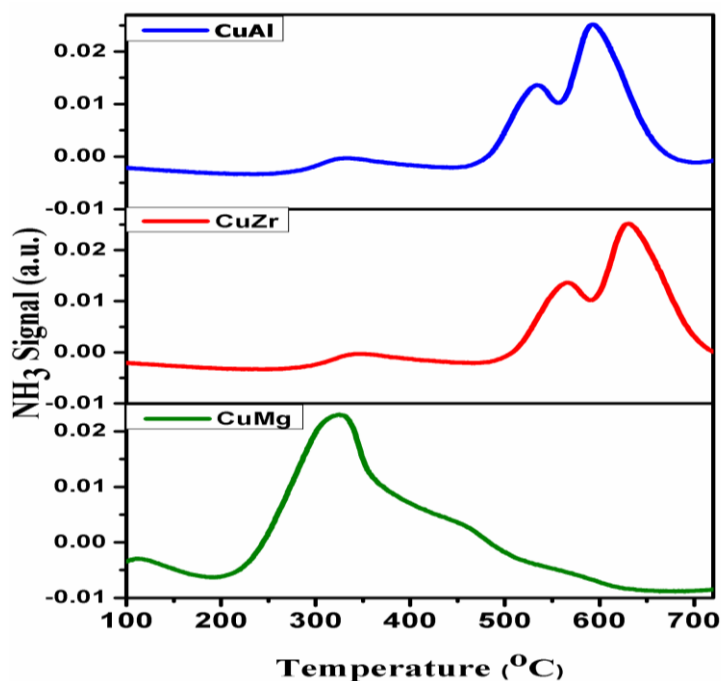
The percentage of Cu, Cu^+ and Cu^{2+} species and relative intensity ratio of $\text{Cu}^{2+}/(\text{Cu}^{1+} \text{ or } \text{Cu}^0)$ calculated based on deconvoluted spectra of Cu $2p_{3/2}$ are expressed in Table 3.1. The lowest ratio of 0.53 in the case of Cu-Al and distribution of (Cu^{1+} or Cu^0) metal and Cu^{2+} was evaluated as 65 % and 35%, respectively indicates most of the Cu was in the form of Cu^0 and/or Cu^{1+} . On the other hand, the highest relative intensity ratio of 1.6 for Cu-Mg was indicative of majority of Cu was in Cu^{2+} form. Interestingly, almost equal distribution of 49% Cu^{2+} and 51 % Cu^{1+} and Cu^0 species was observed from the relative intensity ratio of 0.9 in case of Cu-Zr sample. The presence of oxide species of Cu in all the three samples played a major role in showing the acidic characteristic of the catalyst which affected the activity performance, as discussed later.

Table 3.1 Relative intensity ratio of copper species by XPS in various activated copper catalysts

Catalysts	% distribution of different Cu species		Relative intensity ratio
	Cu ¹⁺ or Cu ⁰	Cu ²⁺	Cu ²⁺ /(Cu ¹⁺ or Cu ⁰)
Cu-Al	65	35	0.53
Cu-Zr	51	49	0.96
Cu-Mg	40	60	1.5

3.3.1.4 NH₃-Temperature programmed desorption

The strength of acid sites was calculated by NH₃-TPD, as they play a significant part in glycerol dehydration and amination reactions. Figure 3.4 and Table 3.2 present the NH₃-TPD profiles and the amount of NH₃ desorbed along with the respective temperature maxima.

**Figure 3.4** NH₃-TPD profiles of different activated copper catalysts

Among these catalysts, Cu-Mg exhibited a broad ammonia desorption peak in the 210-360 °C temperature range, which evidences the presence of only moderate acid sites, while low intensity ammonia desorption peak in the 400-500 °C temperature range, confirms the

existence of strong acidic sites [33]. The NH₃-TPD of both Cu–Zr and Cu–Al catalysts revealed two high intensity peaks for NH₃ desorption in the higher (500–700 °C) temperature region, indicating strong acid sites. From the NH₃-TPD results, the decreasing order of acidity strength is as follows, Cu–Al > Cu–Zr > Cu–Mg. The incorporation of second metal with Cu highly influences the acidic strength by creating the new active sites [34].

Table 3.2 NH₃-TPD results of different copper catalysts

Entry No.	Catalysts	Total NH ₃ desorbed (mL g ⁻¹)	Temperature range-wise desorption of NH ₃ (mL g ⁻¹)		
			40-200 °C	200-400 °C	400-800 °C
1.	Cu-Al	9.51	-	-	3.2, 6.31
2	Cu-Zr	9.4	-	-	3.5, 5.9
3	Cu-Mg	4.57	-	6.71	-

3.3.1.5 Pyridine infrared (Py-IR) spectroscopy

Pyridine infrared (Py-IR) spectroscopy helps in determining the nature of acidic sites (Brønsted and/or Lewis) of the different samples of Cu catalysts. The qualitative measurement of Brønsted and Lewis acid sites was done by subtracting the spectra recorded before and after pyridine adsorption (Figure 3.5). The bands observed at 1458 cm⁻¹ for the Cu–Mg catalyst were due to adsorption of pyridine on Lewis acid sites [35]. In addition to Lewis acidity, all these catalysts showed the adsorption bands pyridine ion at 1532-1557 cm⁻¹ belonging to Brønsted acid sites [36]. Interestingly, both Cu–Al and Cu–Zr catalysts showed the bands corresponding to Brønsted acid sites only in the 1539-1559 cm⁻¹ region. Hence, Brønsted acid sites of Cu–Al and Cu–Zr catalysts have a notable impact on the catalyst activity and product selectivity's, as evidenced by the highest selectivity of oxazoline (95%).

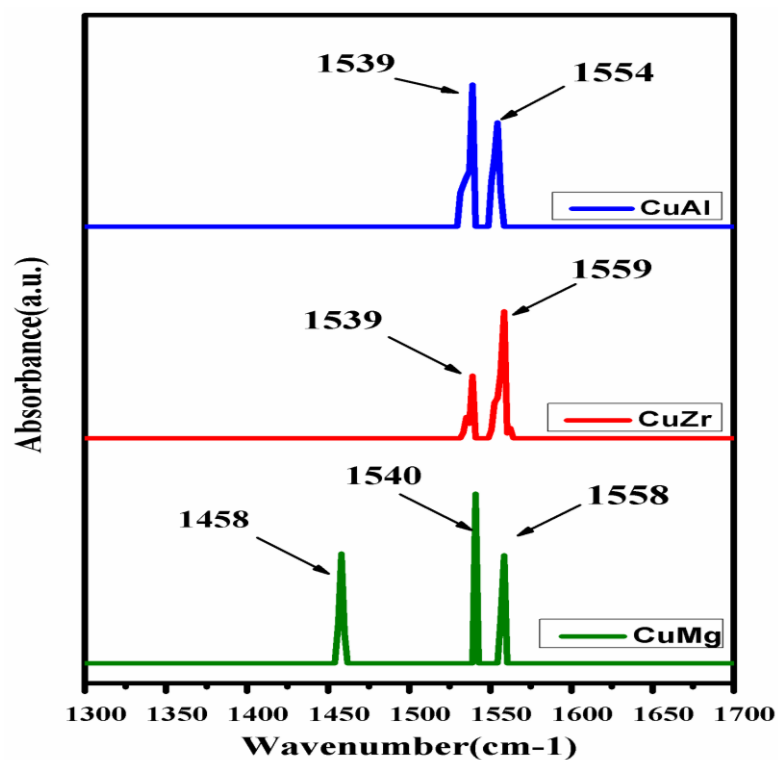


Figure 3.5 Py-IR of different activated copper catalysts

3.3.2 Activity testing

Table 3.3 presents the preliminary results on glycerol dehydration to acetol was performed at 220 °C using various copper catalysts followed by 30% aqueous ammonia passed through the distillate. The final product, oxazoline, was identified by IR spectra, ^1H NMR and ^{13}C NMR as shown in Figures 3.6-3.8.

Table 3.3 Catalyst screening for dehydrative cyclised amination of glycerol

Entry	Catalysts	Glycerol to Acetol ^a				Acetol to Oxazoline ^b			
		Con.	Acetol	1,2-PDO	Other ^c	Con.	Oxazoline	5-methyl imidazole	1,2-dimethyl imidazole
1	Cu-Al	75	77	13	10	99	95	3	2
2	Cu-Zr	78	80	12	8	99	95	3	2
3	Cu-Mg	80	68	20	12	99	95	3	2
4	3% Ru/C	85	30	20	50	99	80	10	8

Reaction conditions: Glycerol to Acetol^a: Glycerol: 20 g, Catalyst: 0.8 g, Temp.: 220 °C, Time: 2 h. Acetol to Oxazoline^b: Distillate: 10 g, NH₃: 15 ml, Catalyst: 0.01 g, Temp.: 50 °C, Time: 2 h. Other^c composed of solketal, ethylene glycol and ethanol mixture.

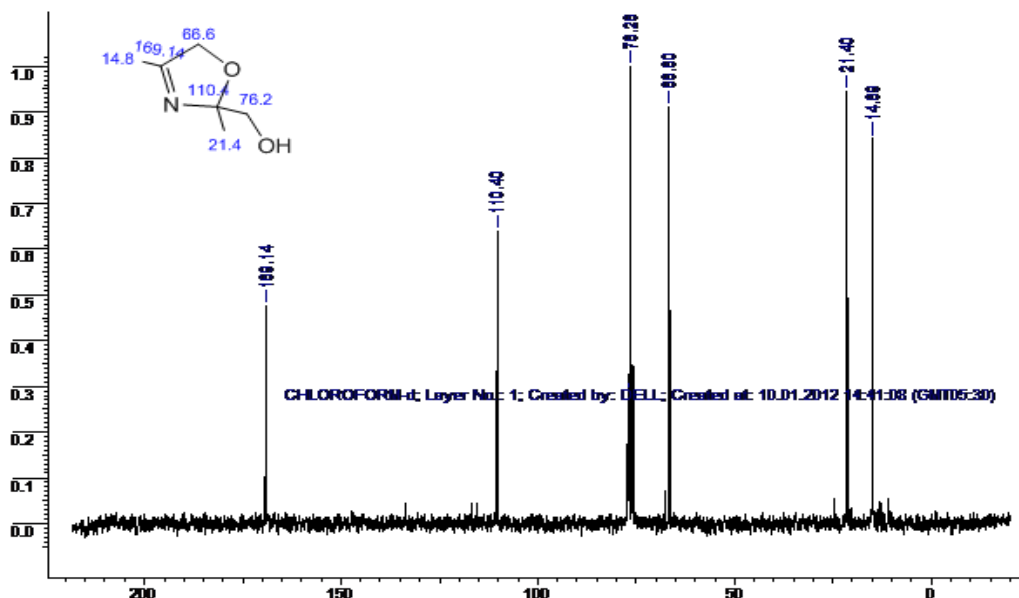


Figure 3.6 ¹³C- NMR spectra of Oxazoline

¹H-NMR (200MHz, CDCl₃): δ 1.39 (CH₃, s, 3H), 2.08 (CH₃, s, 3H), 3.02 (OH, s, 1H), 3.64 (CH₂, d, 2H), 4.58 (CH₂, s, 2H).

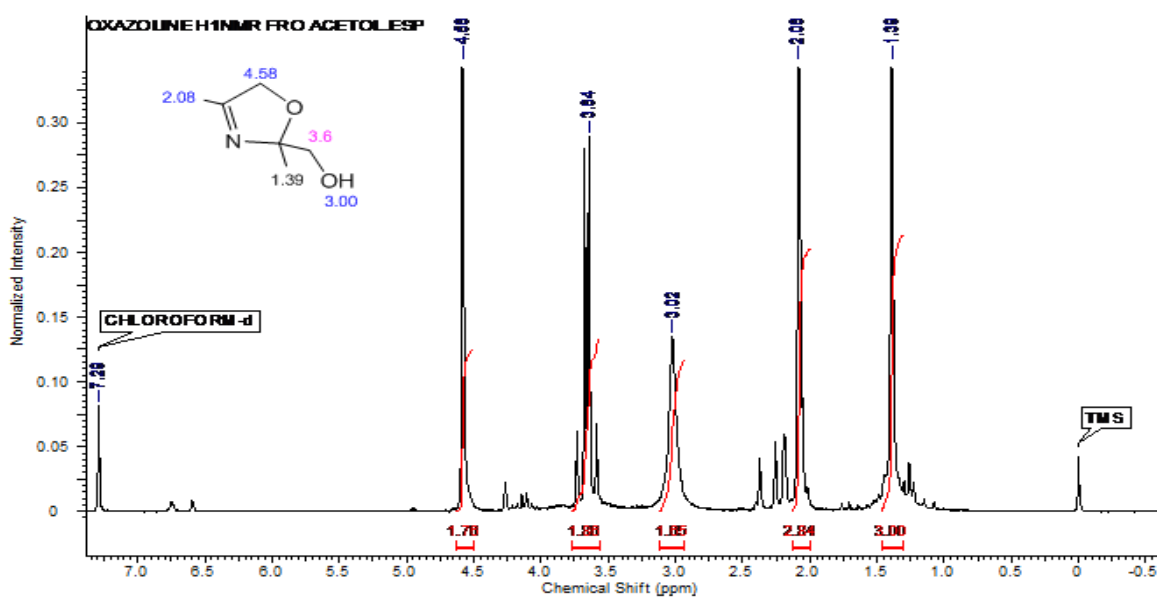


Figure 3.7 ¹H- NMR spectra of Oxazoline

¹³C-NMR (200MHz, CDCl₃): δ 14.89, 21.40, 66.6, 76.26, 110.40, 169.14

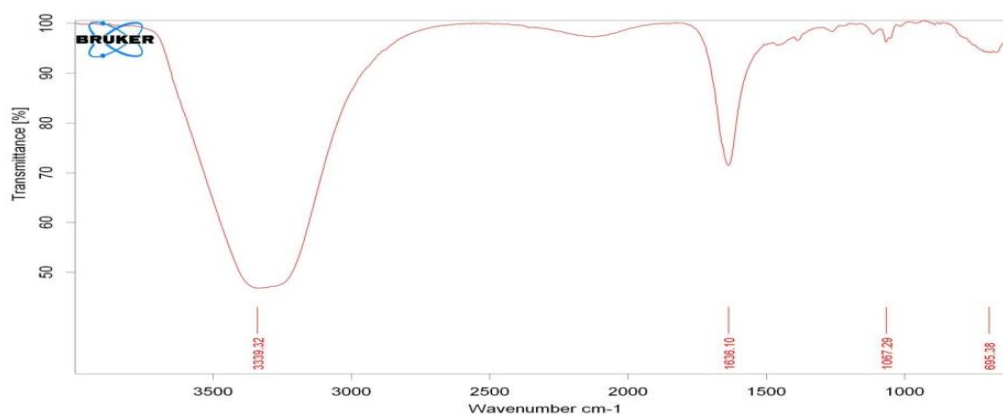
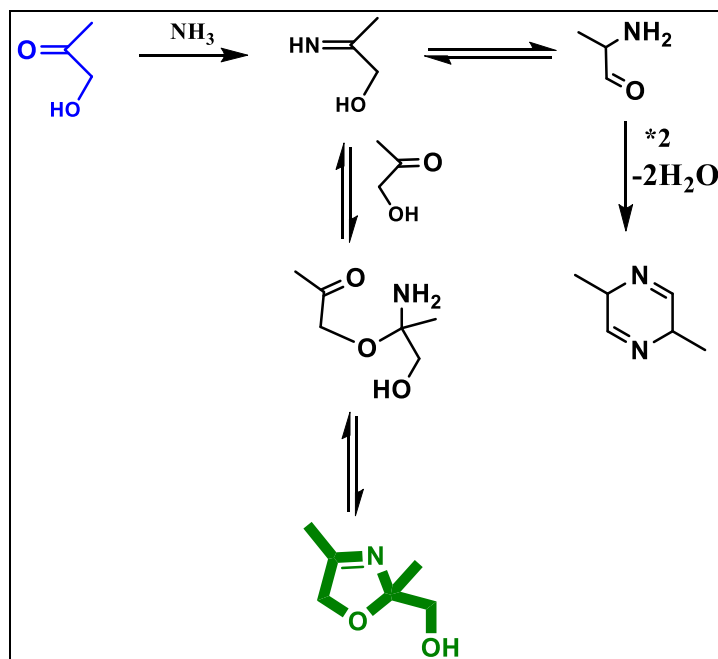


Figure 3.8 IR spectra of oxazoline

For the two-step glycerol conversion to oxazoline, mainly Cu-based catalysts were used and their activities were also compared with those of 3% Ru/C catalyst. It is interesting to note that although among Cu catalysts, copper in combination with Mg showed the highest glycerol conversion of 80%, acetol selectivity was in the order as follows, Cu–Zr > Cu–Al > Cu–Mg (Table 3.3, entries 1-3) with the remaining selectivity's to the acetol hydrogenation product, 1, 2-PDO and other by-products. The glycerol dehydration activity of the catalysts was mainly dependent on the active acid and metal sites [37]. The low selectivity of the Cu–Mg catalyst towards acetol was due to its having moderate acidity and also having lower copper metallic species compared to those present in Cu–Al and Cu–Zr catalysts [Table 3.1], lead to 1, 2-PDO and other by-products formation, mainly solketal [Table 3.3]. 1, 2-PDO formation was due to glycerol hydrogenation by the in situ generated hydrogen by glycerol aqueous phase reforming and/or acetol reforming [12, 38].

Subsequent conversion of acetol to oxazoline observed for all the three catalysts was almost complete (99%) with similar oxazoline selectivity of 95%. Other minor products formed were 5-methyl (2–3%) and 1, 2-dimethyl imidazole (2%). In order to understand the role of a catalyst in acetol amination to oxazoline, a control experiment of acetol (obtained by using Cu–Al catalyst) amination was performed without any catalyst, which gave a lower acetol conversion from 99% to 85% with decreased oxazoline selectivity of 92% and the formation of other side products like dialkyl piperazine (Scheme 3.2 and Table 3.4). A plausible reaction pathway for oxazoline synthesis involves condensation of acetol with ammonia to form α -amino ketone and α -hydroxy imine by tautomerism, which further leads to different products. Self-condensation, dehydration, and dehydrogenation of α -amino ketone forms the

by-product, dialkyl piperazine, while α -hydroxy imine is condensed with second acetol molecule and further cyclises to oxazoline via formation of schiff base.



Scheme 3.2 Reaction mechanism for the glycerol amination

Table 3.4 Effect of catalyst on acetol conversion to oxazoline

Sr. No.	Con. (%)	Selectivity (%)				
		Oxazoline	5-methyl imidazole	1,2-dimethyl imidazole	Dialkyl Pipirazine	Other
1 ^a	99	95	3	2	00	00
2 ^b	85	92	2	1	3	2

Reaction conditions: With catalyst^a: Distillate: 5 g, NH₃: 15 mL, Temp.: 50 °C, Catalyst: 0.05 g, Time: 2 h. Without catalyst^b: Distillate: 5 g, NH₃:15 mL, Temp.: 50 °C, Time: 2 h.

Compared to Cu-based catalysts, although 3% Ru/C catalyst showed the highest glycerol conversion of 85%, the acetol selectivity obtained was the least (30%) (Table 3.3, entry 4). 3% Ru/C favoured increased selectivity to the hydrogenation product 1, 2-PDO and about

50% selectivity to several other by-products, indicating its activity towards glycerol APR and formation of several other products [39]. As the oxazoline formation is via the cyclization of acetol to imine route (Scheme 3.2), obviously, lower acetol selectivity would lead to lower oxazoline yield. Therefore, in the second step over the 3% Ru/C catalyst, although acetol conversion was similar to that of the Cu catalysts (99%), the yield of oxazoline would be less. From these results, it was observed that Cu–Zr was a highly active catalyst for the two-step glycerol conversion to oxazoline. Also, the obvious advantages of this approach are solvent-less conditions, fewer by-products, a significant saving in the operating cost, easy catalyst replacement, and improved product quality.

It was interesting to know that the magnitude of difference in the activities of various catalysts was not in proportion to the difference in their surface area values. This suggests that the catalysts' performance trend cannot be explained solely based on surface area but some other factors such as acidity and the oxidation state of the Cu species influence more catalytic activities.

From the NH₃-TPD results, the decreasing order of acidity strength is in the trend of Cu-Al > Cu-Zr > Cu-Mg. Based on the acidity strength of the catalyst, too strong or too low are not suitable criteria for the glycerol conversion to acetol and subsequently to the oxazoline. This implies that the catalysts having moderate acid sites are sufficient for glycerol conversion to acetol. Strong Brønsted acid sites are also essential for the reaction and played an important role in catalysing the amination of glycerol [40]. In the glycerol-to-oxazoline conversion, both acid sites as well as the metal sites are crucial for the initial activation of glycerol [41]. Metal sites are also necessary for dissociative adsorption of ammonia, while the subsequent conversion of acetol to oxazoline requires acid sites [42].

XPS analysis of all three catalysts showed the presence of three different oxidation states of Cu, viz. Cu⁰, Cu₂O and CuO species (Figure 3.3 and Table 3.1). This could explain the difference observed in the activities of various catalysts. From the characterization data and the activity results, the highest glycerol conversion to acetol and subsequently to oxazoline was possible over the Cu-Zr catalyst. It possessed equal distribution of metallic (Cu⁰) or Cu¹⁺ and Cu²⁺ species along with moderate acidity and more Brønsted acid sites probably being active sites for this reaction.

3.4 Conclusion

We have demonstrated the amination of glycerol with ammonia in an aqueous medium for the production of oxazoline for the first time, using an inexpensive copper based catalyst. In a two step variation, Cu catalysts exhibited almost complete conversion of acetol with 95% selectivity to oxazoline. Interestingly, non-catalytic amination of glycerol was also proceeded but gave less acetol conversion with a decrease in oxazoline selectivity along with multiple side reactions. A possible mechanism for the synthesis of oxazoline from acetol and ammonia was proposed, in which α -amino ketone was the intermediate to produce oxazoline. The role of a catalyst is very prominent for the synthesis of oxazoline from α -amino ketone intermediate selectively while suppressing the further side reaction, which leads to form dialkyl piperazine. The desired product, oxazoline was identified and confirmed by spectral elucidation (IR, ^1H and ^{13}C NMR). An important factor for the high catalytic performance was a moderate acid strength with a high Brønsted acid density. XPS studies and several other characterization techniques confirmed that Cu species present in various oxidation states functioned as highly efficient sites which played a key role in the glycerol dehydration and further amination of acetol. The novel catalyst and the route developed in this work for obtaining value-added oxazoline from biodiesel “waste”, introduces a unique approach in the most cost effective way to realize the concept of biorefinery.

3.5 References

1. B. Katryniok, S. Paul, F. Dumeignil, ACS Catal. 3 (2013) 1819-1834.
2. T. W. Walker, A. H. Motagamwala, J. A. Dumesic, G. W. Huber, J. Catal. 369 (2019) 518-525.
3. X. Dai, S. Adomeit, J. Rabeah, C. Kreyenschulte, A. Bruckner, H. Wang, F. Shi, Angew. Chem. Int. Ed. 58 (2019) 5251-5255.
4. G. Dodekatos, S. Schgnemann, H. Tgysgz, ACS Catal. 8 (2018) 6301-6333.
5. P. N. Amaniampong, Q. T. Trinh, J. J. Varghese, R. Behling, S. Valange, S. H. Mushrif, F. Jerome, Green Chem. 20 (2018) 2730-2741.
6. D. Sun, Y. Yamada, S. Sato, W. Ueda, Appl. Catal. B 193 (2016) 75-92.
7. Q. Sun, S. Wang, H. Liu, ACS Catal. 7 (2017) 4265-4275.
8. Y. Li, M. Nielsen, B. Li, P. H. Dixneuf, H. Junge, M. Beller, Green Chem. 17 (2015) 193-198.
9. B. Katryniok, S. Paul, F. Dumeignil, ACS Catal. 3 (2013) 1819-1834.

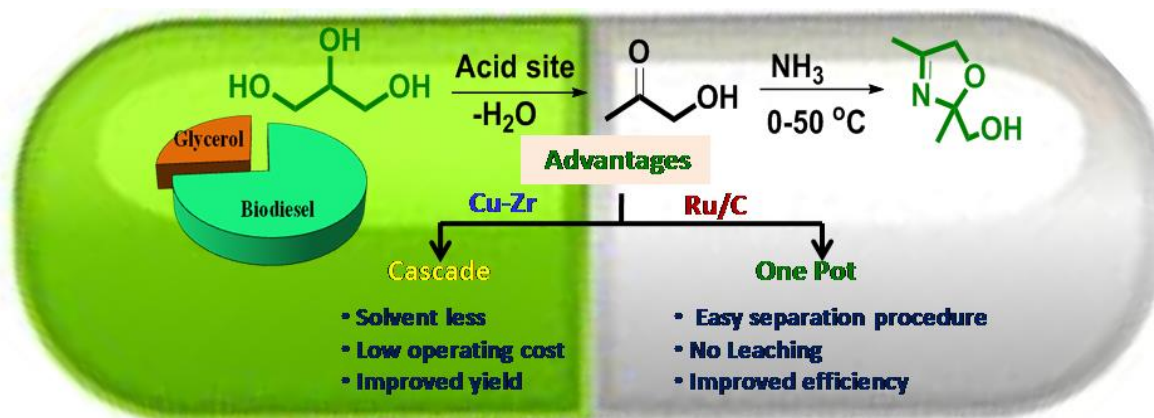
10. H. J. Kim, J. Lee, S. K. Green, G. W. Huber, W. B. Kim, *ChemSusChem* 7 (2014) 1051-1056.
11. S. Lee, H. J. Kim, E. J. Lim, Y. Kim, Y. Noh, G. W. Huber, W. B. Kim, *Green Chem.* 18 (2016) 2877-2887.
12. R. B. Mane, C. V. Rode, *Green Chem.* 14 (2012) 2780–2789.
13. J. Ma, J. Song, H. Liu, J. Liu, Z. Zhang, T. Jiang, H. Fan, B. Han, *Green Chem.* 14 (2012) 1743.
14. G. Liang, A. Wang, L. Li, G. Xu, N. Yan, T. Zhang, *Angew. Chem. Int. Ed.* 56 (2017) 3050–3054.
15. A. Fischer, T. Mallat, A. Baiker, *Catal. Today* 37 (1997) 167-189.
16. H. Kimura, K. Tsuto, *J. Am. Oil Chem. Soc.* 70 (1993) 1027-1030.
17. G. C. Hargaden, P. J. Guiry, *Chem. Rev.* 109 (2009) 2505-2550.
18. X. H. Huang, L. X. Tao, C. Q. Ke, C. Tang, H. Y. Zhang, Y. Ye, L. G. Lin, S. Yao, *Org. Lett.* 19 (2017) 556–559.
19. D. J. Hart, N. A. Magomedov, *J. Am. Chem. Soc.* 123 (2001) 5892–5899.
20. A. Padwa, J. K. Rasmussen, A. Tremper, *J. Am. Chem. Soc.* 98 (1976) 2605–2614.
21. W. J. Middleton, C. G. Krepsan, *J. Org. Chem.* 33 (1968) 3625–3627.
22. G. Prasad, K. N. Mehrotra, *J. Org. Chem.* 47 (1982) 2806–2807.
23. A. Domling, A. Bayler, I. Ugi, *Tetrahedron* 51 (1995) 755–760.
24. M. Ernst, B. W. Hoffer and J. P. Melder, US0240894A1 (2010).
25. V. M. Arredondo, P. J. Corrigan, A. C. Cearley, D. J. Back, M. S. Gibson, N. T. Fairweather, US7619119B2 (2009).
26. W. Himmele, L. Hupfer, H. Toussaint, G. Paul US4105669 (1978).
27. G. Sánchez, J. Friggieri, A. A. Adesina, B. Z. Dlugogorski, E. M. Kennedy, M. Stockenhuber, *Catal. Sci. Technol.* 4 (2014) 3090–3098.
28. C. V. Rode, R. Pandya, R. B. Mane, WO038632A1 (2016).
29. L. Wang, W. Zhu, D. Zheng, X. Yu, J. Cui, M. Jia, W. Zhang, Z. Wang, *React. Kinet. Mech. Catal.* 101 (2010) 365.
30. L. C. Wang, Q. Liu, M. Chen, Y. M. Liu, Y. Cao, H. Y. He, K. N. Fan, *J. Phys. Chem. C* 111 (2007) 16549.
31. J. Agrell, H. Birgersson, M. Boutonnet, I. Melián-Cabrera, R. M. Navarro, J. L. G. Fierro, *J. Catal.* 219 (2003) 389–403.
32. C.D. Wagner, L.H. Gale, R.H. Raymond, *Anal. Chem.* 51 (1979) 466–482.
33. D. Mao, W. Yang, J. Xia, B. Zhang, Q. Song, Q. Chen, *J. Catal.* 230 (2005) 140-149.

34. G. M. S. El Shafei, *J. Colloid Interface Sci.* 182 (1996) 249-253.
35. K. Sagata, N. Imazu, H. Yahiro, *Catal. Today* 201 (2013) 145-150.
36. T. Barzetti, E. Selli, D. Moscotti, L. Forni, *J. Chem. Soc. Faraday Trans.* 92 (1996) 1401-1407.
37. R. B. Mane, A. Yamaguchi, A. Malawadkar, M. Shirai, C. V. Rode, *RSC Adv.* 3 (2013) 16499–16508.
38. M. C. Ramos, A. I. Navascués, L. García, R. Bilbao, *Ind. Eng. Chem. Res.* 46 (2007) 2399-2406.
39. C. Chiu, M. A. Dasari, G. J. Suppes, W. R. Sutterlin, *AIChE J.* 52 (2006) 3543–3548.
40. M. Balaraju, V. Rekha, P. S. S. Prasad, B. L. A. P. Devi, R. B. N. Prasad, N. Lingaiah, *Appl. Catal. A* 354 (2009) 82–87.
41. E. S. Vasiliadou, E. Heracleous, I. A. Vasalos, A. A. Lemonidou, *Appl. Catal. B* 92 (2009) 90–99.
42. S. Li, M. Wen, H. Chen, Z. Ni, J. Xu, J. Shen, *J. Catal.* 350 (2017) 141–148.

Chapter 4

Ru Catalyzed cascade dehydrative amination of glycerol to oxazoline

N-heterocyclic compounds are ubiquitous building blocks in chemical industry. Our previous work suggests that heterogeneous catalysts are convincing to facilitate the synthesis of nitrogen-containing compounds from readily available and cheap raw materials. In this chapter, we will focus on efficient and simple path towards single pot cascade dehydrative amination of glycerol. As glycerol is converted into acetol and acetol converted into oxazoline, the possibility arises that the two steps can be combined using a novel catalytic system. The most selective catalyst in this instance was 3% Ru/C, which shows much enhanced activity (95% selectivity to oxazoline) and robust stability for the single pot oxazoline synthesis. Based on the catalyst characterization integrated with the activity results, a plausible reaction pathway was proposed. The good stability of the 3% Ru/C also helps in recycling experiments without any significant loss of catalytic activity.



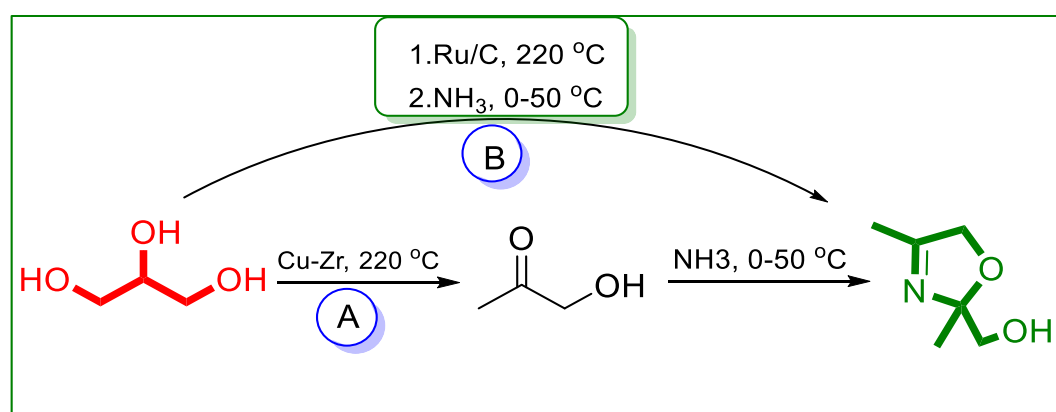
❖ R. Pandya, R. Mane, C. V Rode, *Catal. Sci. Technol.* 8 (2018) 2954–2965.

4.1 Introduction

Triggered by the threat of dwindling fossil resources, the selective biomass conversion has been identified as an alternative, renewable and more sustainable approach to the existing chemical industries [1]. Biomass is considered to be only renewable carbon neutral resource that is abundant and low cost. As already mentioned in chapter 1 (section 1.3.1), biomass serves as a sustainable feedstock for the production of chemicals and fuels.

With the rapid growth in biodiesel production, glycerol has been overproduced worldwide [2]. Glycerol can be used as an important building block for additional valuable chemicals because it is edible, nontoxic, biodegradable compound and has emerged as the top 12 platform chemical from biomass [3]. This sparked attention towards new applications for valorization of glycerol [4]. Therefore, converting glycerol into oxazoline is a promising route, which has received very little attention and their synthesis is less common as already discussed in chapter 3 (section 3.1). Conventional methods for the oxazoline preparation suffer from harsh reaction conditions and/or the use of toxic, corrosive starting materials [5-11]. Therefore, the main objective of this work is to efficiently synthesize oxazoline due to its wide applications in various fields [12-15].

In this regard, our previous work for dehydrative amination of glycerol to oxazoline on a bi-functional Cu catalyst using a simple distillation method (Scheme 4.1 A) has opened a new path towards glycerol amination. As glycerol is converted into acetol and acetol converted into oxazoline, the possibility arises that the two steps can be combined using a novel catalytic system in a single pot reaction.



Scheme 4.1 Two pathways for glycerol amination to oxazoline [A] Dehydrative amination of glycerol to oxazoline using a simple distillation method [B] Cascade dehydrative amination of glycerol to oxazoline

Identifying a suitable catalytic system to allow consecutive dehydration, rearrangement and amination steps to take place efficiently is a major challenge for the new route. Other challenges are: (i) during C–N bond formation, it is possible to have various unstable intermediate such as imines, piperazine and imidazole in various isomeric forms as by-products and (ii) the poisoning of the acid functionalized catalyst in the presence of ammonia. We were also interested in designing and examining the efficiency of a new catalytic system due to difficulties associated with a further increase in oxazoline selectivity.

In this work, we have screened several non-noble as well as noble metal catalysts for one-pot (Scheme 4.1 B) glycerol conversion to oxazoline. We studied here the supported Cu and Ru catalysts for oxazoline synthesis which involves amination in aqueous solution, making the process environmentally benign. The use of an aqueous medium makes the process energy efficient by avoiding the step of separation of glycerol from water. Some important features of this process are i) the use of inexpensive commodity chemicals that make the process economically feasible, ii) the elimination of the intermediary separation step and iii) No leaching of the active metal in the presence of ammonia. It was found that for a single-pot reaction Cu-based catalysts gave lower glycerol conversion and very little oxazoline selectivity compared to that of Ru/C catalysts. In addition, the influence of support, solvent and reaction parameters on the conversion of glycerol and oxazoline selectivity were performed over the 3% Ru/C catalyst for a single-pot reaction.

4.2 Experimental

Cu-Al and 3% supported Ru, Pd, Pt catalysts were prepared by simultaneous co-precipitation and impregnation methods. Chapter 2 (2.3.1 and 2.3.2) has outlined the details of their preparation method. $\text{RuCl}_3 \cdot 3\text{H}_2\text{O}$, H_2PtCl_6 and palladium acetate were purchased from Sigma-Aldrich, India. Aq. ammonia (30%), isopropyl alcohol (IPA), zirconium oxychloride, sulphuric acid, and hexane were obtained from Thomas Baker, India. Nitrate precursors of copper and aluminum, fumed silica, NaBH_4 , alumina and potassium carbonate were obtained from Loba Chemie, Mumbai, India. High purity nitrogen (99.99%) was purchased from M/s. Inox Ltd. Mumbai. Various techniques were used to characterize the catalyst, which is discussed in chapter 2 (Section 2.4). The catalytic test for glycerol amination to oxazoline was performed in a batch reactor and the experimental details are discussed in chapter 2 (section 2.5.2). Liquid samples were analysed by gas chromatography to monitor the progress of the reaction (chapter 2, section 2.6).

4.3 Results and discussion

4.3.1 Characterization techniques

Among various non-noble as well as noble metal catalysts screened in this work, 3% Ru supported on C, SiO₂, and Al₂O₃ showed excellent activity and selectivity for single pot cascade dehydrative amination of glycerol to oxazoline. Therefore, their characterization attempted to identify active sites within these catalysts and the data were compared with the catalytic activity of other catalysts.

4.3.1.1 X-ray diffraction

XRD spectra of 3% Ru supported on C, SiO₂, and Al₂O₃ are shown in Figure 4.1. Ru supported on activated carbon and SiO₂ showed two broad peaks owing to its amorphous nature. The peaks observed for 3% Ru/C at $2\theta = 26.2^\circ$ (002) and 43.3° (101) were attributed to graphitic carbon (JCPDS file no. 752078) while for 3% Ru/SiO₂, the broad peaks in the 2θ range of $10\text{--}30^\circ$ were due to SiO₂ [16]. The XRD spectrum of 3% Ru/Al₂O₃ showed sharp peaks at $2\theta = 18.2^\circ$ (220), 37.3° (311), 39.8° (321), 43.1° (400), 45.9° (210) and 67.1° (440) due to the Al₂O₃ phase (JCPDS file no. 81-1667) [17]. No characteristic Ru peaks were reported in all three Ru-supported catalysts, suggesting either highly dispersed Ru particles or low content of the metal [18].

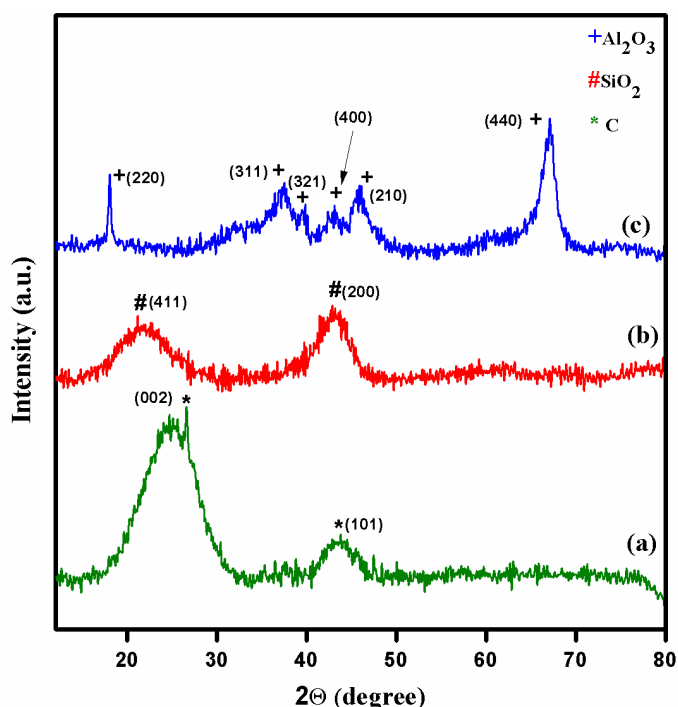


Figure 4.1 XRD spectra of supported Ru catalysts: (a) 3% Ru/C, (b) 3% Ru/SiO₂, and (c) 3% Ru/Al₂O₃

4.3.1.2 BET surface area

Table 4.1 presents the surface area of bare supports and Ru catalysts supported on C, SiO₂, and Al₂O₃. The supports, depending on their nature, dramatically influenced their surface areas, showing a descending trend as follows: C (550 m²/g) > SiO₂ (220 m²/g) > Al₂O₃ (150 m²/g). The highest surface area of C was due to its microporous nature while SiO₂ and Al₂O₃ possessed a micro-mesoporous nature. After Ru loading, the surface area of bare supports decreased significantly due to blockage of surface pores and/or by Ru particle aggregation (TEM images) on the support.

Table 4.1 Surface areas (BET) of supported 3% Ru catalysts

Support	Surface area (m ² /g)	
	As it is	3% Ru loaded
C	550	510
SiO ₂	220	190
Al ₂ O ₃	150	145

4.3.1.3 HRTEM

The support having a higher surface area could be favourable for forming smaller Ru particles and have maximum dispersion which was clearly observed from the HRTEM analysis (Figure 4.2). The HR-TEM image of 3% Ru/C showed smaller Ru particles size of 1–2 nm, suggesting a good ability of C to wet and disperse Ru species (the metal dispersion value of Ru/C obtained was 23). The TEM image of Ru supported on SiO₂ and Al₂O₃ showed slight aggregation of Ru particles with increased Ru particle size of 2-3.5 nm and 2-5 nm, respectively. The alumina support favouring the formation of larger Ru particles was in accordance with previous literature reports [19]. Such intrinsic properties of the support material are known to greatly influence the metal particle size as well as the extent of reduction of the metal and, consequently, the catalytic performance [20, 21]. Figure 4.2 (G and H) displays the TEM images of the 3% Ru/C catalyst after its fifth recycle without any pre-treatment. This clearly revealed that there was an increase in Ru particle size of up to 2-4 nm compared to that of fresh catalyst due to aggregation of Ru particles under aqueous phase reaction conditions.

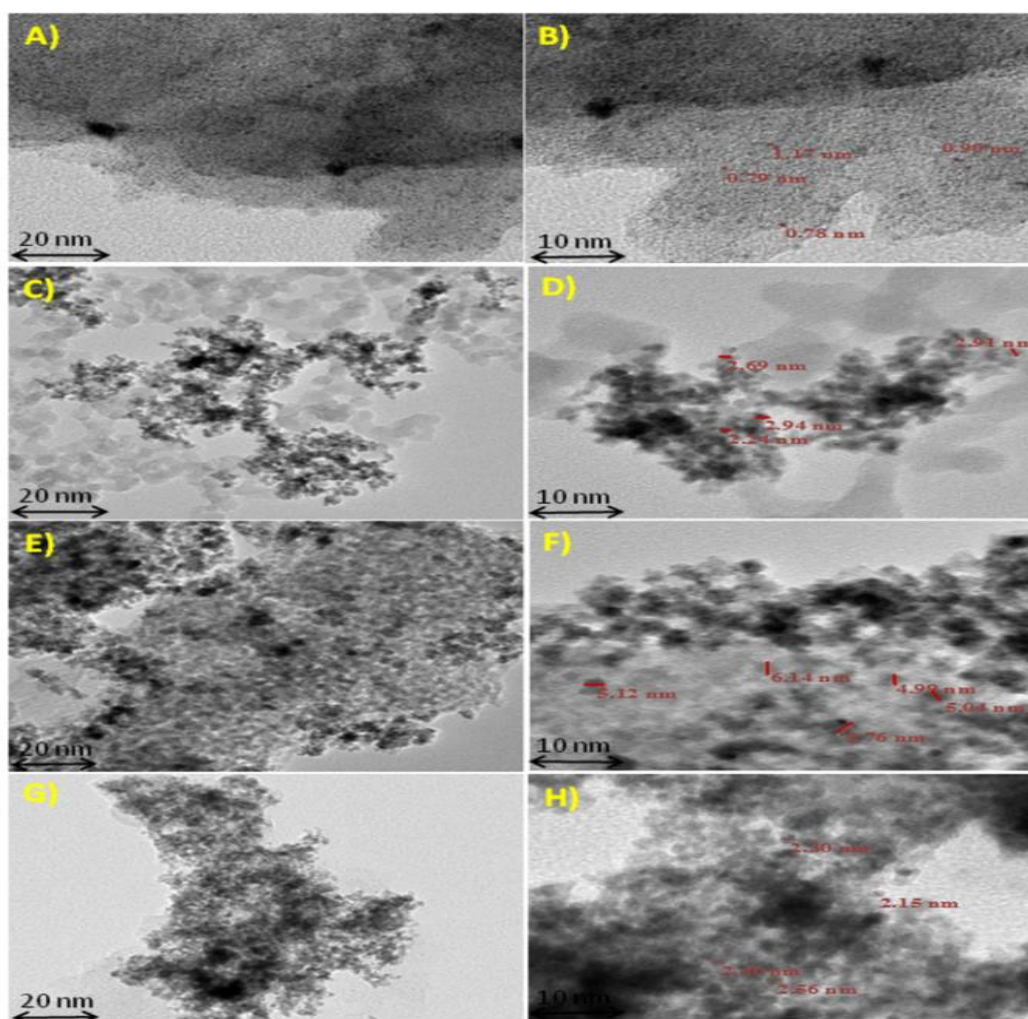


Figure 4.2 TEM images of (a) 3% Ru/C, (b) 3% Ru/C(enlarged), (c) Ru/SiO₂ (d) Ru/SiO₂(enlarged), (e) 3% Ru/Al₂O₃, (f) 3% Ru/Al₂O₃(enlarged), (g) fifth recycled 3% Ru/C (h) fifth recycled 3% Ru/C (enlarged) catalyst

4.3.1.4 SEM

The SEM images of Ru supported on activated carbon and fumed silica also showed the typical porous monolith type structure and amorphous nature with aggregation, respectively, while the SEM image of γ -alumina showed the agglomeration of platy crystals (Figure 4.3) leading to Ru particle aggregation. The electronic states of Ru also varied with a change in the type of support used.

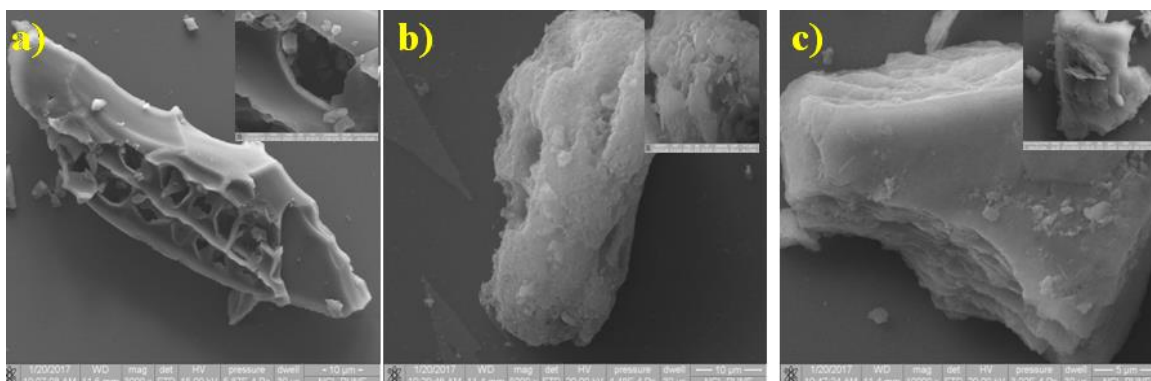
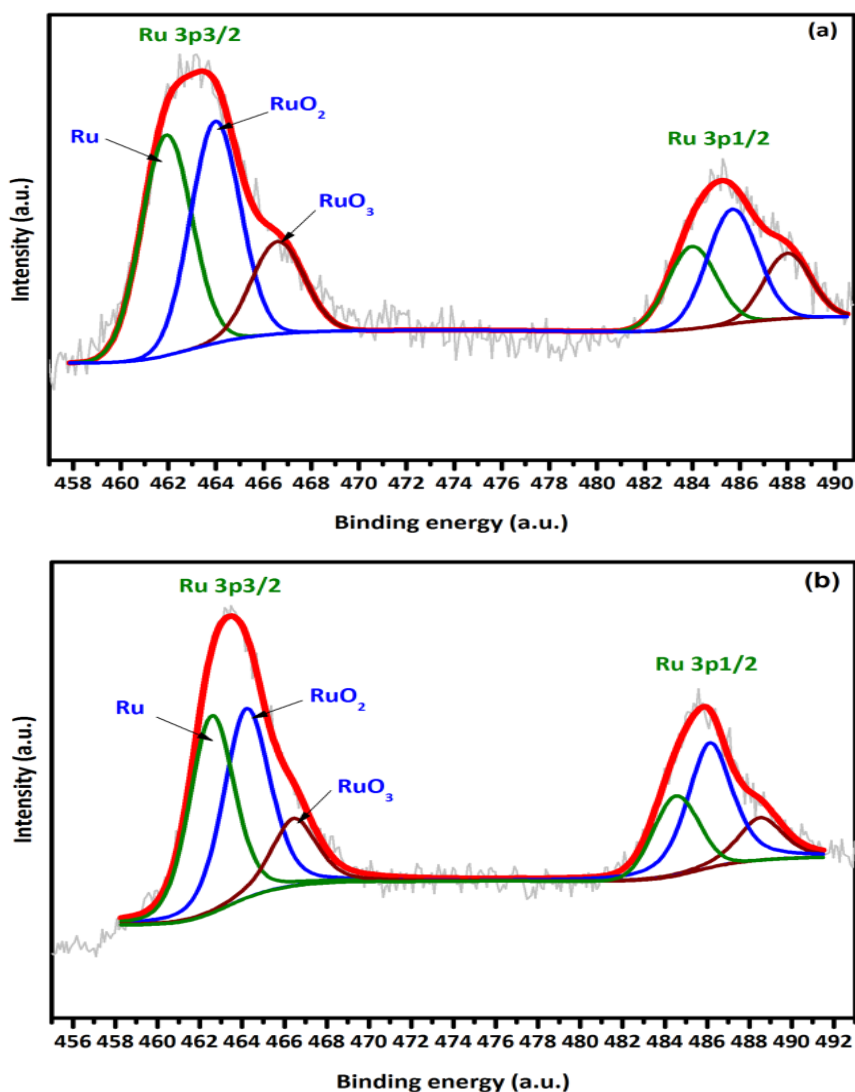


Figure 4.3 SEM images of a) 3% Ru/C, b) 3% Ru/SiO₂ and c) 3% Ru/Al₂O₃ catalysts

4.3.1.5 XPS

The XPS spectra of Ru 3d_{5/2} were overlapping with the C 1s (≈ 284.4) which made it quite difficult to resolve the small Ru peaks from C 1s. Hence, deconvoluted spectra for both Ru 3p_{3/2} and 3d for all the three catalysts are illustrated in Figures 4.4 and 4.5 respectively.



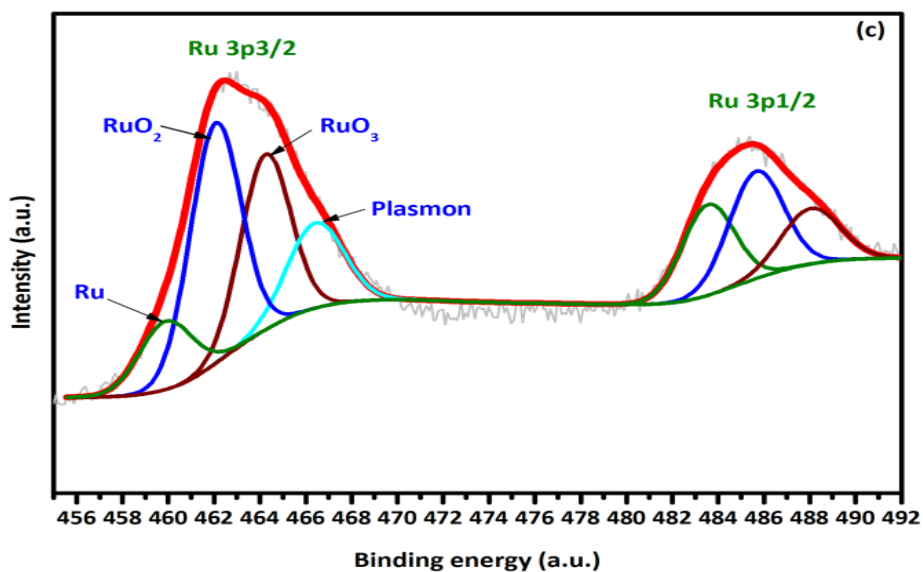
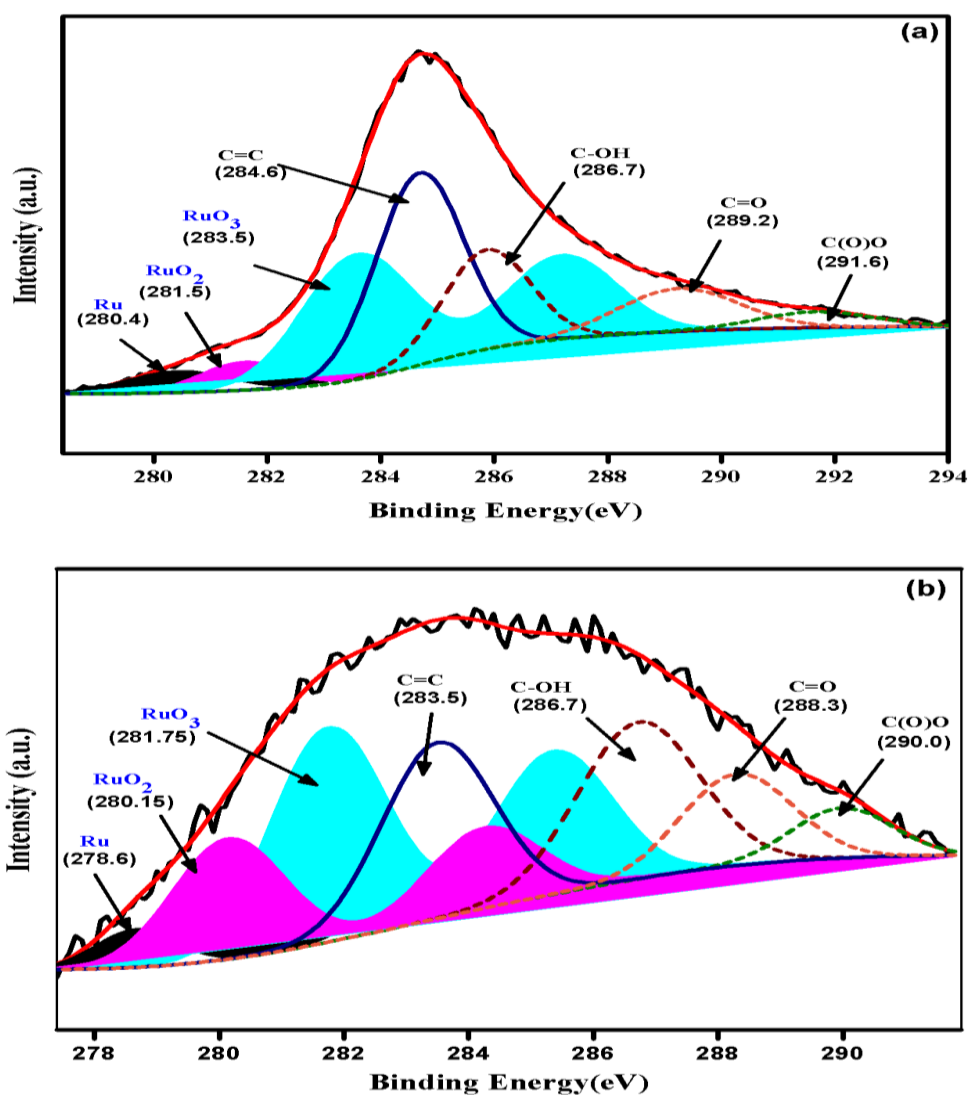


Figure 4.4 XPS spectra for the Ru 3p region (a) 3% Ru/C, (b) 3% Ru/SiO₂ and (c) 3% Ru/Al₂O₃ catalysts



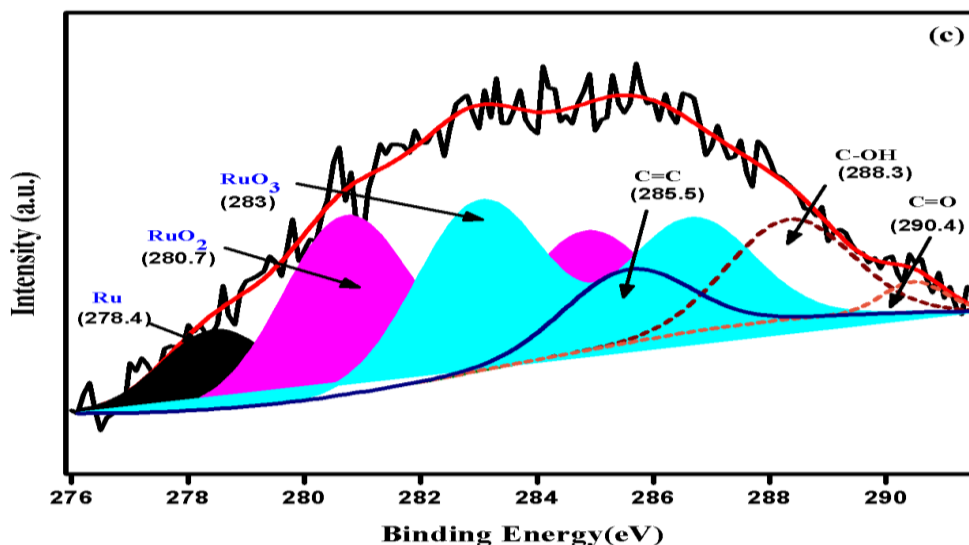


Figure 4.5 XPS spectra for the Ru 3d region (a) 3% Ru/C, (b) 3% Ru/SiO₂ and (c) 3% Ru/Al₂O₃ catalyst

These data revealed the presence of three different oxidation states of Ru, viz. Ru⁰, RuO₂ and RuO₃, in all the three catalysts. The Ru 3p high-resolution XPS spectrum after deconvolution showed three components. The peaks at B. E. of 462.1 and 484.1 eV were characteristic of metallic Ru 3p_{3/2} and 3p_{1/2}, while the peaks at B. E. of 464.10 and 485.82 eV corresponded to the Ru⁴⁺ oxide (RuO₂) and those at B. E. of 466.6 and 488.1 eV represented Ru⁶⁺ (Plasmon and/or RuO₃) [22]. Similarly, the deconvoluted XPS spectra of Ru 3d^{5/2} also showed doublets at binding energy values of 279.9, 281.1 and 283.3 eV separated by spin orbital splitting Ru 3d^{3/2} values of 4.1 eV and 3.6 eV [23, 24]. In the case of the Ru/Al₂O₃ catalyst, the binding energy of the Ru⁰ species was also shifted to a lower value of 278.8 eV, differing by more than 1 eV compared to that reported for bulk ruthenium (280 eV). This could be attributed to the presence of Ru⁰ clusters of very low nuclearity in Ru/Al₂O₃ catalysts [25]. Thus, the electronic state of Ru was sensitive to the type of support material. Nevertheless, the presence of Ru oxide species in all the three samples implies the incomplete reduction of the Ru precursor by sodium borohydride.

The percentage of these different Ru species calculated based on deconvoluted spectra of Ru 3p_{3/2} and Ru 3p_{1/2} varied depending on the nature and structure of the support materials (Table 4.2). The extent of reduction of Ru was found to be the highest in carbon supported catalysts compared to that in catalysts supported on SiO₂ and Al₂O₃ [21]. The presence of

oxide species of Ru in all the three samples played a major role in acidity and hence affected the catalysts activity, as discussed later.

Table 4.2 Percentage of Ru⁰ in different supported catalysts from XPS curve fitting data of Ru 3p peak

Entry	Catalyst	Ru ⁰ / \sum area of oxide species of Ru
1	3% Ru/C	62
2	3% Ru/SiO ₂	57
3	3% Ru/Al ₂ O ₃	25

4.3.1.6 NH₃-Temperature programmed desorption

The strength of acid sites was calculated by NH₃-TPD, as they play a significant part in glycerol amination reactions. Figure 4.6 and Table 4.3 present the NH₃-TPD profiles and acid strengths of the bare supports and supported Ru catalysts. All the three bare supports showed only one low intensity ammonia desorption peak at a temperature range of 50–200 °C corresponds to weak acid sites. However, the total acid strength of the bare support increased in the order of C < SiO₂ < Al₂O₃. Similarly, 3% Ru supported on C and Al₂O₃ also showed weak acid site peaks.

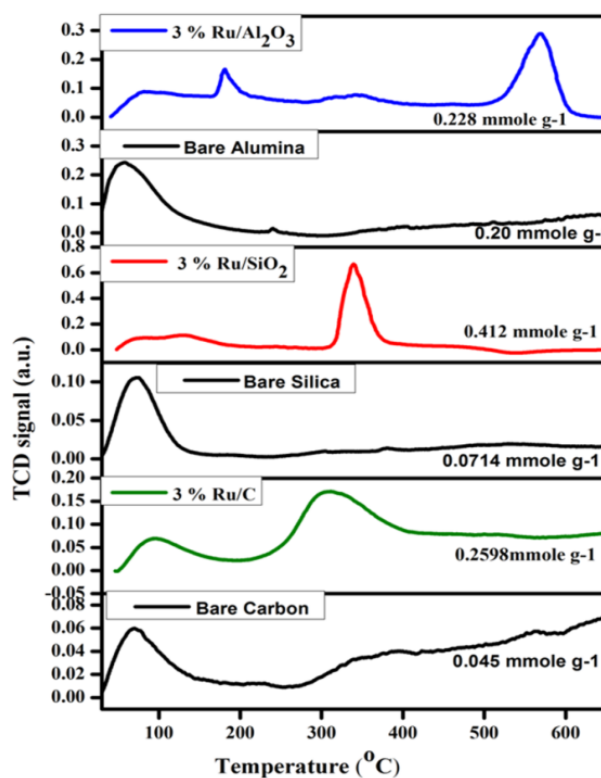


Figure 4.6 NH₃-TPD profiles of supported Ru catalysts

The NH₃-TPD of both 3% Ru/C and 3% Ru/SiO₂ catalysts exhibited broad NH₃ desorption peak in the higher temperature range of 250–360 °C, corresponds to moderate acid sites, while Ru/Al₂O₃ showed a very small and low-intensity peak representing the minimal amount of moderately acidic sites [26]. However, 3% Ru/Al₂O₃ also indicates a sharp NH₃ desorption peak at a high-temperature range of 500– 600 °C corresponding to strong acid sites, which was completely absent in Ru supported on C and SiO₂ samples.

Table 4.3 NH₃-TPD results of bare supports and Ru supported cats

En. No	Catalysts	Total NH ₃ desorbed (mmol g ⁻¹)	Temperature range-wise desorption of NH ₃ (mmol g ⁻¹)		
			40-200 °C	200-400 °C	400-800 °C
1	C	0.045	0.045	-	-
2	Ru/C	0.2598	0.05	0.20	-
3	SiO ₂	0.0714	0.0714	-	-
4	Ru/SiO ₂	0.412	0.13	0.27	-
5	Al ₂ O ₃	0.20	0.20	-	-
6	Ru/Al ₂ O ₃	0.228	0.068	0.0205	0.137

Compared to bare supports, the total acid strength of the Ru supported catalysts showed a somewhat different trend, as acidity increased in the order 3% Ru/Al₂O₃ < 3% Ru/C < 3% Ru/SiO₂ (Table 4.3). These results indicate that strong and new acid sites are formed by the introduction of Ru species. Ru/Al₂O₃ showed the maximum acid strength of strong acid sites, whereas 3% Ru/SiO₂ and 3% Ru/C showed only weak/medium acid sites of similar strengths.

4.3.1.7 Pyridine infrared (Py-IR) spectroscopy

The distinction between Brønsted and Lewis acid sites of the supported Ru catalysts was observed by pyridine infrared (Py-IR) spectroscopy. The qualitative measurement of Brønsted and Lewis acid sites was done by subtracting the spectra recorded before and after pyridine adsorption (Figure 4.7). The quantitative analysis of Brønsted and Lewis acid sites was done using the method proposed by Emeis as discussed in chapter 2 (Section 2.4.6). Table 4.4 summarize the Py-IR results of supported Ru catalysts.

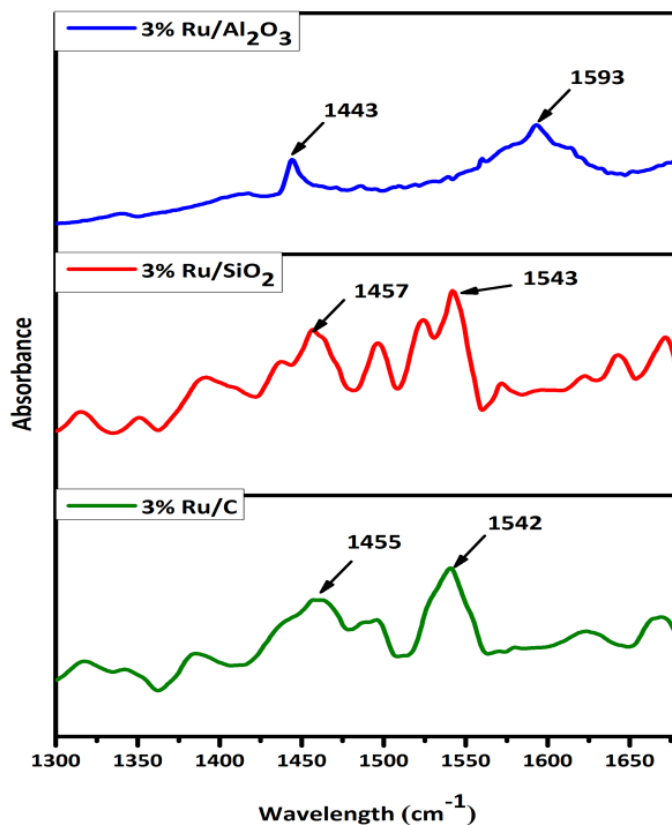


Figure 4.7 Py-IR profiles of supported Ru catalysts

Table 4.4 Py-IR results of supported Ru catalysts

Entry No.	Catalyst	Acidity ^a ($\mu\text{mol pyridine g}^{-1}\text{cat.}$)		
		B	L	B / L
1	3% Ru/C	0.163	0.0259	6.29
2	3% Ru/SiO ₂	0.129	0.0563	2.29
3	3% Ru/Al ₂ O ₃	0.018	0.2258	0.081

L= Lewis acid sites. B=Brønsted acid sites.

For the Ru/C catalyst, the bands appearing at 1542 and 1455 cm^{-1} were due to pyridine adsorbed on Brønsted and Lewis acid sites, respectively. The peak at 1457 and 1555 cm^{-1} for 3% Ru/SiO₂ were common to the various types of acidity present on the surface. The Py-IR spectra of 3% Ru/Al₂O₃ showed very small peaks of pyridine adsorption at 1443 and 1593 cm^{-1} , indicating the presence of Lewis acidity and hydrogen bonded pyridine [27]. The B/L ratio increased in the following order: Ru/Al₂O₃ < Ru/SiO₂ < Ru/C. The strength of the B acid and the B/L ratio has a notable impact on the catalyst activity and product selectivity.

4.3.2 Activity testing

The activity results of several non-noble (mainly Cu) and noble catalysts are shown in Table 4.5. The non-noble metal Cu–Al and Cu–Zr catalysts showed almost similar glycerol conversion of ~19% with very little selectivity to oxazoline (2–3%) with the formation of unreacted acetol (4–10%), 1, 2-PDO (5%) and several other by-products. The probable reason for the lower conversion and selectivity to oxazoline is that compared to the two-step process, acetol remaining in the reaction mixture may lead to less active sites for further adsorption of a substrate. As ammonia is added to the reaction mixture in the second step, Cu which already exists in different oxidation states (Cu, Cu₂O, CuO) as described in chapter 3 (section 3.3.1) in the reaction mixture forms a complex with ammonia and inhibits further reaction [28]. The complex formation was also confirmed by the transformation of the initial colourless reaction solution to a blue colour after the addition of ammonia (Figure 4.8A). However, leaching was not observed in the case of noble metal catalysts (Figure 4.8B).

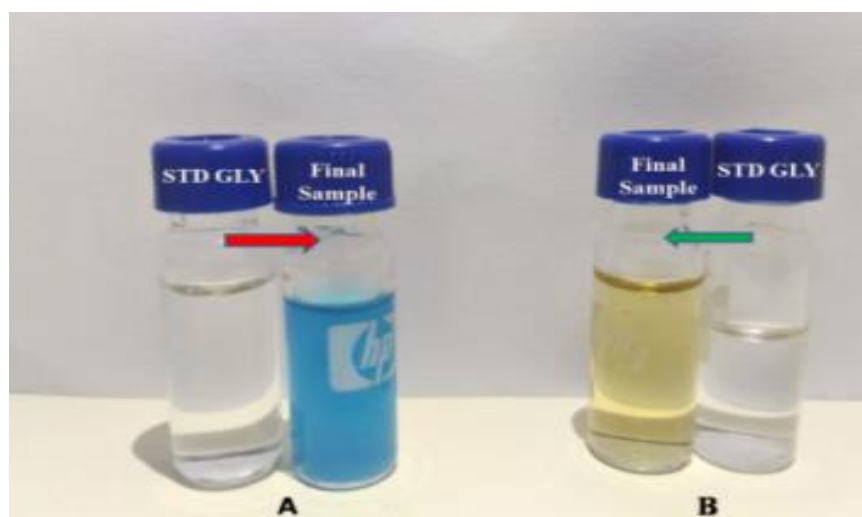


Figure 4.8 Leaching of catalyst a) non-noble catalyst b) noble metal catalyst

In contrast to other noble mono- and bimetallic catalysts, the carbon-supported Ru showed the highest glycerol conversion of 30% and oxazoline selectivity of 90%. The glycerol conversion decreased in the order Ru > Pt > Pd which was in accordance with the available unoccupied d orbitals of the respective metal. This is because the vacant d orbitals have the highest affinity to accept π electrons from the carbonyl intermediates, resulting in the strong adsorption of the carbonyl group [29].

Table 4.5 Catalyst screening for one pot conversion of glycerol to oxazoline

Entry	Catalyst	Con. (%)	Selectivity (%)					
			Oxazoline	Acetol	1,2-PDO	EG	EtOH	Imidazole
1	Cu-Al	18	2	10	5	0	-	-
2	Cu-Zr	19	3	4	5	0	-	-
3	3%Ru/C	30	90	4	3	0	-	3
4	3%Pd/C	15	20	4	5	0	-	-
5	3%Pt/C	18	1	3	40	1	20	20
6	3%Ru/SiO ₂	22	70	5	10	0	5	10
7	3%Ru/ γ -Al ₂ O ₃	20	80	3	5	1	2	9
8	3%Ru-3%Pd/C	10	30	40	5	0	10	15
9	RuO [*]	10	35	10	30	12	8	5
10	3% RuO/C	26	80	6	8	0	0	4

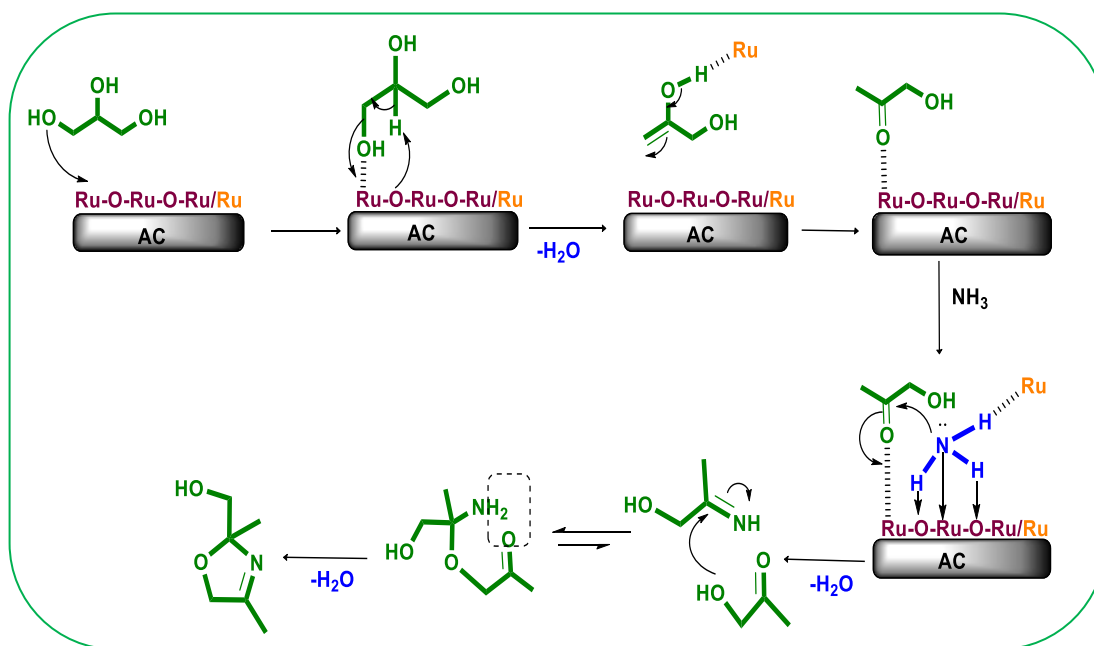
Reaction conditions: Glycerol: 20.0 g, H₂O: 80.0 g, NH₃: 15 ml, Catalyst: 0.8 g, Temp.: 220 °C, * glycerol: 5%), RuO: 0.2g

Similar to the conversion, Ru also showed the maximum oxazoline selectivity (90%) compared to carbon-supported Pt and Pd catalysts (1–20%). However, Pt showed the maximum selectivity to 1, 2-PDO (40%) followed by methanol (20%), imidazole (20%), C–C cleavage product ethylene glycol (EG) and unreacted acetol. The highest selectivity to 1, 2-PDO in the absence of H₂ over Pt catalysts confirmed the high rate of the glycerol aqueous phase reforming (APR) reaction as also reported earlier [30]. Contrary to our expectation, Pd along with Ru (Ru–Pd/C) also gave a very low glycerol conversion of 10% with only 30% selectivity to oxazoline and 40% to acetol. From these results, it was demonstrated that 3% Ru/C was best catalyst for the activity and selectivity of desired product, oxazoline.

It is well known that the intrinsic properties of support greatly influence the Ru particle size and extent of reduction and consequently affect the catalytic performance [31]. Therefore, we compared the performance of Ru supported on SiO₂ and Al₂O₃ catalysts with that of the 3% Ru/C catalyst for glycerol conversion to oxazoline. Among all catalyst, the Ru supported on carbon showed the highest activity. The glycerol conversion and oxazoline selectivity trend observed was 3% Ru/C > 3% Ru/SiO₂ \approx 3% Ru/ γ -Al₂O₃ with glycerol conversion varying from 20% to 35% and selectivity from 70% to 90%. The other products obtained over Al₂O₃ and SiO₂ supported Ru catalysts mainly include imidazole (9–10%), 1, 2-PDO (5–10%) and ethanol (2–5%).

It was interesting to know that the magnitude of difference in the activities of various catalysts was not in proportion to the difference in their surface area values. For example, the activity difference of 3% Ru/C and 3% Ru/SiO₂ was about twofold but the difference in their surface areas was about six-fold (Table 4.1, entry 1). This suggests that the catalysts performance trend cannot be explained solely based on surface area but some other factors such as particle size, acidity and the oxidation state of the Ru species that may influence the catalytic activities. It was found that the carbon-supported Ru catalyst showed well-dispersed smaller Ru particles of 1–2 nm (Figure 4.2) compared to that for the SiO₂ and Al₂O₃ supported Ru catalyst, leading to the highest glycerol conversion for the 3% Ru/C catalyst [32]. Strong Brønsted acidity and a high B/L ratio are also essential for the reaction and played an important role in catalysing the amination of glycerol, as the first step, glycerol dehydration to acetol, was acid catalysed. Although the 3% Ru/Al₂O₃ catalyst possessed strong acid sites (Figure 4.6), it showed lower activity and oxazoline selectivity compared to the C and SiO₂ supported catalysts. This implies that the catalysts having weak and/or moderate acid sites are sufficient for glycerol conversion to acetol [33].

In the glycerol-to-oxazoline conversion, acid sites as well as the metal sites are crucial for the initial activation of glycerol [31]. Metal sites are also necessary for dissociative adsorption of ammonia, while the subsequent conversion of acetol to oxazoline requires acid sites [34]. XPS analysis of 3% Ru/C and 3% Ru/SiO₂ catalysts showed the presence of both metallic Ru and Ru(IV) and Ru(VI) species, while 3% Ru/Al₂O₃ catalyst contained mainly ruthenium in its oxide and hydroxide form (Figures 4.4 and 4.5). This led to the difference observed in the activity of various catalysts. The catalysts having smaller, dispersed Ru particles along with moderate acidity and metallic Ru showed better efficiency of glycerol conversion to oxazoline. This was also supported by the control experiment in which RuO catalyst showed about three times lower glycerol conversion (10%) and oxazoline selectivity (35%) (Table 4.5, entry 9), as compared to that of the Ru/C catalyst (Table 4.5, entry 3). The RuO catalyst supported on carbon (Table 4.5, entry 10) also showed less activity as compared to that shown by 3% Ru/C catalyst, suggesting that both Ru⁰ and RuO are equally important for the catalyst activity. From the characterization data and the activity results, the highest glycerol conversion to acetol and subsequently to oxazoline was possible over 3% Ru/C catalyst as it possessed metallic Ru and Ru oxide species and more Brønsted acid sites probably being active sites leading to excellent performance. Scheme 4.2 shows the plausible reaction pathway for oxazoline synthesis over the Ru/C catalyst.



Scheme 4.2 Plausible mechanistic pathway for glycerol amination to oxazoline

Although the first step of glycerol dehydration is mainly acid catalyzed, metal sites are equally required to activate the glycerol molecule [31]. In this step, the simultaneous abstraction of proton and primary -OH from glycerol by bridging oxygen atom of Ru-O gives enol with the generation of hydrated active sites on the catalyst surface. Further tautomerization to the keto form takes place by abstraction of the proton by Ru^0 to give acetol. This multivalence Ru sites, work bifunctionally because RuO_2 and RuO_3 act as the acid promoters for the activation of the carbonyl group whereas Ru acts as the active site for ammonia dissociation. In this step, NH_3 could be dissociatively adsorbed on the catalyst surface [34] and the lone pair of N attacks on acetol forming a tetrahedral intermediate which is reversibly converted to carbinolamine and then to 2-imino-1-propanol (Scheme 4.2). The imine formation mainly requires acid sites for the elimination of water. 2-Imino-1-propanol thus formed after condensation with a second molecule of acetol undergoes cyclization to obtain oxazoline.

4.3.3 Process optimization studies

For cascade dehydrative amination of glycerol to oxazoline, 3% Ru/C was found to be the most efficient catalyst. Further studies on the effect of process parameters *viz.* metal loading,

catalyst loading, solvent, temperature, and glycerol concentration on conversion of glycerol to oxazoline were carried out using 3% Ru/C catalyst, as discussed below.

4.3.3.1 Effect of metal loading

The effect of Ru loading (1–10%) on dehydrative amination of glycerol at 220 °C is illustrated in Figure 4.9. It can be seen that the glycerol conversion increased linearly with an increase in Ru loading and reached a maximum of 40% at a Ru loading of 5 wt%. However, lower Ru loading (1%) reduces oxazoline selectivity slightly (85%), as fewer active sites are available for the first step of glycerol dehydration. Interestingly, the selectivity to oxazoline decreased even at a higher Ru loading of 5% because the increased active metal sites led to several side products like 1, 2-PDO by aqueous phase reforming of glycerol.

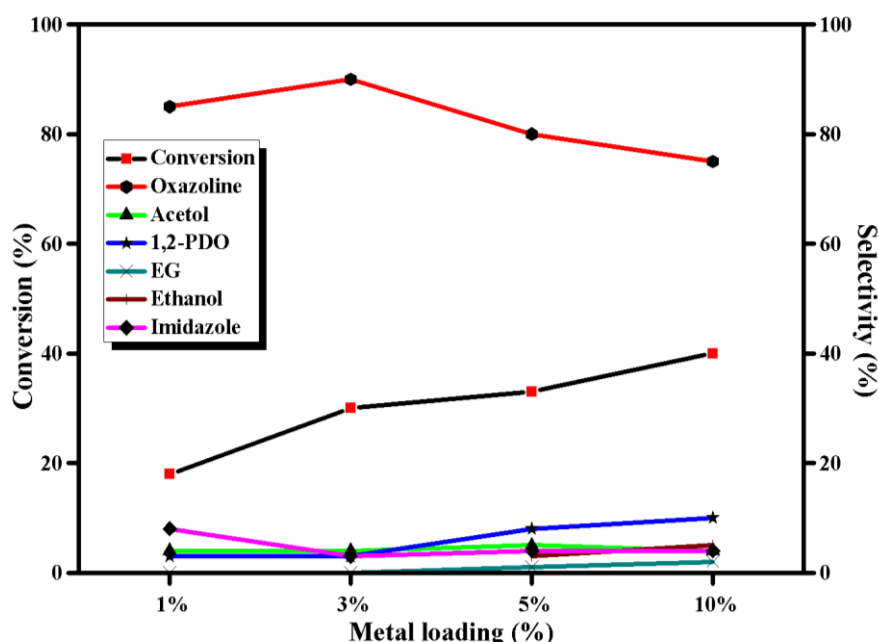


Figure 4.9 Effect of Ru metal loading on cascade dehydrative amination of glycerol

Reaction conditions: Glycerol: 20.0 g, H₂O: 80.0 g, NH₃: 15 ml, Catalyst (Ru/C): 0.8 g, Temp.: 220 °C, Time: 5 h.

4.3.3.2 Effect of glycerol concentration

Feed concentration is a crucial parameter in the economical evaluation of any reactions. Figure 4.10 summarized the influence of glycerol concentration on the dehydrative cyclised amination in the range of 5–30 wt%. The conversion of glycerol decreased from 44% to 15%

as the concentration of glycerol increased from 5 to 30 wt%. This suggests that increased glycerol loading resulted in a substantial lowering of glycerol conversion due to the substrate-inhibited kinetics of the dehydration reaction and/or lower availability of the catalytic sites [33]. The selectivity to oxazoline was found to be minimum at lower (5–10%) and higher (30%) glycerol loadings due to the formation of 1, 2-PDO. 20% glycerol loading was considered as the optimum, as the highest oxazoline selectivity of 90% was obtained at this loading.

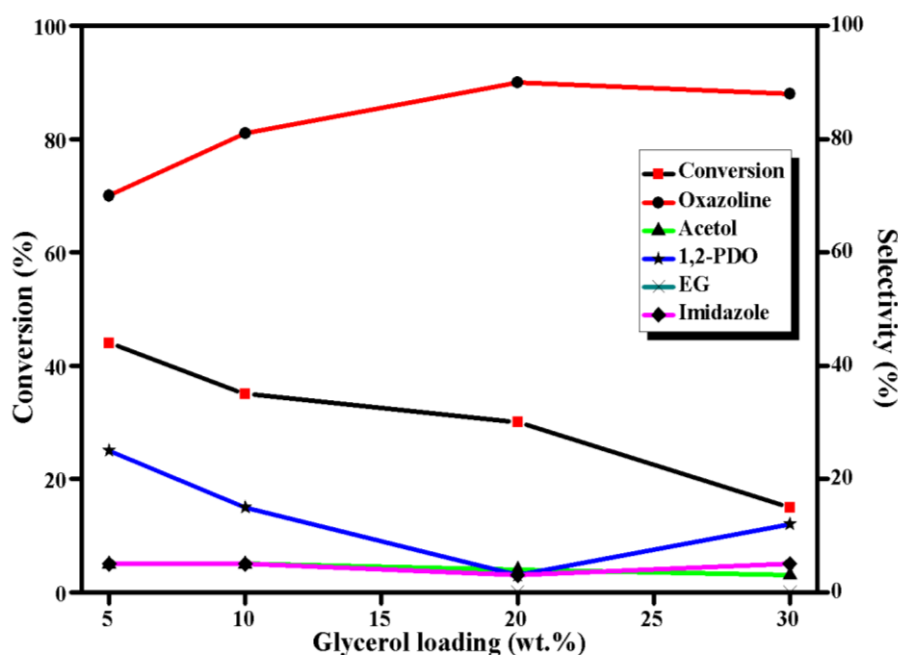


Figure 4.10 Effect of glycerol loading on cascade dehydrative amination of glycerol

Reaction conditions: NH₃: 15 ml, Catalyst (3% Ru/C): 0.8 g, Temp.: 220 °C, Time: 5 h.

4.3.3.3 Effect of solvent

The activity of the 3% Ru/C catalyst was also investigated in different solvents, viz. hexane, 2-propanol (IPA) and water, and the results are given in Table 4.6. Glycerol conversion decreased in the order IPA > hexane > water, while the oxazoline selectivity trend was in the order water > IPA > hexane, different from that observed for glycerol conversion.

Table 4.6 Effect of solvent

Solvent	Con (%)	Selectivity (%)				
		Oxazoline	Acetol	1,2-PDO	Imidazole	Other
Hexane	56	5	5	30	6	50
IPA	60	40	7	30	3	20
Water	30	90	4	3	3	0

Reaction conditions: Glycerol: 20.0 g, H₂O: 80.0 g, NH₃: 15 ml, Catalyst (3% Ru/C): 0.8 g, Temp.: 220 °C, Time: 5 h, other: Oligomeric products of undissolved glycerol.

The activity of the 3% Ru/C catalyst was found to depend mainly on the solubility of glycerol in the respective solvent. The lower solubility of glycerol in an aprotic and non-polar solvent such as hexane resulted in the formation of oligomeric products (56%), which adversely affected selectivity of acetol (10%) and thus oxazoline selectivity [35]. The maximum glycerol conversion (60%) was achieved in IPA, due to higher solubility of glycerol. Nevertheless, due to transfer hydrogenation in IPA [36], acetol more readily converted to 1, 2-PDO (30%), leading to the decreased oxazoline (40%) selectivity than that in water (90%). Therefore, a further study was performed using water as a solvent, which is also a green solvent.

4.3.3.4 Effect of temperature

The effect of temperature on dehydrative amination of glycerol over 3% Ru/C catalyst is illustrated in Figure 4.11. It can be seen that the glycerol conversion increased linearly with reaction temperature. Glycerol conversion increased from 15 to 35% with raising the temperature from 180 to 240 °C. The selectivity to the desired product oxazoline was similar (~84%) at the initial rise in temperature from 180 to 220 °C, but the oxazoline selectivity decreased to 80% upon further increase of temperature to 240 °C. As expected, glycerol reforming was favoured at a higher temperature, which results in improved selectivity for 1, 2-PDO at the cost of oxazoline [37].

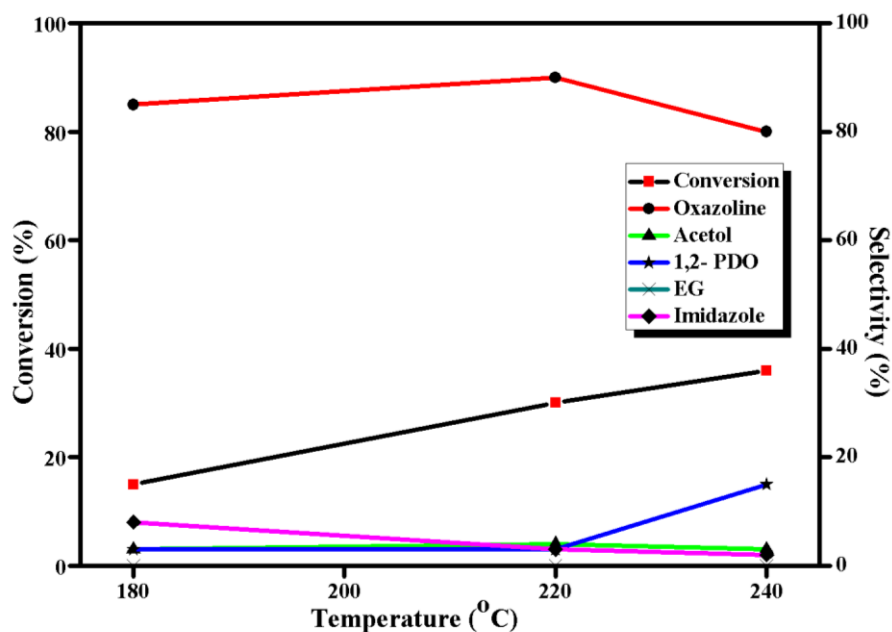


Figure 4.11 Effect of temperature on cascade dehydrative amination of glycerol

Reaction conditions: Glycerol: 20.0 g, H₂O: 80.0 g, NH₃: 15 ml, Catalyst (3% Ru/C): 0.8 g, Time: 5 h.

4.3.3.5 Effect of catalyst loading

The study on the change in glycerol conversion and oxazoline selectivity on varying catalyst concentrations is shown in Figure 4.12. Increasing the catalyst loading from 0.5 to 2.0 g improved the glycerol conversion from 20% to 40%. However, higher catalyst loading improves glycerol conversion, due to the availability of higher active sites. Initially, a lower catalyst loading of 0.5 g led to the formation of imidazole and simultaneously affected the oxazoline selectivity. Further increase in catalyst loading up to 1.5 g hardly affected the oxazoline selectivity, indicating that neither further amination nor any possibility of reversible reaction took place. However, the oxazoline selectivity decreased when catalyst loading increased further from 1.5 to 2 g due to the formation of 1, 2-PDO, indicating aqueous phase reforming was favoured with an increased number of Ru sites [38].

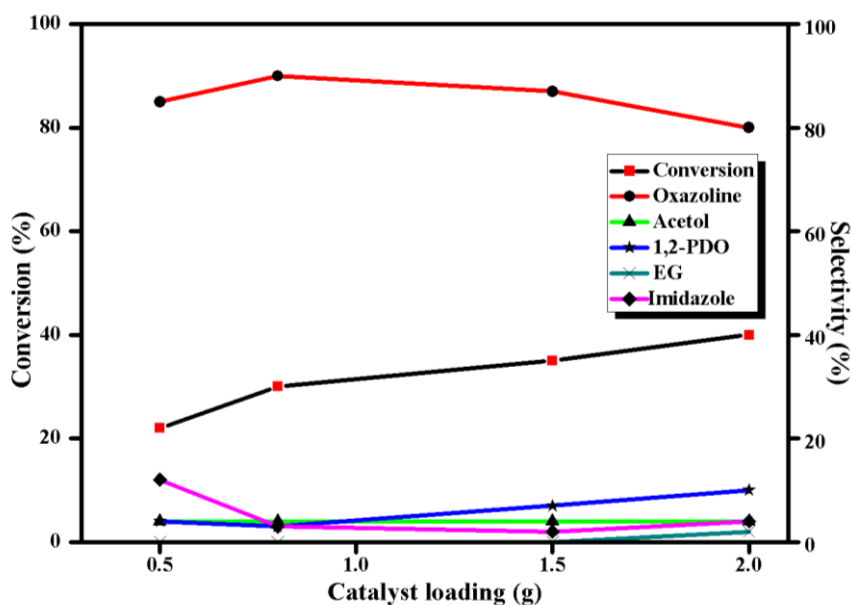


Figure 4.12 Effect of catalyst loading on cascade dehydrative amination of glycerol

Reaction conditions: Glycerol: 20.0 g, H₂O: 80.0 g, NH₃: 15 ml, Temp.: 220 °C, Time: 5 h.

4.3.4 Recycling of catalyst

From an economic and environmental perspective, recycling of heterogeneous catalysts is advantageous. The catalysts (3% Ru/C) could be recycled simply by filtration and further washed with methanol to remove any surface adsorbed organic species. The catalyst recovered from the first run was charged using fresh reactants and the same procedure was repeated for 5 times. 3% Ru/C catalyst was found to be highly active and showed an excellent performance up to the fourth recycle as shown in Figure 4.13, while after the fifth recycle, the activity dropped which could be due to sintering and/or agglomeration of the metal particles as shown in the TEM image (Figure 4.2).

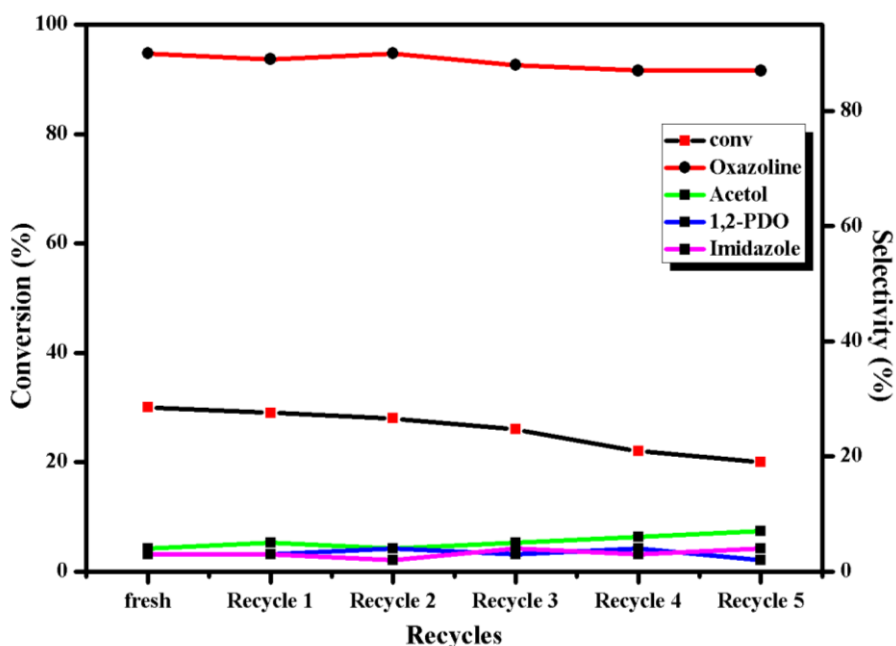


Figure 4.13 Recycling studies on the 3% Ru/C catalyst on cascade dehydrative amination of glycerol

Reaction conditions: Glycerol: 20.0 g, H₂O: 80.0 g, NH₃: 15 ml, Catalyst (3% Ru/C): 0.8 g, Temp.: 220 °C, Time: 5 h.

4.4 Conclusion

Herein, we report 3% Ru/C catalyst for single pot cascade novel strategy which coupled catalytic dehydration of glycerol and its subsequent ammonization directly convert glycerol to valuable oxazoline with high selectivity. In a single-step cascade process, supported Ru catalysts showed excellent activity and most importantly, stability against poisoning by ammonia. XPS studies and several other characterization techniques confirmed that the multivalent Ru association species functioned as a highly efficient catalyst that played a key role in the amination of glycerol. A moderate acid strength with high Brønsted acid density was beneficial for the reaction. Py-IR spectroscopy evidenced that increasing the B/L ratio led to better performance of 3% Ru/C with higher activity and oxazoline selectivity. Based on the catalyst characterization integrated with the activity results, a plausible reaction pathway was proposed. The first step of the reaction, glycerol dehydration, is mainly catalyzed by acid sites; further tautomerization to the keto form takes place by abstraction of the proton by metallic Ru to give acetol. The subsequent amination of acetol provides imine, which

undergoes cyclization with another molecule of acetol to obtain oxazoline. The effects of different variables such as metal and catalyst loadings, temperature, and solvents on the dehydrative amination of glycerol were also investigated.

4.5 References

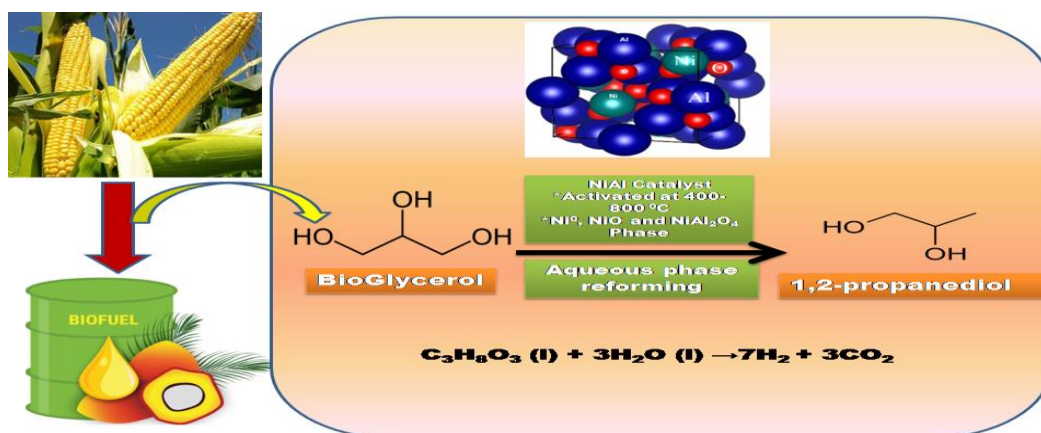
1. L. T. Mik, E. Csefalvay, A. Nemeth, *Chem. Rev.* 118 (2018) 505.
2. C. H. C. Zhou, J. N. Beltramini, Y. X. Fan, G. Q. M. Lu, *Chem. Soc. Rev.* 37 (2008) 527-549.
3. A. Behr, J. Eilting, K. Irawadi, J. Leschinski, F. Lindner, *Green Chem.* 10 (2008) 13-30.
4. M. Pagliaro, R. Ciriminna, H. Kimura, M. Rossi, C. Della Pina, *Angew. Chem.* 119 (2007) 4516-4522.
5. A. Padwa, J. K. Rasmussen, A. Tremper, *J. Am. Chem. Soc.* 98 (1976) 2605–2614.
6. W. J. Middleton, C. G. Krepsan, *J. Org. Chem.* 33 (1968) 3625–3627.
7. G. Prasad, K. N. Mehrotra, *J. Org. Chem.* 47 (1982) 2806–2807.
8. A. Domling, A. Bayler, I. Ugi, *Tetrahedron* 51 (1995) 755–760.
9. M. Ernst, B. W. Hoffer, J. P. Melder, US0240894A1 (2010).
10. V. M. Arredondo, P. J. Corrigan, A. C. Cearley, D. J. Back, M. S. Gibson, N. T. Fairweather, US7619119B2 (2009).
11. W. Himmele, L. Hupfer, H. Toussaint, G. Paul US4105669 (1978).
12. J. A. Frump, *Chem. Rev.* 71 (1971) 483–505.
13. G. C. Hargaden, P. J. Guiry, *Chem. Rev.* 109 (2009) 2505-2550.
14. X. H. Huang, L. X. Tao, C. Q. Ke, C. Tang, H. Y. Zhang, Y. Ye, L. G. Lin, S. Yao, *Org. Lett.* 19 (2017) 556–559.
15. D. J. Hart, N. A. Magomedov, *J. Am. Chem. Soc.* 123 (2001) 5892–5899.
16. J. L. Liu, L. J. Zhu, Y. Pei, J. H. Zhuang, H. Li, H. X. Li, M. H. Qiao, K. N. Fan, *Appl. Catal. A* 353 (2009) 282–287.
17. C. Sui, F. Yuan, Z. Zhang, C. Zhang, X. Niu, Y. Zhu, *Catalysts* 6 (2016) 173–191.
18. M. Wang, H. Yang, Y. Xie, X. Wu, C. Chen, W. Ma, Q. Dong, Z. Hou, *RSC Adv.* 6 (2016) 29769–29778.
19. E. S. Vasiliadou, E. Heracleous, I. A. Vasalos and A. A. Lemonidou, *Appl. Catal. B* 92 (2009) 90–99.
20. T. W. Hansen, P. L. Hansen, S. Dahl and C. J. H. Jacobsen, *Catal. Lett.* 84 (2002) 7–12.

21. J. Feng, H. Fu, J. Wang, R. Li, H. Chen and X. Li, *Catal. Commun.* 9 (2008) 1458–1464.
22. J. Wambach, M. Schuberta, M. Döbelib, F. Vogel, *Chimia* 66 (2012) 706–711.
23. I. A. Carbajal-Ramos, M. F. Gomez, A. M. Condó, S. Bengiío, J. J. Andrade-Gamboa, M. C. Abello, F. C. Gennari, *Appl. Catal. B* 181 (2016) 58–70.
24. J. Y. Shen, A. Adnot, S. Kaliaguine, *Appl. Surf. Sci.* 51 (1991) 47–60.
25. M. A. Sánchez, V. A. Mazzieri, M. A. Vicerich, C. R. Vera, C. L. Pieck, *Ind. Eng. Chem. Res.* 54 (2015) 6845–6854.
26. T. Finke, M. Gernsbeck, U. Eisele, C. Vincent, M. Hartmann, S. Kureti, H. Bockhorn, *Thermochim. Acta* 473 (2008) 32–39.
27. Z. M. El-Bahy, R. Ohnishi, M. Ichikawa, *Appl. Catal. B* 40 (2003) 81–91.
28. J. Mehlig, *Ind. Eng. Chem. Anal. Ed.* 13 (1941) 533–535.
29. S. Wang, K. Yin, Y. Zhang, H. Liu, *ACS Catal.* 3 (2013) 2112–2121.
30. R. R. Davda, J. W. Shabaker, G. W. Huber, R. D. Cortright, J. A. Dumesic, *Appl. Catal. B* 43 (2003) 13–26.
31. E. S. Vasiliadou, E. Heracleous, I. A. Vasalos, A. A. Lemonidou, *Appl. Catal. B* 92 (2009) 90–99.
32. T. Miyazawa, Y. Kusunoki, K. Kunimori, K. Tomishige, *J. Catal.* 240 (2006) 213–221.
33. M. Balaraju, V. Rekha, P. S. S. Prasad, B. L. A. P. Devi, R. B. N. Prasad, N. Lingaiah, *Appl. Catal. A* 354 (2009) 82–87.
34. S. Li, M. Wen, H. Chen, Z. Ni, J. Xu, J. Shen, *J. Catal.* 350 (2017) 141–148.
35. A. Martin and M. Richter, *Eur. J. Lipid Sci. Technol.* 113 (2011) 100–117.
36. M. G. Musolino, L. A. Scarpino, F. Mauriello, R. Pietropaolo, *Green Chem.* 11 (2009) 1511–1513.
37. D. Roy, B. Subramaniam, R. V. Chaudhari, *Catal. Today* 156 (2010) 31–37.
38. T. Hirai, N. Ikenaga, T. Miyake, T. Suzuki, *Energy Fuels* 19 (2005) 1761–1762.

Chapter 5

Role of catalyst pre-treatment in aqueous-phase reforming of glycerol to propylene glycol

Supported nickel-based catalysts were investigated for aqueous-phase reforming (APR) of glycerol. A series of Ni catalysts supported on different support (C, Al₂O₃, ZnO₂, Mont, ZrO₂ or SiO₂) were prepared by wet impregnation method and tested in glycerol APR which gave in situ glycerol hydrogenolysis product, 1, 2-propanediol (propylene glycol) at 220 °C for 5 h in a batch reactor. The effects of catalyst reduction temperature (between 400-800 °C) on physicochemical properties of NiAl catalyst were investigated and tested for APR of glycerol. The excellent activity performance of the catalyst was explained based on its detailed characterization by XRD, XPS, NH₃-TPD and Py-IR. Under APR conditions, dehydration of glycerol to acetol and in situ reforming of glycerol to hydrogen was considered to occur synergistically. This hydrogen produced *In situ* is then available for producing 1, 2-PDO from acetol. Under these conditions, the Ni/Al₂O₃ activated at 600 °C catalysts exhibited the highest glycerol conversion, 35 %, with propylene glycol yield around 40 %. The good stability of the spinel phase of the studied catalyst helps in recycling experiments without any significant loss of catalytic activity.



5.1 Introduction

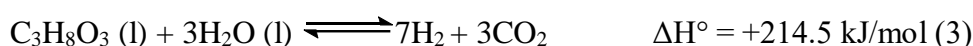
For the last couple of decades, several efforts have been made towards the development of carbon-neutral hydrogen by utilizing biomass [1]. These green and renewable sources are beneficial for the substitution of non-renewable, polluting fossil energy sources as already discussed in chapter 1 (section 1.3.1). During the last decades, APR of biomass derived oxygenated compounds (sugars, sugar alcohols, and glycerol) represents a green and effective method for hydrogen production [2].

The large scale production of biodiesel has forced us to think of glycerol (GLY) transformation into high value products, as it is a low-cost, ever increasing by-product of biodiesel industry. However; it is still a key challenge to develop efficient processes for converting glycerol into commercially valued products [3]. Among possible downstream products from glycerol, hydrogen production from glycerol has been considered as an attractive process [4]. Some of the reforming techniques used to produce hydrogen from glycerol include APR, steam reforming (SR), pyrolysis, gasification, and supercritical water [5-8]. Based on the nature of catalyst and reaction conditions, glycerol APR leads to in-situ hydrogenation to produce various industrially important products such as acetol, 1, 2-propanediol (1, 2-PDO), 2-propanols (2-Prop) and ethylene glycol (EG). These chemicals are useful in many industrial applications such as industrial solvent, thermo set plastics, antifreeze, flavours and fragrances, and approved additive in food, cosmetic and pharmaceutical industries as discussed in section 1.5 [9].

Ideally, glycerol APR involves two parallel reactions, which leads to CO and H₂ by C–C cleavage [10]:



The overall APR reaction is the sum of Reactions (1) and (2):



And the methanation reactions,





Thus the most favoured catalyst for hydrogen production is the one that promotes cleavage of C-C and C-H bond followed by WGS reaction, with the least activity towards methanation reaction i.e. C-O bond breaking [11]. Generally, Pt, Pd and Group VIII metals are preferred for higher APR activity [12, 13].

Supported Pt catalysts are known to be active for C-C and C-H cleavage and thus used for H₂ production by APR of oxygenated hydrocarbons [14] but have significant activity towards methanation reaction [15]. In addition, due to the high cost, use of pt based catalysts becomes prohibitive for commercial exploitation [16-18].

In recent years, non-noble nickel based catalysts has attracted more attention for APR process due to its low cost and higher activity in C-C scission, which increases with smaller particles [19-22]. However, Nickel supported on conventional γ -alumina has been widely studied, but under APR hydrothermal conditions, it shows low stability due to catalyst deactivation where it is transformed into more acidic bohemite (AlOOH) phase by hydration [23].

The nature of oxide supports also influence catalytic activity of the glycerol APR [24, 25]. Nickel aluminate (NiAl₂O₄) is partially inverted spinel structure in which Ni²⁺ ions occupy the octahedral sites and Al³⁺ in tetrahedral sites [26]. In addition, the reduction step can alter the structural and catalytic properties and also have a great impact on the particle size and dispersion of Ni [27]. Thus, better catalytic behaviour could be obtained if metal support interaction is improved [28]. During the reduction process, the formation of oxygen vacancy induces microstructural changes with high concentration of metallic nickel particles on the surface. This would prevent sintering by creating a nickel aluminate layer between Ni and the alumina. [29].

It is well known that altering the reduction temperature influence the arrangement of Ni in the aluminate matrix, where Ni crystallites are smaller and stable [30, 31]. However, detailed parametric studies and the role of activation temperature for aqueous phase reforming has not been studied so far to systematically explore the concept and demonstrate the potential advantages of aqueous phase reforming.

In this chapter, nickel aluminate spinel was synthesized by an incipient wetness impregnation method with a stoichiometric mole ratio of nickel to alumina mole ratio and the effect of reduction temperature on the catalytic behaviour in glycerol aqueous phase reforming was evaluated. Further studies of process parameters for APR of glycerol *viz.* glycerol concentration, temperature and catalyst concentration are also presented.

5.2 Experimental

10% Ni catalysts on different supports were prepared by wet impregnation method. In a typical preparation, $\text{Ni}(\text{NO}_3)_2$ were dissolved in DI water, and a known amount of powdered support was added afterward. After 1 h of rotation for homogenization, the water was removed by evaporation at 80 °C under vacuum. Finally, the obtained material was dried at 110 °C for 12 h, calcined at 400 °C for 3 h and activated at 400°C for 12 h. For NiAl, the catalysts were reduced in a horizontal oven, under H_2 atmosphere (flow rate of 10 mL min⁻¹) at different temperatures: 400, 600 and 800 °C (these samples were labelled as NiAl-400, NiAl-600 and NiAl-800 respectively). Nickel nitrate, 1, 2-propanediol and acetol were purchased from Sigma-Aldrich, India. Nitrogen and hydrogen gas cylinder (purity 99.99%) was purchased from M/s. Inox Ltd. Mumbai. Zirconia, alumina and fumed silica were supplied by Loba Chemie, India. Various techniques were used to characterize the catalyst, which is discussed in chapter 2 (Section 2.4). The catalytic test for glycerol hydrogenolysis to 1, 2-PDO was performed in a batch reactor and the experimental details are discussed in chapter 2 (section 2.5.2). Liquid samples were analysed by gas chromatography to monitor progress of the reaction (chapter 2, section 2.6).

5.3 Results and discussion

5.3.1 Characterization techniques

From the various Ni catalysts supported on different support (C, Al_2O_3 , ZnO_2 , Mont, ZrO_2 or SiO_2) screened for this work, 10% Ni supported on Al_2O_3 showed the excellent activity and selectivity for APR of glycerol. Therefore, their characterization attempted to identify active sites within these catalysts and the data were compared with the catalytic activity of other catalysts.

5.3.1.1 X-ray diffraction

The XRD spectra of Ni supported on Al_2O_3 reduced at different activation temperatures are shown in Figure 5.1. All samples showed characteristic peaks for $\gamma\text{-Al}_2\text{O}_3$ at $2\theta = 37.7^\circ$ and 66.5° (JCPDS 86-1410). The characteristic peaks of cubic spinel structure NiAl_2O_4 were ascribed by diffraction peak at $2\theta = 19.0^\circ$, 45.1° , 59.6° (440) (JCPDS 78-1601). Nickel aluminate formation suggests a strong interaction between metal and support [31]. No characteristic nickel oxide (NiO) peak (expected at $2\theta = 43.5^\circ$ and 63.1°) was reported in any samples, suggesting either low content or smaller crystallite size, which is below the detection range of XRD [32].

It is interesting to note that on increasing the reduction temperature from 400 to 800 °C, the intensities of Al_2O_3 and NiAl_2O_4 peaks decreased and small peaks appeared at $2\theta = 44.5^\circ$, 51.8° and 76.4° representing the formation of metallic nickel (JCPDS 01-087-0712). The intensity of peaks corresponds to metallic Ni increased with an increase in reduction temperature from 400 to 800 °C [33]. It was also observed that the presence of peaks relevant to both NiAl_2O_4 and metallic nickel phases at given 2θ in the NiAl-600 changes with an increase in the reduction temperature (NiAl-800) and resulted in a slight decrease in peaks for nickel aluminate at $2\theta = 19.0^\circ$, 45.1° , 59.6° , while the peak intensity at $2\theta = 44.5^\circ$, 51.8° , 76.4° increased, which represented metallic nickel (JCPDS 79-1558).

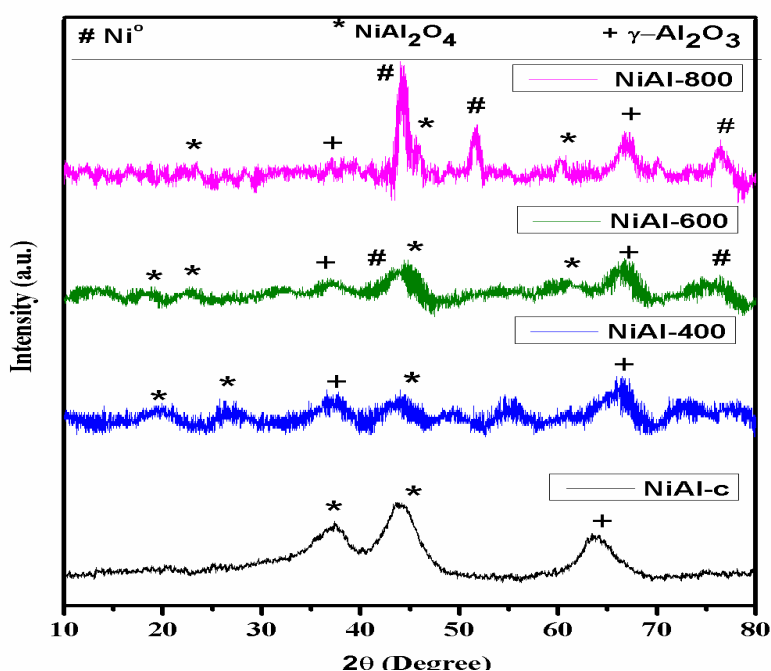


Figure 5.1 XRD spectra of activated NiAl catalysts at different temperature: (a) NiAl-calcined (b) NiAl-400 (c) NiAl-600 and (d) NiAl-800

5.3.1.2 BET surface area

The activation temperature influenced the BET surface areas of the alumina supported Ni samples reduced at different temperatures, showing a descending trend as follows: Bare- Al_2O_3 (130) > Ni-Al-400 ($98 \text{ m}^2 \text{ g}^{-1}$) > Ni-Al-600 ($95 \text{ m}^2 \text{ g}^{-1}$) > Ni-Al-800 ($90 \text{ m}^2 \text{ g}^{-1}$). This was mainly because of blocking of support pore after Ni loading due to slight aggregation of the Ni particles (TEM images) on the support, with an increase in reduction temperature.

5.3.1.3 HRTEM

Tem image of the reduced $\text{Ni}/\text{Al}_2\text{O}_3$ catalysts used to obtain information about the morphology and particle size distribution (Figure 5.2). For all samples, metallic Ni having a

particle size in the range of 5-8 nm. It is evident from the previous literature that NiAl_2O_4 exerted a positive effect on Ni sintering [34] by stabilizing the Ni particles against sintering and reduce their surface mobility. This also suggests the strong interaction of nickel with nickel aluminate than that with the alumina [31].

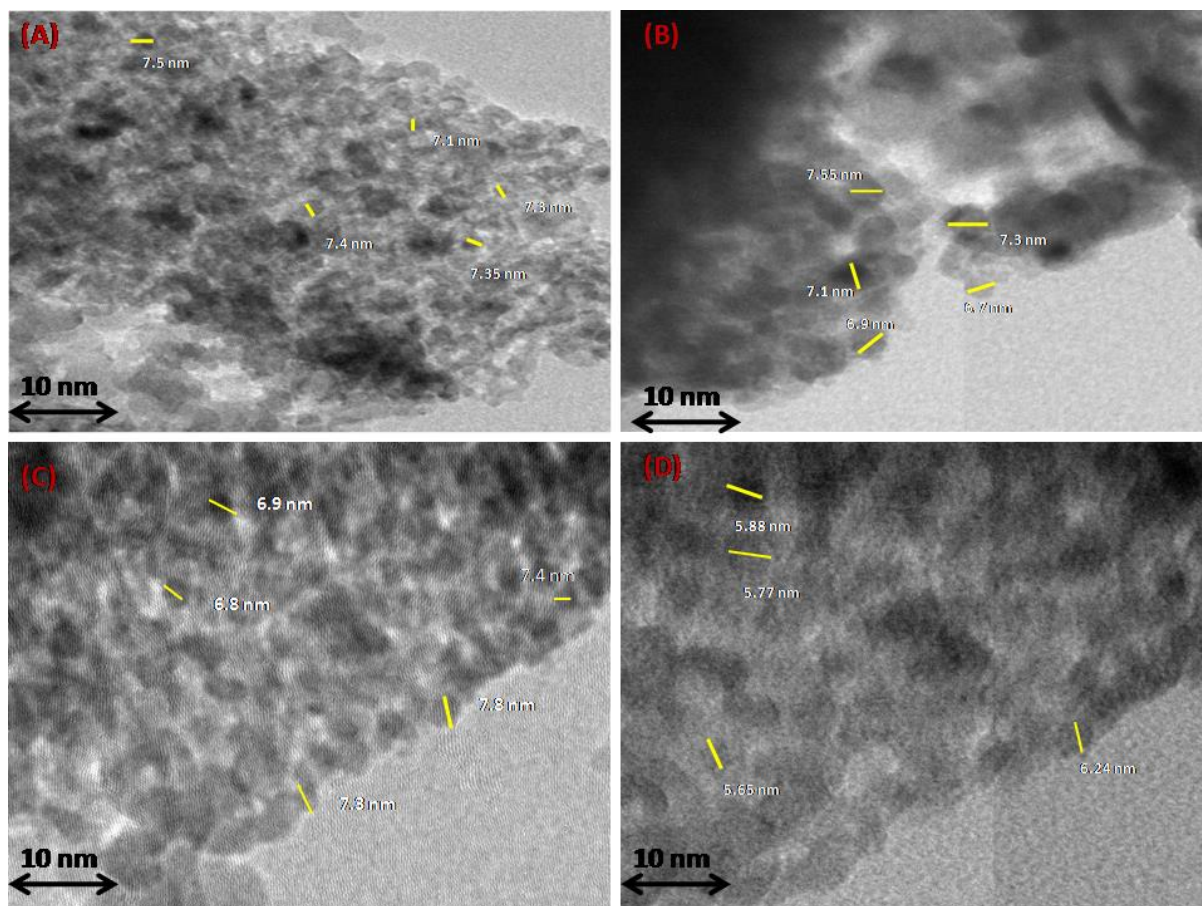
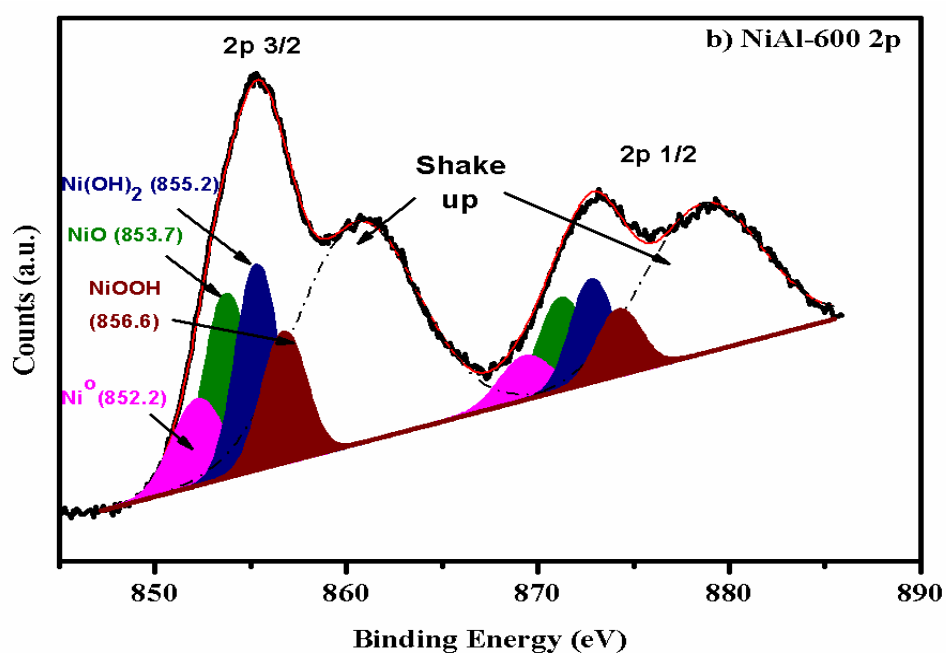
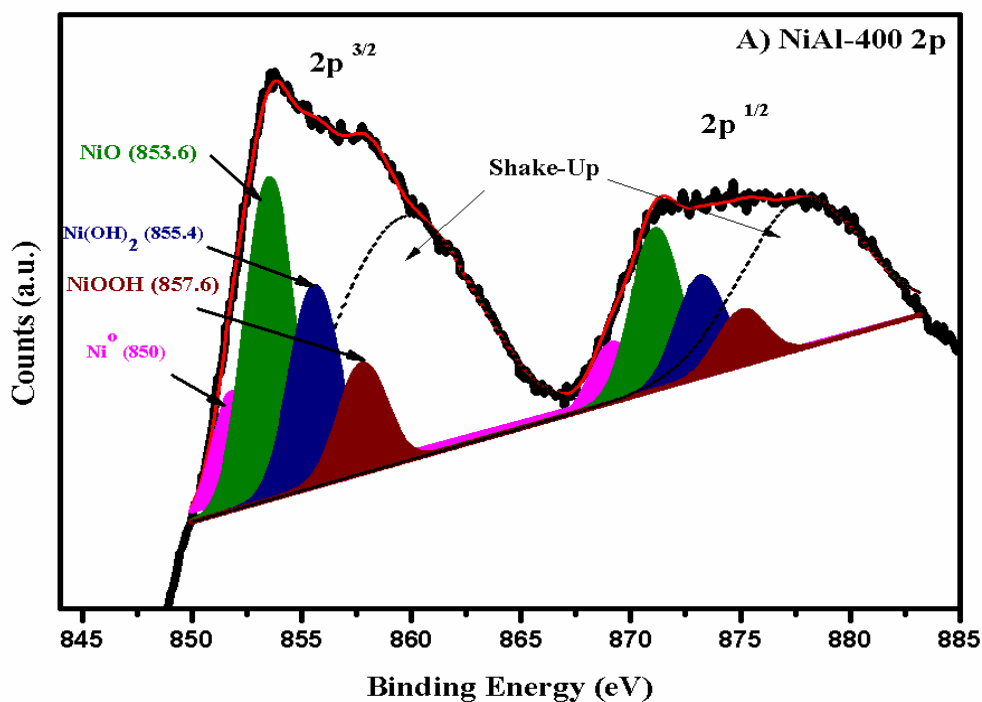


Figure 5.2 TEM images of activated NiAl catalysts at different temperature: (a) NiAl-calcined (b) NiAl-400 (c) NiAl-600 and (d) NiAl-800

5.3.1.4 XPS

The Ni 3p high-resolution XPS spectrum of $\text{Ni}/\text{Al}_2\text{O}_3$ catalysts reduced at various temperatures (Figure 5.3) shows that the electronic states of Ni varied with a change in the activation temperature. These spectra revealed the presence of different oxidation states of Ni, viz. Ni^0 , NiO , $\text{Ni}(\text{OH})_2$, and NiOOH . It seems that the applied experimental conditions for activation did not completely reduce the NiO into Ni^0 . The intense satellite peak found at

the high binding energy side of the Ni $2p_{3/2}$ spectrum is due to multi electron excitation [35]. Ni $2p_{3/2}$ XPS spectra for Ni⁰, NiO, Ni(OH)₂, and NiOOH have binding energies of 850, 853.6, 855.4 and 857.6 eV respectively. Based on previous studies, the deconvoluted XPS spectra for Ni $3p_{1/2}$ also shows binding energy values of 279.9, 281.1 and 283.3 eV with a spin-orbit splitting of 17.5 eV [36].



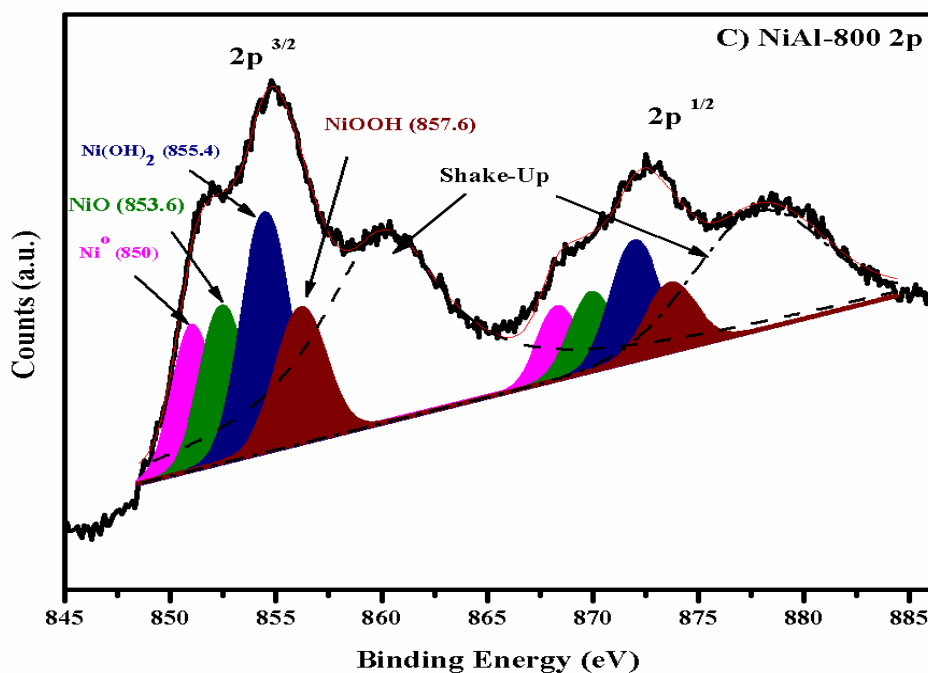


Figure 5.3 XPS spectra for the Ni 3p region (a) NiAl-400 (b) NiAl-600 (c) NiAl-800

XPS provides details about the surface elemental composition, which is a very critical parameter, in order to understand the catalytic activity of the sample. The area obtained from deconvoluted spectrum shows that reduction temperature affects Ni metal reducibility (Table 5.1). The percentage of Ni⁰ species calculated based on deconvoluted spectra of Ni 2p_{3/2} and Ni 2p_{1/2} varied depending on the temperature used for the activation showing an increasing trend as follows: Ni-Al-400 (13%) < Ni-Al-600 (16%) < Ni-Al-800 (18%). The reduction temperature parallelly affects the nickel contents of these samples as expected from their increasing nickel contents. The presence of oxide species of Ni with respect to Ni⁰ in all the three samples played a major role in the catalysts activity, as discussed later.

Table 5.1 Effect of activation temperature on the % of Ni⁰ from XPS curve fitting data of the Ni 2p peak

Catalyst	Area of different species present on the surface (%)			Ni ⁰ /Σarea of oxide species of Ni
	Ni	Ni ⁺² (As NiO)	Ni ^{2+/3+} (as Ni(OH) ₂ /NiOOH)	
NiAl-400	13	43	44	15
NiAl-600	16	30	54	19
NiAl-800	18	21	61	23

5.3.1.5 NH₃-Temperature programmed desorption

As the acid sites also play an important role in aqueous phase reforming of glycerol, their strength was determined by NH₃-TPD. Figure 5.4 and Table 5.2 represent the NH₃-TPD profiles and acid strengths of the bare alumina and supported Ni catalysts activated at different temperatures. In this study, weak, medium and strong acid sites correspond to the peaks observed in the low (below 250 °C), medium (250-500 °C) and high temperature (above 500 °C) regions, respectively.

The low intensity peak of ammonia desorption in the 50–200 °C range indicates the presence of weak acid sites in all samples. The NH₃-TPD of both NiAl-400 And NiAl-600 catalysts shows a broad peak of NH₃ desorption in the higher temperature region of 300 and 450 °C respectively, indicating the presence of moderate acid sites. The reaction of reduced Ni with strong acid sites induces a reduction of Ni to NiO and thus slight shift is observed in the moderate acidity region [37]. NiAl-800 showed a very small and low-intensity peak representing the minimal amount of moderate acidic sites. The fact that the moderate acidic sites decreased in NiAl-800 compared to NiAl-600 sample suggested that density of Ni^{+2/+3}.

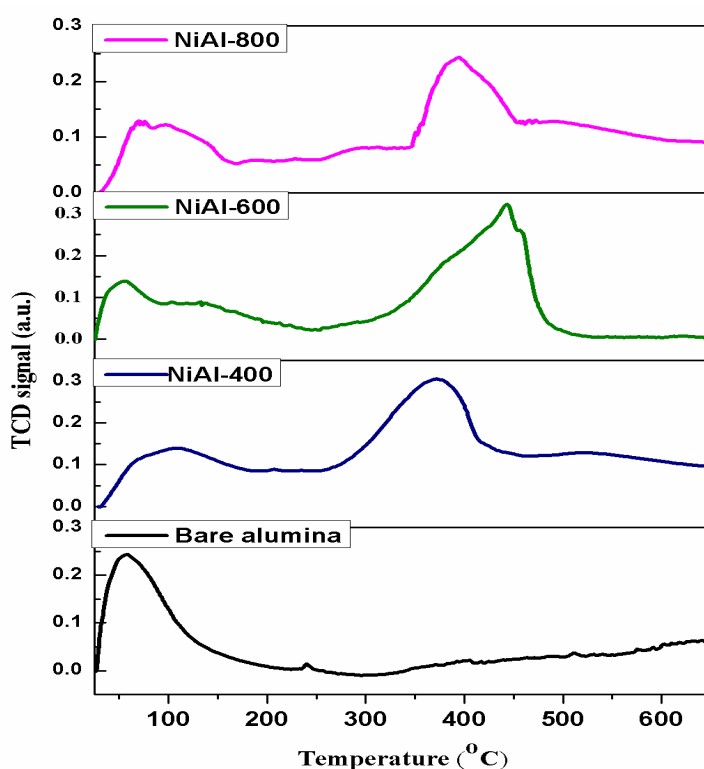


Figure 5.4 NH₃-TPD profiles of NiAl catalysts activated at different temperature

Table 5.2 NH₃-TPD results of NiAl catalysts activated at different temperature

Sr. No.	Catalysts	Total NH ₃ desorbed (mmol g ⁻¹)	Temperature range-wise desorption of NH ₃ (mmol g ⁻¹)		
			40-200 °C	200-500 °C	500-800 °C
1	Al ₂ O ₃	0.20	0.30	-	-
2	NiAl-400	1.1	0.424	0.685	-
3	NiAl-600	1.5	0.414	1.112	-
4	NiAl-800	1.3	0.450	0.875	

These results indicate that at high activation temperature, Ni⁰ surface density increased as revealed by XRD and XPS. It can be concluded that these differences in the acidic properties have significant impact on catalyst performance as discussed later.

5.3.1.6 Pyridine infrared (Py-IR) spectroscopy

The distinction between Brønsted and Lewis acid sites of the supported Ni catalysts was observed by pyridine infrared (Py-IR) spectroscopy. The qualitative measurement of Brønsted and Lewis acid sites was done by subtracting the spectra recorded before and after pyridine adsorption (Figure 5.5).

For all the NiAl catalysts, the bands appearing at 1542 and 1456 cm⁻¹ were due to pyridine adsorbed on Brønsted and Lewis acid sites, respectively. Table 5.3 summarize the Py-IR results of NiAl catalysts. Quantitative determination of Brønsted and Lewis surface acidity was done using the method proposed by Emeis as discussed in chapter 2 (section 2.4.6). The ratio of Brønsted to Lewis acid sites of these samples decreased as follows: NiAl-400 > NiAl-600 > NiAl-800. However, Lewis acidity of catalyst was almost constant but the Brønsted acidity decreased with an increase in activation temperature. The strength of the B acid and the B/L ratio has a notable impact on the catalyst activity and product selectivity.

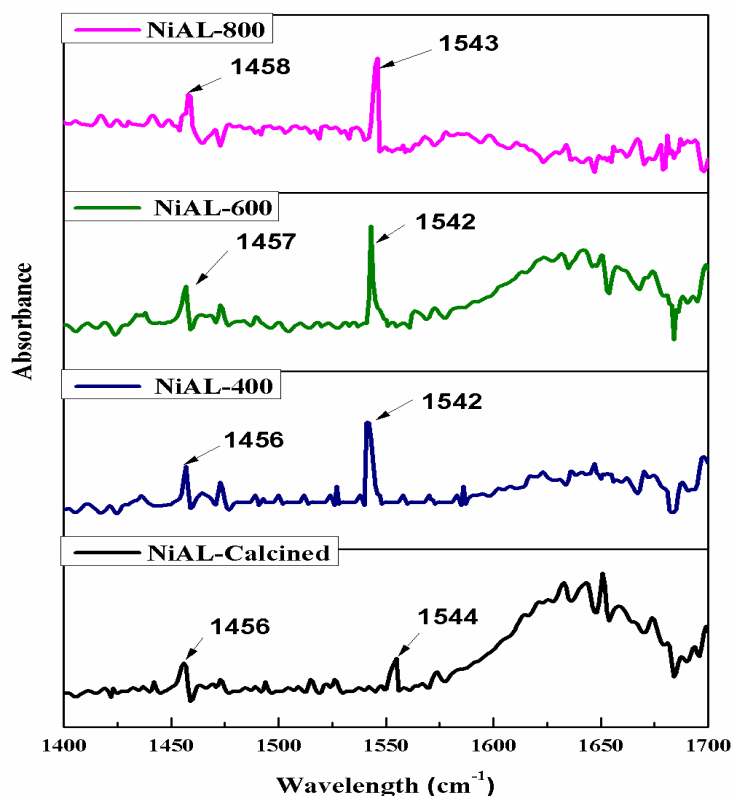


Figure 5.5 Py-IR profiles of NiAl catalysts activated at different temperature

Table 5.3 Py-IR spectroscopy results of NiAl catalysts activated at different temperature

Entry No.	Catalyst	Acidity ^a ($\mu\text{mol pyridine per g cat}$)		
		B	L	B/L
1	NiAl-C	0.35	0.29	1.20
2	NiAl-400	0.39	0.28	1.39
3	NiAl-600	0.38	0.28	1.35
4	NiAl-800	0.36	0.27	1.33

^aAcidity calculated from the extinction coefficients given in chapter 2 (section 2.4.6). L= Lewis acid sites. B=Brønsted acid sites.

5.3.2 Activity testing

The preliminary results on the screening of various Ni supported catalysts and the effect of activation temperature of NiAl catalysts on its performance for aqueous phase reforming of glycerol are presented in Table 5.4.

Table 5.4 Catalyst activity for APR of glycerol

Sr. NO.	Catalyst	Con.	1,2 PDO	EG	ACETO L	2- PROP ANOL	Metha nol	Etha nol
APR 1	Ni/C	25	23	7	54	10	2	4
APR 2	Ni/ZrO ₂	15	15	7	65	6	1	6
APR 3	Ni/SiO ₂	16	20	6	60	4	5	5
APR 4	Ni/ZnO ₂	10	16	6	68	2	6	2
APR 5	Ni/Mont	6	10	3	58	16	9	3
APR 6	Ni/Al ₂ O ₃	34	29	6	52	7	3	3
APR 7	γ -alumina	-	-	-	-	-	-	-
APR 8	Ni/Al C	5	20	6	53	10	4	7
APR 9	Ni/Al-400	35	30	5	53	7	2	3
APR 10	Ni/Al-600	38	40	6	30	14	5	5
APR-11	Ni/Al-800	40	25	6	29	11	10	19

Reaction conditions: Glycerol: 10.0 g, H₂O: 90.0 g, Catalyst: 0.8 g, Temp.: 220 °C, Time: 5 h.

In order to understand the role of a catalyst, blank tests under the same reaction conditions but without a catalyst showed no glycerol conversion. In the case of an unreduced 10% Ni-Al₂O₃ catalyst (Ni/Al-C), substantially less activity was observed for the glycerol APR reaction.

Table 5.4 provides a comparison of the catalytic performances of Ni impregnated on various supports. The nature of the support significantly influence the conversion of glycerol and the selectivity to 1, 2-PDO. As Nickel is well known for aqueous phase reforming, Ni on various support (C, Al₂O₃, ZnO₂, Mont, ZrO₂ or SiO₂) were evaluated for the Apr of glycerol (Table 5.4). Various oxide supports used in this work can be categorized into three classes: Mont and ZnO₂ oxides are basic; Al₂O₃, SiO₂, ZrO₂ are acidic and C is nearly neutral [39]. The Ni catalysts supported on Al₂O₃ showed the highest conversion of glycerol (34%) with 29% 1, 2-PDO selectivity, compared to the nickel on other support, although the loading amount was constant (Table 5.4). The catalytic activities of Ni-based catalysts increased as Ni/Mont < Ni/ZnO₂ < Ni/SiO₂ \approx Ni/ZrO₂ < Ni/C < Ni/Al₂O₃ (Table 5.4). The results showed that acidic support was more favourable for the Ni-based catalysts than the basic support for the formation of 1, 2-PDO.

Among several other catalysts, Ni supported on alumina was chosen in this work, because of its highest ability for catalyzing hydrogenation–dehydrogenation, due to acid properties

contributing to its bifunctional nature [40, 41]. The catalytic performance for Ni-Al₂O₃ reduced at different temperatures is shown in Figure 5.6. The temperature of catalyst pre-treatment for activation influences the degree of reduction and consequently the catalytic performance of the NiAl samples.

It was observed that the catalyst reduced at the lowest temperature (NiAl-400) mainly favour dehydration reactions and the major product were hydroxyacetone together with small amounts of methanol and ethanol.

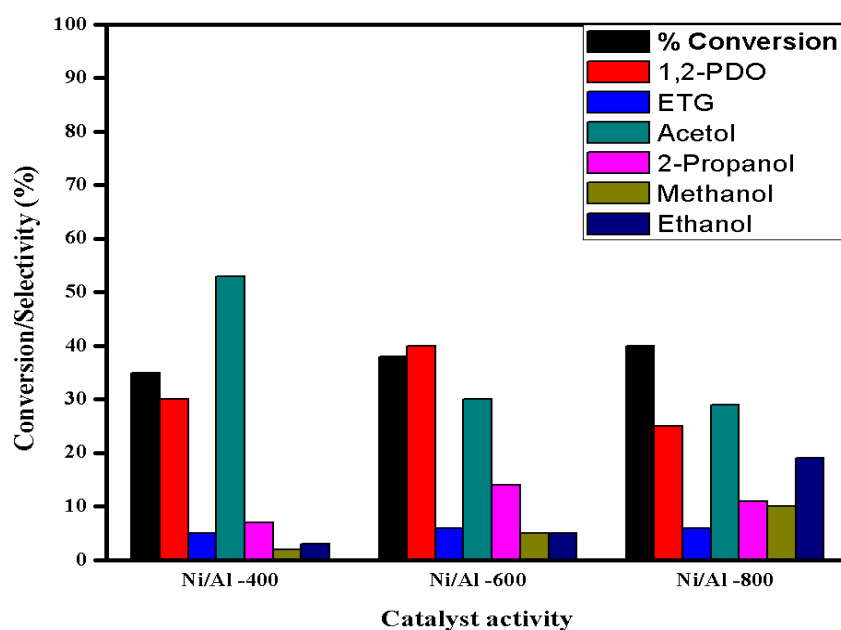


Figure 5.6 Catalyst activity of NiAl catalysts activated at different temperature

Reaction conditions: Glycerol: 10.0 g, H₂O: 90.0 g, Catalyst: 0.8 g, Temp.: 220 °C, Time: 5 h.

For NiAl-600, the main liquid products are found to be 1, 2-PDO (40%), hydroxyacetone (30%), 2-propanol (14%), ethylene glycol (6%), and much lesser concentration of ethanol (5%) and methanol (5%). Additional dehydration and hydrogenation of 1, 2-propylene glycol in the presence of hydrogen can result in 2-propanol formation [43] as shown in Scheme 5.1. This conversion of glycerol relies on many complex processes including dehydrogenation, dehydration and hydrogenolysis reactions [42].

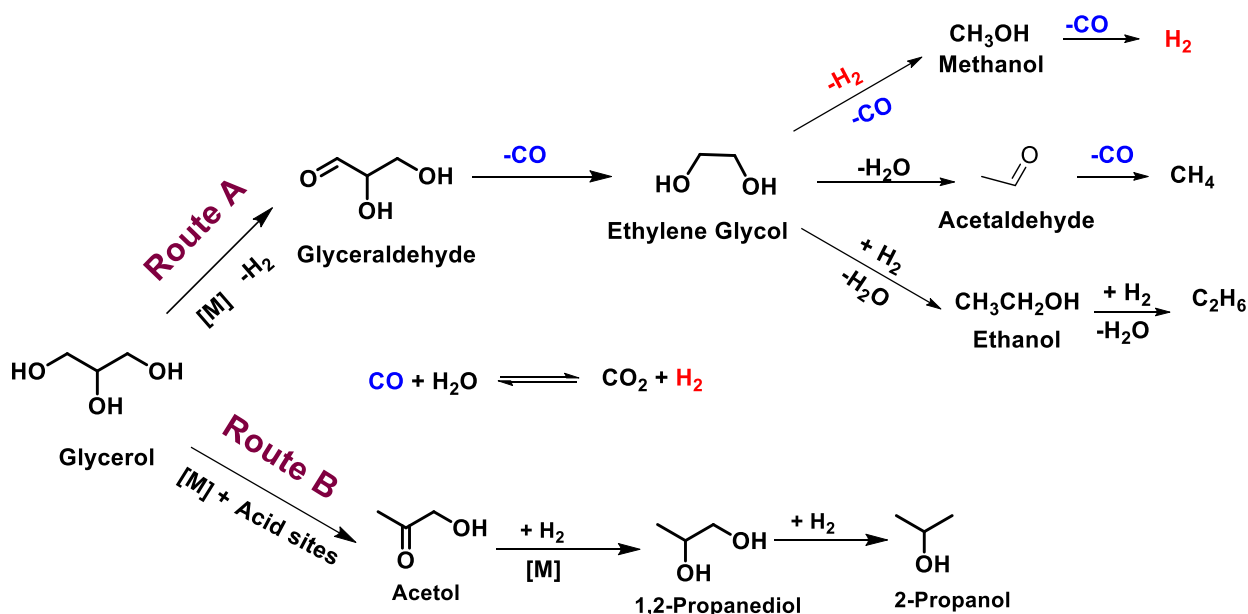
Higher activation temperature of the catalyst adversely affects the liquid phase product distribution. For the catalyst reduced at 800 °C (NiAl-800), the conversion of 1, 2-PDO dropped from 40% to 25% as the reduction temperature increased. In contrast, the production of methanol and ethanol increased in proportional quantities.

It was interesting to know that even though the surface area and particle sizes of catalysts (NiAl-400, NiAl-600 and NiAL-800) were almost similar but there is a wide difference in their activities (Figure 5.6). This suggests that the catalysts performance trend cannot be explained solely based on surface area and particle size but some other factors such as acidity and the oxidation state of the Ni species influence the catalytic activities. Strong acid sites of NiAl-600 are also essential for the reaction and played an important role in catalysing the glycerol dehydration to acetol in the first step which was acid catalysed. It was found that NiAl-600 showed highest acidity among NiAl-400 and NiAl-800, leading to highest 1, 2-PDO selectivity with 38% conversion of glycerol. The reason for slight increase in acidity was partial reduction of Ni species during the activation process, which generate new oxidized species. Surprisingly, the NiAl-800 catalyst possessed strong B acidity and a high B/L ratio yet it showed less selectivity of 1, 2-PDO than of NiAl-600 catalysts. This implies that the catalysts having strong acidity with a moderate ratio of B to L acid sites are sufficient for glycerol conversion to 1, 2-PDO. These trends are strongly in agreement with our XPS and XRD data as discussed above.

In the glycerol APR, the acid sites as well as the metal sites are crucial for the initial activation of glycerol. XPS analysis of NiAl catalyst activated at different temperatures showed the presence of both metallic Ni and Ni^{2+/3+} species. The area percentage of different species present on the surface plays a crucial role in defining the activity of catalyst. The percentage of NiO progressively decreased with the reduction temperature with area percentage in order of NiAl-400 (43%) > NiAl-600 (30%) > NiAL-800 (21%). From the XRD and XPS, it was observed that Ni species were present in different forms like nickel spinel phase, surface free nickel oxide, Ni^{2+/3+} in nonstoichiometric spinel. Previous research by Braidy et al. [44] concluded that diffusion of Ni in nonstoichiometric spinel forms NiAl₂O₄ and metallic Ni eventually under H₂ atmosphere. Small particle size 6 - 8 nm of Ni calculated by TEM confirmed the diffusion of metallic nickel and its interaction with the bulk. According to the XPS, higher area percentage of the NiAl₂O₄ [NiAl-400 (44%) < NiAl-600 (51%) < NiAL-800 (64%)] revealed that majority of Ni exists as NiAl₂O₄ in the reduced catalyst. The coexistence of Ni⁰, Ni²⁺ and Ni³⁺ species in this catalyst was responsible for

improved activity in APR of glycerol due to its multifunctional ability to catalyze C–C cleavage, dehydration and hydrogenation reactions.

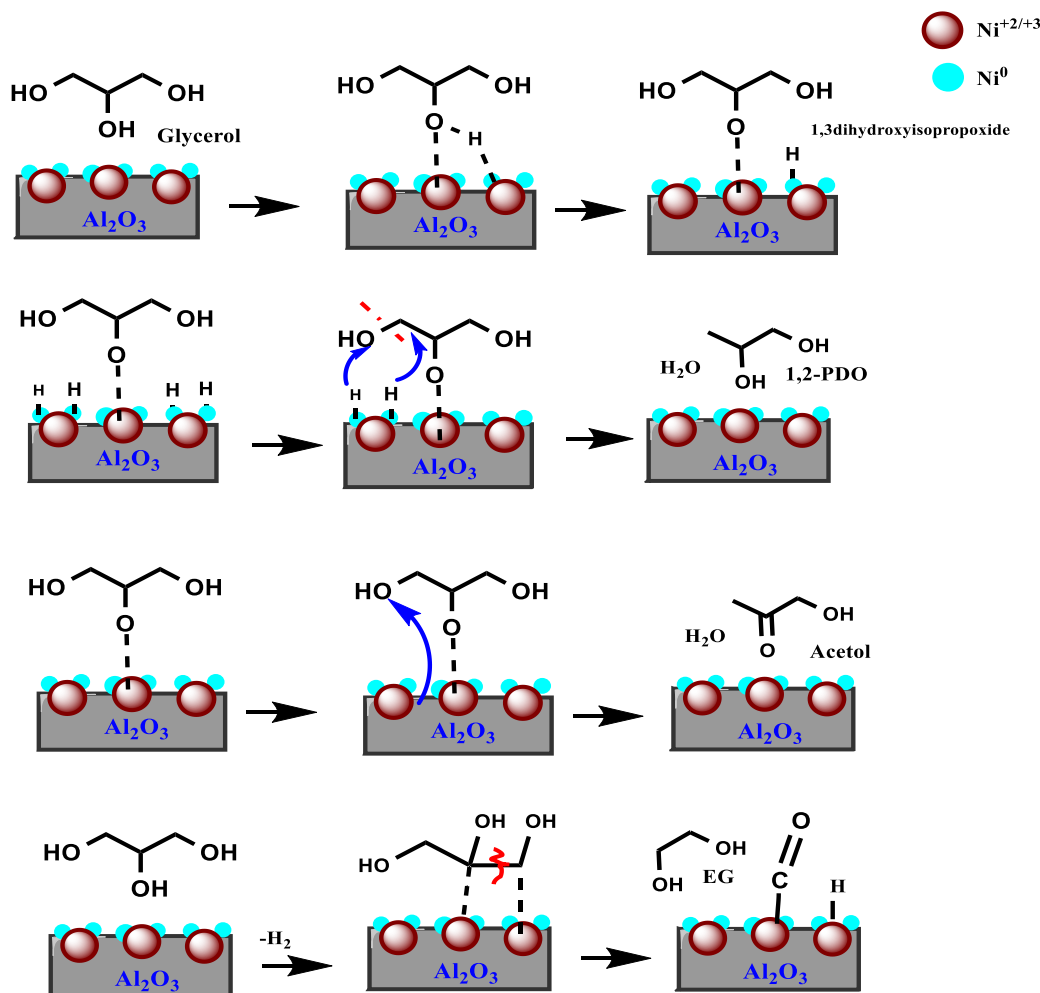
Two reaction routes (A and B) for glycerol hydrogenolysis have been proposed involving dehydration and dehydrogenation reactions (Scheme 5.1). In route B, glycerol dehydrates to acetol (over acid sites) and then hydrogenates in a second step to produce 1, 2-PDO (over metal sites), while excessive hydrogenolysis of 1, 2-PDO gives 2-propanol. In route A, glycerol leads to the formation of glyceraldehyde through dehydrogenation, which can further go through decarbonylation reactions to produce EG (on metal sites).



Scheme 5.1 Reaction pathway proposed for the glycerol APR on nickel catalyst

For instance, for catalysts reduced at lower reduction temperature (NiAl-400) mainly, dehydration products appeared and hydroxyacetone was the major product probably due to its slow hydrogenation rate. This reaction occurs via adsorption of terminal hydroxyl group of glycerol on Ni metal which is subsequently dehydrated to produce acetol over an acidic alumina supports (Scheme 5.2). In contrast, higher reduction temperature favours dehydrogenation products (methanol, ethylene glycol and ethanol) for NiAl-800, but a concomitant decrease of dehydration/ hydrogenation products (acetol and 1, 2-PDO) could be

confirmed. The mechanism involves C–C cleavage and further decarbonylation which is also reported by others [45]. However, increased yield of ethanol suggested that in-situ hydrogen was mainly consumed in hydrogenolysis reactions



Scheme 5.2 Proposed reaction pathway for hydrogenation/dehydration and dehydrogenation of glycerol with aqueous phase reforming over Ni-Al catalyst

Hence to maintain the balance between dehydration/hydrogenation products and dehydrogenation products an intermediate temperature was selected for the activation of catalyst (NiAl-600). Here, hydrogen produced during APR is transferred to terminal carbon of the glycerol and both glycerol and hydrogen undergo surface reaction on Ni sites. Here the protonation of the terminal hydroxyl group of glycerol facilitating C–O bond cleavage followed by subsequent hydrogenation to yield 1, 2-PDO on metal sites [46]. Thus the activation temperature of catalyst plays a significant role in the production of 1, 2-PDO, which was formed through the dehydration/hydrogenation route.

From the characterization data and the activity results, the best catalytic performance was exhibited by NiAl-600 as it possessed both metallic Ni and Ni oxide species, moderate Brønsted acid sites with strong acidity probably being active sites leading to excellent performance. In addition, the effect of various process parameters on conversion of glycerol to 1, 2-PDO was determined over the NiAl-600 catalyst.

5.3.3 Process optimization studies

For APR of glycerol, NiAL-600 was found to be the most efficient catalyst. In addition, the effect of process parameters *viz.* metal loading, glycerol concentration and temperature on conversion of glycerol to 1, 2-PDO were determined over NiAl-600 catalyst and the results are discussed below.

5.3.3.1 Effect of metal loading

The effect of Ni loading (10–40%) on APR of glycerol at 220 °C is illustrated in Figure 5.7. The glycerol conversion increases linearly from 33% to 40% with increment in Ni loading (10–40%). However, selectivity of 1, 2-PDO decreased to 20% from 28% at the highest Ni loading of 40%, due to the sintering of Ni particles at higher loading.

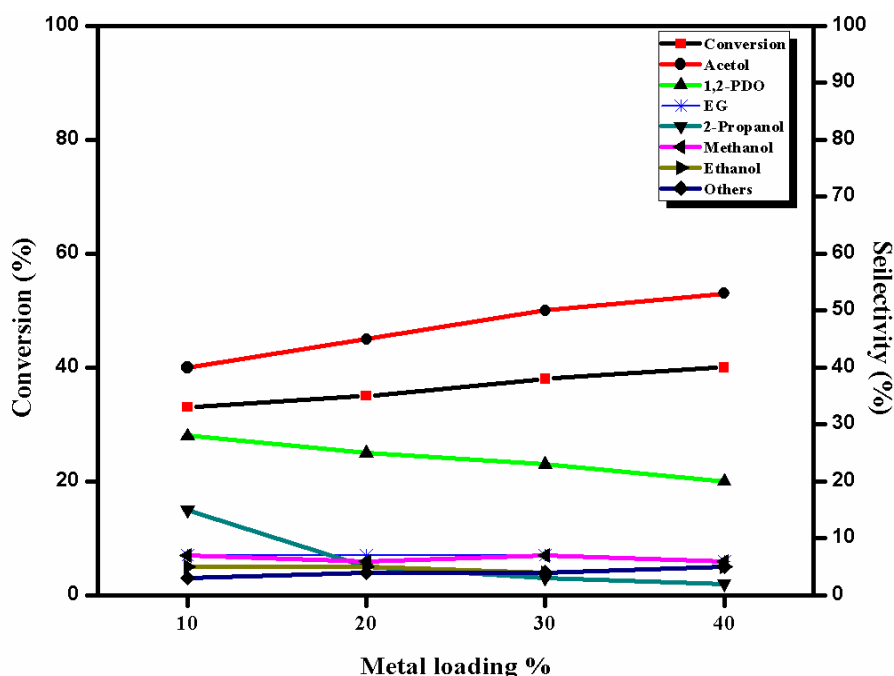


Figure 5.7 Effect of metal loading on glycerol APR reaction

Reaction conditions: Glycerol: 10.0 g, H₂O: 90.0 g, Catalyst (NIAI-600): 0.8 g, Temp.: 220 °C, Time: 5 h.

5.3.3.2 Effect of glycerol concentration

Feed concentration is a crucial parameter in the economical evaluation of any reactions. Figure 5.8 summarized the influence of glycerol concentration on the APR of glycerol in the range of 10–30 wt%, at a constant temperature of 220 °C. Glycerol conversion decreases from 32 % to 20%, if the concentration of glycerol increases from 10% to 30%. This lowering of glycerol conversion could be due to lower availability of the catalytic sites. However, selectivity of 1, 2-PDO was also decreased up to 25% due to formation of side products like EG(6%), 2-PrOH(6%), Me-OH(5%), Et-OH(7%). 10% glycerol loading was considered as the optimum, as the highest 1, 2-PDO selectivity of 30% was obtained at this loading.

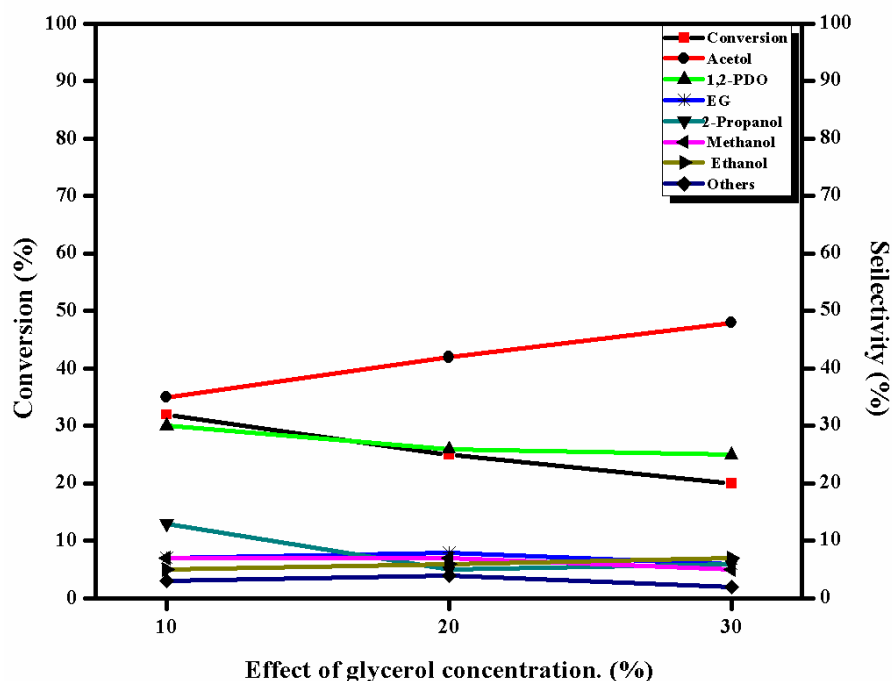


Figure 5.8 Effect of glycerol loading on glycerol APR reaction

Reaction conditions: Glycerol: 10.0 g, H₂O: 90.0 g, Catalyst (NIAI-600): 0.8 g, Temp.: 220 °C, Time: 5 h.

5.3.3.3 Effect of temperature

The effect of temperature from 200 to 240 °C on the conversion and selectivity pattern for the glycerol APR reaction over NiAl-600 catalyst is illustrated in Figure 5.9. Glycerol conversion increased from 25% to 40% with raising the temperature from 200 to 240 °C [47]. The selectivity to the desired product 1, 2-PDO was maximum (32%) at the initial rise in temperature from 200 to 220 °C. As expected, the selectivity of the in situ hydrogenation product has increased due to the reforming of glycerol. On further increase in the temperature from 220 to 240 °C, increased selectivity to small chain alcohols [Like MeOH(12%) and EtOH(13%)] was observed due to excessive hydrogenation of 1, 2-PDO.

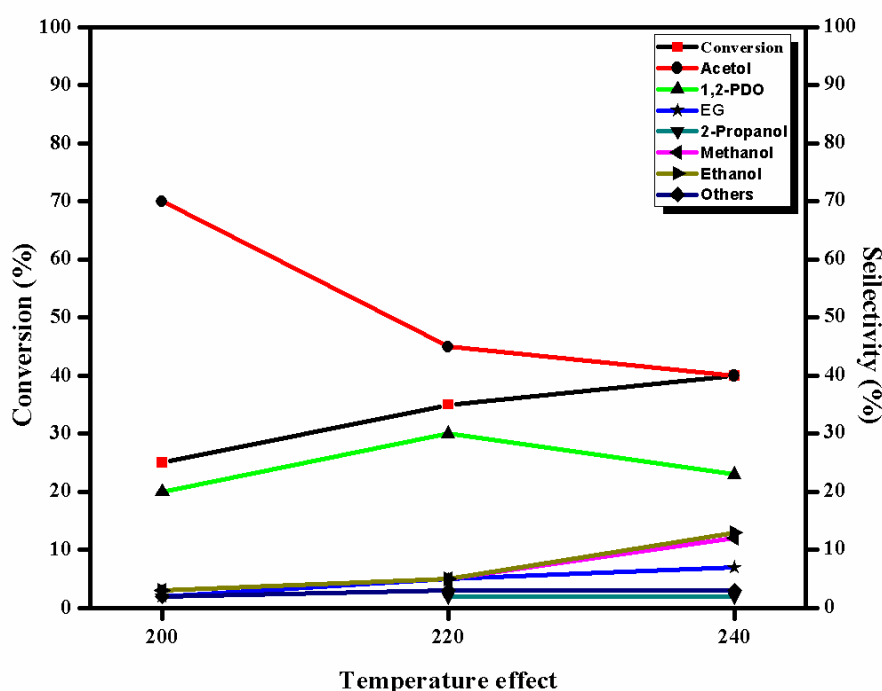


Figure 5.9 Effect of temperature on APR of Glycerol

Reaction conditions: Glycerol: 10.0 g, H₂O: 90.0 g, Catalyst (NiAl-600): 0.8 g, Time: 5 h.

5.3.4 Recycling of catalyst

Heterogeneous catalysts offer the advantage of recycling and making a process economically viable, the catalyst recycle studies were carried out by separating the catalyst after the first run from the product mixture simply by filtration and washed it with methanol to remove any adsorbed organic species. The catalyst recovered from the first run was charged using fresh reactants and the same procedure was repeated for 3 times. NiAl-600 catalyst was found to be highly active and its stability was confirmed by successful recycle experiments (Figure 5.10).

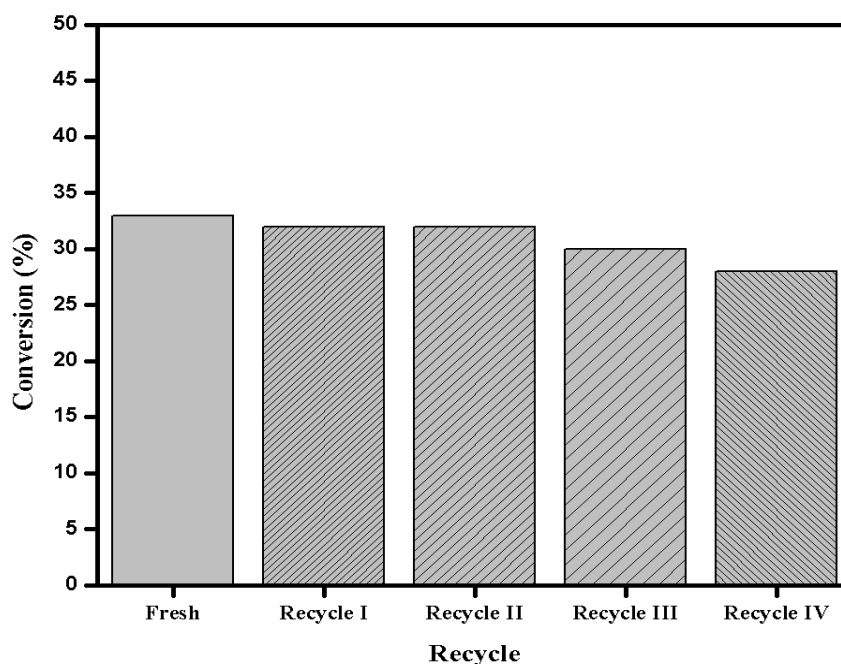


Figure 5.10 Recycling studies on the NiAl-600 catalyst for the APR reaction

Reaction conditions: Glycerol: 10.0 g, H₂O: 90.0 g, Catalyst (NiAl-600): 0.8 g, Temp.: 220 °C, Time: 5 h.

5.4 Conclusion

For APR of glycerol, a series of Ni catalysts supported on different support (C, Al₂O₃, ZnO₂, Mont, ZrO₂ or SiO₂) were prepared by wet impregnation method. Among these, alumina support 10% Ni catalyst displayed a maximum glycerol conversion of 34% with 29% selectivity to 1, 2-PDO. The activation temperature has a strong influence on the structural properties where the Ni in the aluminate matrix is rearranged to provide small Ni particles with better textual stability. Hence, the effect of the reduction temperature between 400 and 800 °C on the catalytic performance of 10% Ni/Al₂O₃ for the APR of glycerol was also investigated. From the characterization data and the activity results, the best catalytic performance was exhibited by 10% Ni/Al₂O₃ catalyst activated at 600 °C temperature (NiAl-600), with 38% glycerol conversion and 40% 1, 2-PDO selectivity.

The XRD results affirmed the formation of NiAl₂O₄ spinel phase due to surface diffusion of metallic Ni causing interaction with the bulk of NiO. TEM images depicted the formation of very small metallic nickel particles (< 8 nm). XPS studies along with XRD confirmed the

presence of multivalent Ni species which played key roles in the APR of glycerol. The presence of a moderate Brønsted and Lewis acidities with B/L ratio of 1.35 was a crucial factor for the high catalytic performance. NH₃ TPD revealed that increasing the acid strength led to better performance of NiAl-600 with higher activity and 1, 2-PDO selectivity. Based on the catalyst characterization integrated with the activity results, two plausible reaction pathways were proposed for glycerol reforming: dehydrogenation to glyceraldehyde, and the dehydration-hydrogenation mechanism to yield 1, 2-PDO. It was observed that too low or too high activation temperature is not suitable for the effective liquid phase reforming of glycerol. At low activation temperature mainly dehydration product (acetol) was observed while, at higher activation temperature mainly dehydrogenation mechanism was dominant. Hence the catalyst activated at 600 °C showed major selectivity towards C-O and C-C bond cleavage products with very less amount of EG (6%), EtOH (5%) and MeOH(5%). In addition, the effect of process parameters *viz.* metal loading, glycerol concentration and temperature on conversion of glycerol to 1, 2-PDO was also studied. NiAl-600 catalyst was found to be highly active and its stability was confirmed by four successful recycling runs.

5.5 References

1. O. O. James, S. Maity, M. A. Mesubi, K. O. Ogunniran, T. O. Siyanbola, S. Sahu, R. Chaubey, *Green Chem.* 13 (2013) 2272–2284.
2. P. D. Vaidya, J. A. Lopez-Sanchez, *ChemistrySelect* 2 (2017) 6563–6576.
3. R. Pandya, R. Mane, C. V Rode, *Catal. Sci. Technol.* 8 (2018) 2954–2965.
4. G. Wen, Y. Xu, H. Ma, Z. Xu, Z. Tian, *Inter. J. of Hydrogen Energy* 33 (2008) 6657-6662.
5. N. H. Tran, G. S. K. Kannangara, *Chem. Soc. Rev.* 42 (2013) 9454-9479.
6. Y. Wang, M. Chen, Z. Yang, T. Liang, S. Liu, Z. Zhou, X. Li, *Appl. Catal. A* 550 (2018) 214-227.
7. S. J. Yoon, Y. M. Yun, M. W. Seo, Y. K. Kim, H. W. Ra, J. G. Lee, *Int. J. Hydrogen Energy* 38 (34) (2013) 14559-14567.
8. M. N. N. Shahirah, J. Gimburn, A. Ideris, M. R. Khan, C. K. Cheng, *Renew. Energy* 107 (2017) 223-234.
9. Y. Nakagawa, K. Tomishige, *Catal. Sci. Technol.* 1 (2011) 179-190.
10. A. Seretis, P. Tsiakaras, *Fuel Process. Technol.* 142 (2016) 135–146.
11. M. El Doukkali, A. Iriondo, P. L. Arias, J. Requies, I. Gandarías, L. Jalowiecki-Duhamel, F. Dumeignil, *Appl. Catal. B Environ.* 125 (2012) 516-529.

12. Y. C. Lin, *Int. J. Hydrogen Energ.* 38 (6) (2013) 2678-2700.
13. R. L. Manfro, A. F. da Costa, N. F. P. Ribeiro, M. M. V. M. Souza, *Fuel process Technol.* 92 (3) (2011) 330-335.
14. N. H. Tran, G. S. Kannangara, *Chem. Soc. Rev.* 42 (24) (2013) 9454–9479.
15. R. R. Davda, J.W. Shabaker, G.W. Huber, R.D. Cortright, J.A. Dumesic, *Appl. Catal. B Environ.* 56 (2005) 171–186.
16. F. Bastan, M. Kazemeini, A. S. Larimi, *Renew. Energy* 108 (2017) 417–424.
17. B. Meryemoglu, B. Kaya, S. Irmak, A. Hesenov, O. Erbatur, *Fuel* 97 (2012) 241–244.
18. J. W. Shabaker, G. W. Huber, J.A. Dumesic, *J. Catal.* 222 (2004) 180–191.
19. R. L. Manfro, A. F. da Costa, N. F. P. Ribeiro, M. M. V. M. Souza, *Fuel process Technol.* 92 (3) (2011) 330–335
20. R. L. Manfro, T. P. M. D. Pires, N. F. P. Ribeiro, M. M. V. M. Souza, *Catal. Sci. Technol.* 3 (2013) 1278-1287.
21. R. B. Mane, C. V. Rode, *Green Chem.* 14 (2012) 2780-2789.
22. Remón, J.R. Giménez, A. Valiente, L. García, J. Arauzo, *Energy Convers. Manag.* 110 (2016) 90-112.
23. M. El Doukkali, A. Iriondo, J. F. Cambra, P. L. Arias, *Top. Catal.* 57 (2014) 1066-1077.
24. C. Jiménez-González, Z. Boukha, B. de Rivas, J. J. Delgado, M. A. Cauqui, J. R. González-Velasco, J. I. Gutiérrez-Ortiz, R. López-Fonseca, *Appl. Catal. A* 466 (2013) 9-20.
25. H. Özdemir, M. A. F. Öksüzömer, M. A. Gürkaynak, *Fuel* 116 (2014) 63–70.
26. H. S. C. O'Neill, W. A. Dollase, C. R. Ross II, *Phys. Chem. Minerals* 18 (1991) 302–319.
27. A. Khan, P.G. Smirniotis, *J. Mol. Catal. A* 280 (2008) 43–51.
28. F. P. Ribeiro, R. C. R. Neto, S. F. Moya, M. M. V. M. Souza, M. Schmal, *Int. J. Hydrogen Energ.* 35 (21) (2010) 11725–11732.
29. C. Jiménez-González, Z. Boukha, B. de Rivas, J. J. Delgado, M. A. Cauqui, J. R. González-Velasco, J. I. Gutiérrez-Ortiz, R. López-Fonseca, *Appl. Catal. A* 466 (2013) 9–20.
30. F.P. Ribeiro, R.C.R. Neto, S. F. Moya, M. M. V. M. Souza, M. Schmal, *Int. J. Hydrogen Energ.* 35 (21) (2010) 11725–11732.
31. Morales-Marín, A., J. L. Ayastuy, U. Iriarte-Velasco, and M. A. Gutierrez-Ortiz. *Appl. Catal. B* 244 (2019) 931-945.

32. Z. Boukha, C. Jiménez-González, B. de Rivas, J. R. González-Velasco, J. I. Gutiérrez- Ortiz, R. López-Fonseca, *Appl. Catal. B* 158-159 (2014) 190–201.
33. A. Al-Ubaid, E. E. Wolf, *Applied Catalysis* 40 (1988) 73-85.
34. L. Zhou, L. Li, N. Wei, J. Li, J. Basset, *ChemCatChem* 7 (2015) 2508–2516.
35. K. W. Park, J. H. Choi, B. K. Kwon, S. A. Lee, Y.E. Sung, H. Y. Ha, S. A. Hong, H. Kim, A. Wieckowski, *The Journal of Physical Chemistry B* 106 (2002) 1869-1877.
36. P. Dufresne, E. Payen, J. Grimblot, J. P. Bonnelle, *The Journal of Physical Chemistry* 85 (1981) 2344-2351.
37. B. C. Miranda, R. J. Chimentão, F. Gispert-Guirado, J. Llorca, F. Medina, F. LópezBonillo, J. E. Sueiras, *Appl. Catal. B* 147 (2014) 464-480.
38. C. A. Emeis, *J. Catal.* 141 (1993) 347–354.
39. G. Wen, Y. Xu, H. Ma, Z. Xu, Z. Tian, *Int. J. Hydrogen Energy* 33 (2008) 6657–6666
40. C. V. Rode, R. B. Mane, A. S. Potdar, P. B. Patil, P. S. Niphadkar, P. N. Joshi, *Catal. Today* 190 (2012) 31–37.
41. I. Chen, D. W. Shiue, *Ind. Eng. Chem. Res.* 27 (1988) 429-434.
42. J. ten Dam, U. Hanefeld, *ChemSusChem* 4 (2011) 1017-1034.
43. I. Gandarias, P. L. Arias, J. Requies, M. B. Güemez, J. L. G. Fierro, *Appl. Catal. B* 97 (2010) 248-256.
44. N. Braidy, S. Bastien, J. Blanchard, C. Fauteux-Lefebvre, I. E. Achouri, N. Abatzoglou, *Catal. Today* 291 (2017) 99-105.
45. Y. S. Yun, D. S. Park, J. Yi, *Catal. Sci. Technol.* 4 (2014) 3191-3202.
46. I. Gandarias, P. L. Arias, J. Requies, M. El Doukkali, M. B. Güemez, *J. Catal.* 282 (2011) 237-247.
47. E. B. Pereira, N. Homs, S. Martí, J. L. G. Fierro, P. Ramírez de la Piscina, *J. Catal.* 257 (2008) 206-214.

Chapter 6

Conclusions and Future scope

This chapter summarizes the important conclusions derived from the results obtained in the present work. Finally, some ideas for future work are suggested for chemo catalytic pathways for value addition of bioglycerol.

6.1 Conclusions

This thesis discussed advancements in the catalytic conversion of glycerol, into useful chemicals and materials. The performance of various types of catalysts, influence of synthesis and activation methods on catalytic performance and stability were thoroughly characterized and evaluated for amination and aqueous phase reforming of glycerol to give commercially important chemicals. The significant achievement of my research was to explore the scope of reactions for converting glycerol into nitrogen containing molecules like oxazoline, because all the strategies mentioned in the previous literature only offer oxygen containing chemicals from glycerol. The novel catalyst and the route developed in my work open up a new way to revalorize the waste produced by the biodiesel plant into value-added oxazoline, which adds a new approach in realizing the biorefinery concept in a most cost effective way. In addition, role of catalyst pre-treatment was also shown to successfully catalyze the aqueous-phase reforming of glycerol to propylene glycol, which is again an important commodity product and having important industrial applications as industrial solvent, thermo set plastics, antifreeze, flavours and fragrances, and approved additive in food, cosmetic and pharmaceutical industries. The major outcome of the thesis was the understanding of structure-activity correlation to identify the factors that are important to enhancing the performance of catalyst for all these reactions. The key findings are summarized below:

- ④ In the preliminary stage of this work, copper based catalyst was developed for the amination of glycerol with ammonia in aqueous medium for the production of oxazoline. In this two-step strategy, Cu catalysts exhibited almost 78% of glycerol conversion with complete selectivity to acetol while, the amination of acetol carried out separately gave 95% selectivity to oxazoline. A possible mechanism for the synthesis of oxazoline from acetol and ammonia was proposed, in which α -amino ketone was the intermediate to produce oxazoline. Role of a catalyst is very prominent for the synthesis of oxazoline from α -amino ketone intermediate selectively while suppressing the further side reaction, which leads to form dialkyl piperazine. The desired product, oxazoline was identified and confirmed by spectral elucidation (IR, ^1H and ^{13}C NMR). XPS studies and several other characterization techniques confirmed that Cu species present in various oxidation states, functioned as highly efficient sites which played a key role in the glycerol dehydration and further amination of acetol. A high Brønsted acid density with moderate acid strength was a crucial factor for the high catalytic performance.

- ⊙ Encouraged by the initial results on a bi-functional Cu catalyst for dehydrative amination of glycerol to oxazoline using a simple distillation method has opened a new path towards glycerol amination. Considering that the conversion of glycerol into acetol and the conversion of acetol into oxazoline have both been achieved, an opportunity arises to combine the two steps in a single pot reaction using a novel catalytic system. We have demonstrated a single-pot oxazoline synthesis using 3% Ru/C as the most stable catalyst to achieve 95% selectivity to oxazoline without any leaching. In a single-step cascade process, supported Ru catalysts showed excellent activity and most importantly, stability against poisoning by ammonia. XPS studies and several other characterization techniques confirmed that the multivalent Ru association species functioned as a highly efficient catalyst that played a key role in the amination of glycerol. A high Brønsted acid density with moderate acid strength was a crucial factor for the high catalytic performance. Py-IR spectroscopy evidenced that increasing the B/L ratio led to better performance of 3% Ru/C with higher activity and oxazoline selectivity. Based on the catalyst characterization integrated with the activity results, a plausible reaction pathway was proposed. The first step of the reaction, glycerol dehydration, is mainly catalyzed by acid sites; further tautomerization to the keto form takes place by abstraction of the proton by metallic Ru to give acetol. The subsequent amination of acetol provides imine, which undergoes cyclization with another molecule of acetol to obtain oxazoline. The effect of various reaction parameters such as temperature, metal and catalyst loadings, and solvents on the conversion and oxazoline selectivity were also studied.
- ⊙ Another very unique achievement of this work was the aqueous phase reforming (APR) of glycerol over supported nickel-based catalysts was investigated. A series of Ni catalysts supported on different support (C, Al₂O₃, ZnO₂, Mont, ZrO₂ or SiO₂) were prepared by wet impregnation method and tested for glycerol APR. Among these, alumina support 10% Ni catalyst showed the highest glycerol conversion of 35% and selectivity of 30% to 1, 2 PDO. Hence the effect of reduction temperature of 10% Ni/Al₂O₃ between 400 and 800 °C, on its physicochemical properties and catalytic performance in the APR of glycerol was investigated. The activation temperature is found to strongly influence the structural properties where the nickel in the aluminate matrix is rearranged and relatively small Ni crystallites with better textual stability can be obtained. 10% Ni/Al₂O₃ catalyst activated at 600 °C temperature showed the highest glycerol conversion 38% and the maximum

selectivity of 40% to 1, 2-PDO. The XRD results affirmed the formation of NiAl_2O_4 spinel phase where metallic nickel diffused to the solid surface, strongly interacting with the bulk of NiO. TEM images depicted the formation of very small metallic nickel particles (< 8 nm). XPS studies along with XRD confirmed the presence of multivalent Ni species which played key roles in the APR of glycerol. The presence of a moderate Brønsted and Lewis acidities with B/L ratio of 1.35 was a crucial factor for the high catalytic performance. NH_3 TPD revealed that increasing the acid strength led to better performance of NiAL-600 with higher activity and 1, 2-PDO selectivity. Based on the catalyst characterization integrated with the activity results, a plausible reaction pathway was proposed which involved glycerol reforming occurring through both the dehydrogenation to glyceraldehyde, and through dehydration of terminal hydroxyl groups, and subsequent hydrogenation to yield 1, 2-propylene glycol. It was observed that too low or too high activation temperature is not suitable for the effective liquid phase reforming of glycerol. At low activation temperature mainly dehydration product (acetol) was observed while, at higher activation temperature mainly dehydrogenation mechanism was dominant. Hence the catalyst activated at 600 °C showed major selectivity to the C-O and C-C bond cleavage products with very less amount of EG (6%), EtOH (5%) and MeOH(5%). The effect of various reaction parameters such as temperature, glycerol and catalyst loadings on the conversion and 1, 2-PDO selectivity was also studied and the studied catalyst could be recycled successfully for four times without any significant loss of catalytic activity.

6.2 Future prospects

As a result of rapid economic growth with significant environmental challenges, there is an essential requirement to implement sustainable manufacturing at every step of the process, from sourcing the raw materials to production, end use and eventual disposal. Green chemistry is the key to sustainable development, as they seek to establish more environmentally friendly, cleaner and safer industrial processes. Biomass derived glycerol molecule has the potential to serve as a sustainable feed stock for producing a variety of value-added chemicals and fuels, but the astonishing possibilities of glycerol are still unexploited. The future of green chemistry will depend on a multidisciplinary approach, innovative reactor engineering, and new catalyst, which will make a significant contribution towards sustainable development.

Research papers published in peer reviewed journals

Papers

1. Solvothermal synthesis of mesoporous manganese oxide with enhanced catalytic activity for veratryl alcohol oxidation
Ajay Jha, Tejansh Chandole, **Rajan Pandya**, Hyun-Seog Roh and Chandrashekhar V. Rode, *RSC Adv.*, 2014, 4, 19450-19455.
2. Cascade dehydrative amination of glycerol to oxazoline
Rajan Pandya, Rasika Mane and Chandrashekhar V. Rode, *Catalysis Science & Technology*, 2018, 8(11), 2954-2965.
3. Role of catalyst pre-treatment in aqueous-phase reforming of glycerol to propylene glycol
Rajan Pandya, Chandrashekhar V. Rode (to be submitted)
4. Selective hydrogenolysis of glycerol to 1, 2-PDO over La_2CuO_4 catalyst
Rajan Pandya, Chandrashekhar V. Rode (to be submitted)
5. Catalytic production of amino alcohol from waste glycerol
Rajan Pandya, Chandrashekhar V. Rode (to be submitted)

Patent

1. A one pot process for synthesis of oxazoline and imidazole compounds from glycerol
Chandrashekhar V. Rode, **Rajan Pandya** and Rasika Mane, WO 2016/038632 A1
2. A one pot process for synthesis of oxazoline and imidazole compounds from glycerol
Chandrashekhar V. Rode, **Rajan Pandya** and Rasika Mane, US Patent 2019/10385029 B2

Posters presentation for national/international symposium

1. **Rajan Pandya, Chandrashekhar V. Rode**
Cu–ZrO₂ nanocomposite catalyst for selective hydrogenation of levulinic acid and its ester to γ -valerolactone
Science Day 2014, CSIR-NCL, Pune, India
2. **Rajan Pandya, Chandrashekhar V. Rode**
Novel process for the preparation of oxazoline from glycerol
New Frontiers in Chemistry-From Fundamentals to Applications (**NFCFA2015**),
Goa, India.
3. **Rajan Pandya, Chandrashekhar V. Rode,**
Oxazoline Preparation from glycerol using a bimetallic catalyst
International Conference on Sustainable Chemistry & Engineering (**SusChemE 2015**), Mumbai, India.
4. **Rajan Pandya, C.V. Rode**
Novel process for the preparation of oxazoline from glycerol
22nd National Symposium on Catalysis (**CATSYMP-22, 2015**), CSMCRI, Bhavnagar,
Gujarat, India

About the Author

Rajan Pandya was born on 30th April 1990 in Banskara in district of Rajasthan, India. He completed his Bachelors in Chemistry (Honours) from The Maharaja Sayajirao University of Baroda, Gujarat (2007-2010). He went on to pursue Masters in Analytical Chemistry (2011-2012) from The Maharaja Sayajirao University of Baroda, Gujarat. He was awarded with Science excellence award (1st prize) at Gujarat University; Ahmadabad (2009) for the project titled hard melamine softens in milk. He was also qualified Joint CSIR-UGC (NET) JRF held in JUNE, 2012 with all India ranking 75. He then registered for his doctorate degree in August 2013 with AcSIR under the supervision of Dr. Chandrashekhhar Rode, Chief Scientist in Chemical Engineering and Process Development Division, CSIR-NCL, Pune. His work mainly focuses on design and development of new heterogeneous catalyst system to find chemo catalytic pathways for value addition of bioglycerol, which have been presented in this thesis.

1

Solvothermal synthesis of mesoporous manganese oxide with enhanced catalytic activity for veratryl alcohol oxidation†

Cite this: DOI: 10.1039/c4ra00184b

2

Ajay Jha, Tejansh Chandole, Rajan Pandya and Chandrashekhar V. Rode*

Catalyst activities of manganese and cobalt oxides prepared by solvothermal and co-precipitation methods were studied for veratryl alcohol oxidation. Manganese oxides showed higher activity performance than that of cobalt oxides irrespective of the method of preparation. The solvothermal method yielded mesoporous manganese oxide without using any template giving mixed phases of monoclinic Mn_2O_3 and hausmannite Mn_3O_4 . The mesoporous manganese oxide exhibited excellent activity for liquid phase aerobic oxidation of veratryl alcohol under base free conditions, with 96% conversion and almost complete selectivity towards veratraldehyde. The detailed characterization results on morphology, size and composition of the prepared mesoporous manganese oxide obtained by XRD, XPS, H_2 -TPR, N_2 adsorption–desorption isotherms, FE-SEM and HR-TEM techniques were used to understand the role of morphological and structural features in enhancement of the observed catalytic activity.

Received 8th January 2014
Accepted 1st April 2014

DOI: 10.1039/c4ra00184b

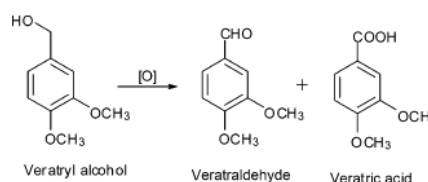
www.rsc.org/advances

Introduction

The activity of a catalyst strongly depends upon its morphology, crystallite size and the crystal planes hosting the active sites. These in turn depend upon the catalyst preparation method.^{1,2} During the past decade, rapid development in materials science has offered an opportunity to prepare metal and/or metal oxides with tailored structural characteristics for efficient catalysis. Among these, the most critical factor is the exposure of a specific crystal plane which is responsible for the type of active sites required in a particular reaction.³ Our earlier studies on Co_3O_4 material synthesized by solvothermal method showed that [111] plane of the cobalt oxide was highly active, due to presence of higher concentration of Co^{3+} , responsible for the oxidation reaction.⁴ From this perspective, it was thought appropriate to compare two methods *viz.* co-precipitation and solvothermal for the preparation of manganese and cobalt oxides as these are versatile oxidation catalysts. In this contribution, we have compared the performances of manganese and cobalt oxide catalysts for veratryl alcohol oxidation. The structural characterization studies of cobalt oxide catalyst used in this work, have been already discussed in our previous paper.⁴

Co-precipitation is a simple and well known method, reported for the synthesis of most of the metal oxides^{5,6} whereas, solvothermal method has been reported as a powerful



tool to synthesize the nanomaterial with reproducible quality and quantitative yield.⁷ The prepared catalysts were evaluated for liquid phase oxidation of veratryl alcohol (Scheme 1). Manganese oxide is mainly used for this purpose because of its non-toxic and cost-efficient nature, and also predominantly due to the wide range of stable oxidation states (+2, +3, +4, and +7) of Mn.⁸ In heterogeneous catalysis, manganese oxides are used as selective catalysts for a wide range of catalytic applications including ozone decomposition,⁹ photocatalytic oxidation of organic pollutants,¹⁰ nitric oxide reduction,¹¹ selective oxidations of carbon monoxide,¹² volatile organic compounds and decomposition of hydrogen peroxide.¹³ Recently, spinel Co_3O_4 , prepared by simple co-precipitation method has been reported for selective oxidation of veratryl alcohol in water by using molecular oxygen. The catalyst showed the highest conversion of 85% with 96% selectivity to veratraldehyde in 7 hours.⁵ As a derivative of coniferyl alcohol (a primary monomer of lignin), veratryl alcohol bearing 3,4-dimethoxy group has been extensively studied for understanding the chemistry of lignin valorization and exploring efficient transformation routes. Oxidation of veratryl alcohol to veratraldehyde was also



Scheme 1 Aerobic oxidation products of veratryl alcohol.

Chemical Engineering & Process Development Division, CSIR-National Chemical Laboratory, Pune-411008, India. E-mail: cv.rode@ncl.res.in; Fax: +91 20 2590 2621; Tel: +91 20 2590 2349

† Electronic supplementary information (ESI) available: XPS of used $MnOx$ -ST catalyst. See DOI: 10.1039/c4ra00184b

Cite this: *Catal. Sci. Technol.*, 2018,
8, 2954Cascade dehydrative amination of glycerol to
oxazoline†R. Pandya,  R. Mane and C. V. Rode *

Transformation of biomass into valuable nitrogen-containing compounds is highly desired, yet less explored. Here, we report a simple and efficient method for the direct conversion of bioglycerol to oxazoline involving glycerol dehydration to acetol followed by its amination using an aqueous solution of ammonia. For the two-step strategy a non-noble metal Cu–Zr catalyst was developed, giving a glycerol to acetol conversion of 78% followed by amination separately with 95% selectivity to oxazoline. Moreover, we have demonstrated a single-pot oxazoline synthesis using Ru/C as the most stable catalyst to achieve 95% selectivity to oxazoline without any leaching. XPS studies revealed the co-existence of multivalent Ru species in different percentages depending on the nature and structure of the support. These multivalent species (RuO₂ and RuO₃) have a synergistic effect on the activation of the carbonyl group, whereas Ru⁰ is an active site for ammonia dissociation. NH₃-TPD and Py-IR spectroscopy results also suggest that the presence of relatively moderate acid sites and a higher Brønsted/Lewis acid ratio in the catalyst promote the selective production of oxazoline. The reaction pathway involves first glycerol dehydration to acetol. In the subsequent step, NH₃ is dissociatively adsorbed on the catalyst surface and the imine thus formed is condensed with a second molecule of acetol to obtain oxazoline. The studied catalyst could be recycled successfully without any significant loss of catalytic activity.

Received 25th January 2018,
Accepted 29th April 2018

DOI: 10.1039/c8cy00185e

rsc.li/catalysis

1. Introduction

In recent years, downstream processing of biomass resources has attracted much attention for the development of sustainable industrial processes and efficient management of greenhouse gas emission. Biomass represents a prominent and easily accessible renewable source of organic carbon and its processing needs viable catalytic routes. Glycerol is a by-product of biodiesel production involving transesterification of vegetable oils and animal fats. As a consequence of government mandates in various countries to blend biodiesel with diesel, the production of biodiesel is forecasted to reach 37 million metric tons in 2020, ultimately leading to the surplus availability of glycerol.¹ Therefore, although glycerol has a traditional market, it is incapable of absorbing the huge surplus quantity of glycerol in the near future which already resulted in a crash in the price of glycerol. Thus, the valorisation of glycerol will not only improve the biodiesel economy but also provide an excellent opportunity for the usage of renewable resources in synthetic chemistry.^{2,3}

Glycerol is a trihydroxy reactive molecule and much effort has been devoted to its transformation to value-added chemicals with diverse applications.⁴ The most commonly studied reactions of glycerol are oxidation,^{5,6} hydrogenolysis,^{7,8} reforming,^{9,10} and dehydration,^{11,12} while amination of glycerol has been less explored despite its numerous applications. Depending upon the choice of catalyst and reaction conditions, glycerol amination affords various industrially important chemicals such as amino alcohol, serinol, and oxazolines.¹³ Oxazolines have a wide variety of uses as pharmaceuticals, flavouring agents, gasoline and lube oil additives, adhesives, monomers for the production of polymers, as a protecting group for carboxylic acids in asymmetric catalysis and in photography.^{14,15} Some of the 3-oxazoline derivatives (or 2,5-dihydro oxazoles) are recognized as useful intermediates^{16,17} and have been used in various total syntheses (Fig. 1). Two dimeric diterpenoids, taxodikaloids (a and b), have been identified from the seeds of *Taxodium ascendens* which possess an unprecedented oxazoline ring linkage between two monomers, and *ent*-alantrypinone (c) is the enantiomer of a natural product produced by the fungus *Penicillium thymicola*.

Despite the compelling synthetic utility and substantial biological as well as material applications of 3-oxazolines, their synthesis is less common, which includes photocatalytically induced ring opening of 2*H*-azirines,¹⁸ reaction of α -aminoperfluoronitrile¹⁹ or diazo derivatives,²⁰ condensation

Chemical Engineering and Process Development Division, CSIR-National Chemical Laboratory, Dr. Homi Bhabha Road, Pune, India-411008.

E-mail: cv.rode@ncl.res.in; Fax: +91 020 2590 2621; Tel: +91 020 2590 2349

† Electronic supplementary information (ESI) available. See DOI: 10.1039/c8cy00185e

(12) INTERNATIONAL APPLICATION PUBLISHED UNDER THE PATENT COOPERATION TREATY (PCT)

(19) World Intellectual Property
Organization
International Bureau



(43) International Publication Date
17 March 2016 (17.03.2016)

(10) International Publication Number
WO 2016/038632 AI

- (51) **International Patent Classification:**
C07D 233/58 (2006.01) C07D 263/14 (2006.01)
- (21) **International Application Number:**
PCT/IN20 15/050 108
- (22) **International Filing Date:**
11 September 2015 (11.09.2015)
- (25) **Filing Language:** English
- (26) **Publication Language:** English
- (30) **Priority Data:**
2621/DEL/2014 12 September 2014 (12.09.2014) IN
- (71) **Applicant: COUNCIL OF SCIENTIFIC AND INDUSTRIAL RESEARCH [IN/IN];** Anusandhan Bhawan, Rafi Marg, New Delhi 110 001 (IN).
- (72) **Inventors: RODE, Chandrashekhar Vasant;** National Chemical Laboratory, Dr. Homi Bhabha Road, (Maharashtra), Pune 411 008 (IN). **PANDYA, Rajan;** National Chemical Laboratory, Dr. Homi Bhabha Road, (Maharashtra), Pune 411 008 (IN). **MANE, Rasika Bharat;** National Chemical Laboratory, Dr. Homi Bhabha Road, (Maharashtra), Pune 411 008 (IN).
- (74) **Agent: REMFRY & SAGAR;** Remfry House At The Millennium Plaza, Sector 27, Gurgaon, Gurgaon 122 009 (IN).
- (81) **Designated States (unless otherwise indicated, for every kind of national protection available):** AE, AG, AL, AM, AO, AT, AU, AZ, BA, BB, BG, BH, BN, BR, BW, BY, BZ, CA, CH, CL, CN, CO, CR, CU, CZ, DE, DK, DM, DO, DZ, EC, EE, EG, ES, FI, GB, GD, GE, GH, GM, GT, HN, HR, HU, ID, IL, IN, IR, IS, JP, KE, KG, KN, KP, KR, KZ, LA, LC, LK, LR, LS, LU, LY, MA, MD, ME, MG, MK, MN, MW, MX, MY, MZ, NA, NG, NI, NO, NZ, OM, PA, PE, PG, PH, PL, PT, QA, RO, RS, RU, RW, SA, SC, SD, SE, SG, SK, SL, SM, ST, SV, SY, TH, TJ, TM, TN, TR, TT, TZ, UA, UG, US, UZ, VC, VN, ZA, ZM, ZW.
- (84) **Designated States (unless otherwise indicated, for every kind of regional protection available):** ARIPO (BW, GH, GM, KE, LR, LS, MW, MZ, NA, RW, SD, SL, ST, SZ, TZ, UG, ZM, ZW), Eurasian (AM, AZ, BY, KG, KZ, RU, TJ, TM), European (AL, AT, BE, BG, CH, CY, CZ, DE, DK, EE, ES, FI, FR, GB, GR, HR, HU, IE, IS, IT, LT, LU, LV, MC, MK, MT, NL, NO, PL, PT, RO, RS, SE, SI, SK, SM, TR), OAPI (BF, BJ, CF, CG, CI, CM, GA, GN, GQ, GW, KM, ML, MR, NE, SN, TD, TG).
- Declarations under Rule 4.17:**
- as to applicant's entitlement to apply for and be granted a patent (Rule 4.17(H))
 - of inventorship (Rule 4.17(iv))
- Published:**
- with international search report (Art. 21(3))



WO 2016/038632 AI

- (54) **Title:** A ONE POT PROCESS FOR SYNTHESIS OF OXAZOLINE AND IMIDAZOLE COMPOUNDS FROM GLYCEROL
- (57) **Abstract:** The present invention disclose a single step one pot process for synthesis of oxazoline and imidazole derivatives from glycerol using solid acid metal catalyst with improved yield.



US010385029B2

(12) **United States Patent**
Rode et al.

(10) **Patent No.:** **US 10,385,029 B2**
(45) **Date of Patent:** **Aug. 20, 2019**

(54) **ONE POT PROCESS FOR SYNTHESIS OF OXAZOLINE AND IMIDAZOLE COMPOUNDS FROM GLYCEROL**

(71) Applicant: **COUNCIL OF SCIENTIFIC & INDUSTRIAL RESEARCH**, New Delhi (IN)

(72) Inventors: **Chandrashekhhar Vasant Rode**, Pune (IN); **Rajan Pandya**, Pune (IN); **Rasika Bharat Mane**, Pune (IN)

(*) Notice: Subject to any disclaimer, the term of this patent is extended or adjusted under 35 U.S.C. 154(b) by 148 days.

(21) Appl. No.: **15/510,184**

(22) PCT Filed: **Sep. 11, 2015**

(86) PCT No.: **PCT/IN2015/050108**

§ 371 (c)(1),
(2) Date: **Mar. 9, 2017**

(87) PCT Pub. No.: **WO2016/038632**

PCT Pub. Date: **Mar. 17, 2016**

(65) **Prior Publication Data**

US 2017/0240515 A1 Aug. 24, 2017

(30) **Foreign Application Priority Data**

Sep. 12, 2014 (IN) 2621/DEL/2014

(51) **Int. Cl.**
C07D 233/58 (2006.01)
C07D 263/14 (2006.01)

(52) **U.S. Cl.**
CPC **C07D 263/14** (2013.01); **C07D 233/58** (2013.01); **Y02P 20/127** (2015.11)

(58) **Field of Classification Search**
CPC C07D 263/14; C07D 233/58
See application file for complete search history.

(56) **References Cited**

U.S. PATENT DOCUMENTS

2008/0045749 A1* 2/2008 Arredondo C07C 29/145
564/503

FOREIGN PATENT DOCUMENTS

GB 1554176 * 10/1979 C07C 91/04

* cited by examiner

Primary Examiner — Joseph R Kosack

(74) *Attorney, Agent, or Firm* — Seyfarth Shaw LLP

(57) **ABSTRACT**

The present invention disclose a single step one pot process for synthesis of oxazoline and imidazole derivatives from glycerol using solid acid metal catalyst with improved yield.

8 Claims, 3 Drawing Sheets

Erratum